Investigating and predicting landslides using a rainfall-runoff model in Southern Norway

Eline Haga Kråbøl

Thesis submitted for the degree of

Master of Science in Hydrology

60 credits

Institute of Geosciences

Faculty of Mathematics and Natural Sciences

UNIVERSITY OF OSLO

May 2016

Investigating and predicting landslides using a rainfall-runoff model in Southern Norway

Eline Haga Kråbøl

Thesis submitted for the degree of

Master of Science in Hydrology

60 credits

Institute of Geosciences

Faculty of Mathematics and Natural Sciences

UNIVERSITY OF OSLO

May 2016

Investigating and predicting landslides using a rainfall-runoff model in Southern Norway

This thesis is published digitally through DUO – Digitale Utgivelser ved UiO.

http://www.duo.uio.no/

Trykk: Reprosentralen, Universitetet i Oslo

Abstract

Landslides are amongst the most destructive natural hazards, causing damage to infrastructures, such as roads, railways and houses, and can, in a worst-case scenario, take lives. By studying the effect and response of rainfall using the temporal and spatial distribution of the storage and discharge, a better understanding of landslide processes and a more detailed prediction can be possible. This study employs a parameter-parsimonious rainfall-runoff model, the Distance Distribution model (DDD), to simulate hydrological conditions for rainfall induced landslide events. The DDD model represents the subsurface in 2D in that it calculates the storage along a hillslope representing the entire catchment in question. Model simulations for 76 debris avalanches and debris flows in Southern Norway have been investigated at catchment scale and at three points along the hillslope. The main objectives were to determine if the model has any capacity to predict hydrological conditions triggering landslides and to investigate how storage-discharge hysteresis is represented in the model and how it can relate to landslide occurrences.

Evaluated for the entire catchment, 70 % of the landslide events occurred during completely saturated conditions and more than 90 % of the events are characterized by sharp gradients and/or a prolonged high saturation in the temporal dynamics of saturation. This results suggests that the DDD model has capacity to predict hydrological conditions triggering landslides. The simulation of overland flow proved to be relevant for landslide occurrence found for 87 % of the events. The results for lower, middle and upper point of hillslope show that the storage has a distribution that varies along the hillslope and with time. The 2D representation of the hillslope has the potential to be used in landslide investigation, however, only if the registration of landslide events improves, starting with landslide initiation points.

Simulations employing hysteretic curves indicate that the structure of the DDD model allows addressing the non-linear, hysteretic relationship between storage and discharge. Hysteresis are complex processes, however, and there are still many aspects which are not known, suggesting that further exploration of the changes in storage and discharge, *dS/dt and dQ/dt,* would be useful. In terms of relating the landslide occurrence with hysteresis, no connections were found. A reduced uncertainty related to the timing of the landslide events and the use of input data of hourly resolution may allow for a better correlation between landslides and hysteresis.

Acknowledgements

I would like to thank all the people who contributed, one way or another, to complete my education and finish my thesis successfully.

I would like to begin expressing my gratitude to my supervisors Chong-Yu Xu (UiO), Thomas Skaugen (NVE) and Kolbjørn Engeland (UiO and NVE) for providing me with the topic, for great support and for showing a genuine interest in my work. I am especially grateful for your motivation and for giving me the opportunity to present my work at the EGU General Assembly 2016. A special thank you to Thomas Skaugen for your engagement and valuable guidance throughout my work.

I would like to thank the Norwegian Resources and Energy Directorate (NVE) for letting me use their data, programs and applications. I am also very grateful to Graziella Devoli and Søren Boje at NVE for sharing their vast knowledge about landslides with me.

A great thank you to my fellow students at the University of Oslo. Especially, my fellow student in Hydrology, Lisa, for your support, help, good corporation and friendship from the very beginning to the very end. We have had many wonderful experiences during our time at the University of Oslo and this journey would not have been the same without you!

Also warm thanks to my friends and family, especially my mom and dad, for the love and support. A special thank you to my best friend and boyfriend, Helge, for believing in me and encouraging me.

I wish you a good read.

Eline Haga Kråbøl Oslo, 31.05.16

Contents

1 Introduction

Landslides are amongst the most destructive natural hazards, causing damage to infrastructures, such as roads, railways and houses, and can, in a worst-case scenario, take lives. During the last decade, many debris flows and debris avalanches (all herein referred to as "landslides") have occurred during severe rainfall and snowmelt in Norway and the number of landslide events is expected to increase in the future (Lied, 2014). This scenario, based on the 2012 report on climate extremes from the Intergovernmental Panel of Climate Change (Seneviratne et al., 2012) emphasizes the importance of a good understanding of where the landslides occur, their spatial extent of runout and their prediction.

Hydro-meteorological events, especially heavy rainstorms and the succession of medium rainstorms in wet seasons, serve as the most frequent triggering factors of landslides in many regions in the world (Ebel et al., 2010). The current conceptual understanding of rainfall-induced landslides involves the reduction of effective stress due to development of positive pore-water pressure (Fannin and Jaakkola, 1999). Amount of rainfall together with the antecedent wetness controls the amount of water the soil can absorb before being completely saturated, thus developing positive pore-water pressures (Hennrich and Crozier, 2004).

That landslide occurrences are closely related to hydrologic responses are widely recognized (Ebel et al., 2010). The hydrological responses involves the spatial and temporal distribution of water moving through the catchment, which is strongly affected by threshold behaviors, and hysteresis (Camporese et al., 2014). Threshold behavior includes, amongst others, the formation of overland flow controlled by soil capacity and infiltration rate, while hysteresis refers to the non-linear relationship between two variables observed in nature. Hysteresis in the storage-discharge relationship refers to the changing relationship depending on whether the soil is wetting or drying, has long been investigated (Beven, 2006; Zehe et al., 2007; Detty and McGuire, 2010; Spence, 2010). Despite the importance of hydrological response in controlling landslides, investigations of the connection between storage-discharge hysteresis and landslides are rare.

Norway is considered an important region for landslide investigation as it is particularly prone to landslide hazards due to topography, geology and weather (Dyrrdal et al., 2012; Lied, 2014). Since 2013, a landslide early warning system (EWS) has been operational at The Norwegian Water Resources and Energy Directorate (NVE) in synergy with the flood forecasting service operating since 1989 (Boje et al., 2014; Devoli et al., 2014). Two rainfall

runoff models are currently in use at the flood and landslide forecasting service, namely Hydrologiska Byråns Vattenbalansavdelning model (HBV) operational since 1989, and the Distance Distribution Dynamics model (DDD), operational since 2013. The DDD model at the present is only used for flood predictions, not for landslides. In the recently published DDD model (Skaugen and Onof, 2014; Skaugen and Mengistu, 2015) the subsurface has a 2-D representation in that it calculates the storage along a hillslope representing the entire catchment in question. The model estimates the capacity of the subsurface reservoir at different levels of saturation and predicts overland flow.

Objectives

This thesis is carried out in cooperation with NVE. The primary objectives of this study are to 1) determine if the subsurface representation of soil and groundwater in the DDD model has any capacity to predict the hydrological conditions triggering landslides and 2) investigate how the storage-discharge hysteresis associated with the landslide events are represented in the DDD model and how the landslides can relate to the hysteretic loops. By studying the effect and response of rainfall using the temporal and spatial distribution of the storage and discharge, a better understanding of landslide processes and a more detailed prediction can be possible (Wieczorek and Glade, 2005; Boje, 2011). The objectives of the study are achieved through the following sub-objectives;

- Investigate the characteristics of the subsurface states as represented by the DDD model, in a suitable window of time surrounding the landslides. Do the landslides occur during partially or completely saturated conditions?

- Investigate of the temporal dynamics of saturation in a suitable window of time surrounding the occurrence of landslides in the catchment - Does the saturation exhibits sharp gradients or prolong high saturation prior to the landslide events?

- Investigate the relationship between overland flow and landslides - is the model simulation of overland flow relevant for landslide occurrences?

- Investigate the relationship between the storage-discharge hysteresis and landslides - Can the occurrence of landslides be associated with either the rising limb or the recession, and how does the DDD model represent hysteresis in the subsurface at the time of the landslide events?

2 Theory - Hillslope hydrology and landslides

To study the triggering factors of landslides knowledge of landslides and hillslope hydrology are needed. This chapter briefly discusses hillslope hydrology and landslide theory.

2.1 Hillslope hydrology

The main aim of studying hillslope hydrology is to investigate the catchment response to water, which involves the movement of water through the hillslope to the river network. The relationships between storage, including residence time and subsurface flow, overland flow and discharge is especially important.

2.1.1 Overland flow

Overland flow, also referred to as surface runoff, is the flow of water on the surface caused by excess stormwater, meltwater or other flow sources (Kirkby, 1988). Its cause vary with season, region and within events (Kendall et al., 1999). Overland flow is produced as either Hortonian overland flow or saturation overland flow, where the saturation overland flow is produced when the soil capacity is completely filled so that the water is forced to flow on the surface. The less common Hortonian overland flow occurs when the rainfall rate exceeds the current infiltration capacity of the soil (Kirkby, 1988; Fannin and Jaakkola, 1999).

2.1.2 Subsurface flow

Subsurface flow is the water that infiltrates and percolates through the unsaturated and saturated subsurface. The water is either stored in the soil or travels within the soil as lateral through-flow (Kirkby, 1988). The flow of water can occur as a homogenous flow through micropores or as preferential flow through macropores (e.g. tree roots, burrow holes from animals or fractures) and is mainly driven by gravity and capillarity. The formation of the subsurface flow depends on antecedent conditions, topography, soil and bedrock layer characteristics and the magnitude of the water input (Beven and Germann, 1982).

2.1.3 Hydrological response - Hysteresis

The spatial and temporal distribution of water moving in the catchment is strongly affected by catchment thresholds (e.g. storage capacity, maximum velocity and infiltration rate), and

hysteresis. Typically, hysteresis occurs when a time lag exists between two variables and when a response variable (e.g. discharge, storm runoff and water table depth) not only depends on the value of a driving variable (e.g. subsurface storage, storm rainfall and soil moisture), but also on its past history (Visintin, 2006; Norbiato and Borga, 2008; Ebel et al., 2010; Camporese et al., 2014; Zuecco et al., 2015). Threshold behavior and hysteresis occurs at different levels of complexity, at various scales and may limit the predictability of hydrological processes and the repeatability of hydrological observations (Zehe et al., 2010; Penna et al., 2011). Examples of storage-discharge hysteresis are seen in Figure 1.

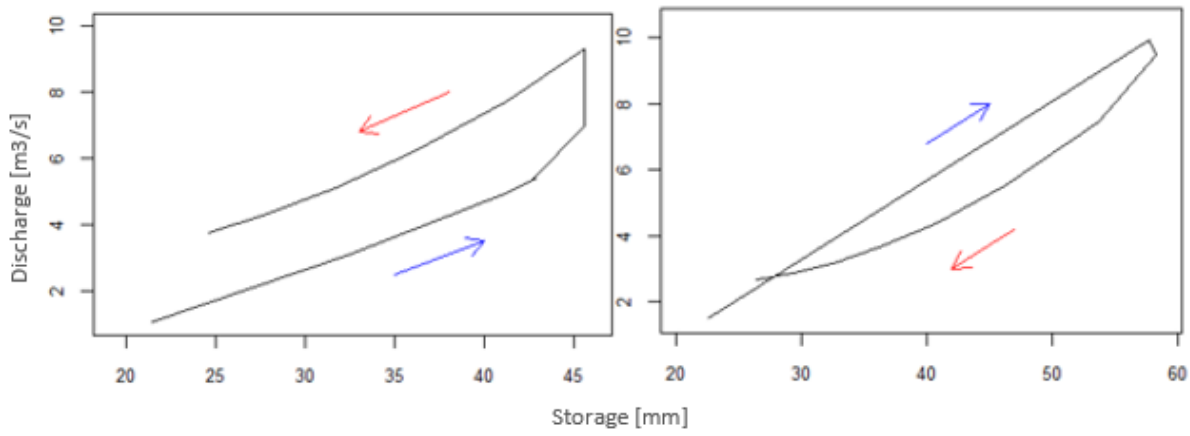

Figure 1) Hysteresis in the relationship between storage and discharge. The arrows indicate the recharge and recession, i.e. the direction of the loop; anti-clockwise (left) and clockwise (right).

It is well documented that storage (here referring to any variable quantifying or reflecting the volume of water stored in the subsurface such as saturated storage, groundwater level and soil moisture content) regulates discharge in a non-linear way creating hysteresis in the storage-discharge relationship (Myrabø, 1997; McGlynn and McDonnell, 2003; Beven, 2006; Lehmann et al., 2007; Zehe et al., 2007; Detty and McGuire, 2010; Zehe et al., 2010; Penna et al., 2011; Radatz et al., 2013; Weill et al., 2013). The directions of the loops can be clockwise (i.e. lower storage on the rising limb than on the falling limb for a given discharge), or anti-clockwise. The shape of the loops vary from simple elliptical circles to more complex or ”non-classifiable” shapes. In the past, it has been suggested that the shape and scale of the hysteretic relationships are controlled by various factors, including catchment characteristics such as area and topography, antecedent wetness conditions and catchment connectivity (i.e. the connectivity between the riparian zone and hillslope, influencing which area contributes to discharge). The loops are also found to vary with

location, i.e. adjacent to river or at the hillslope, and the size of the rainfall event/snowmelt (Myrabø, 1997; Allen et al., 2010; Weill et al., 2013; Camporese et al., 2014). Larger catchments experience greater travel distances resulting in a more damped hydrological response. Thus, the delay to peak flow following rainfall events decreases with decreasing scale, causing greater hysteresis (Davies and Beven, 2015). Greater hysteresis is also found during dry antecedent conditions and less steep slopes due to a decreased displacement of water (Camporese et al., 2014; Davies and Beven, 2015)

Hysteresis has been found in literature to vary according to location (Myrabø, 1997; Kendall et al., 1999; Penna et al., 2011). Myrabø (1997) and Kendall et al (1999), found the hysteretic loops of the relationship between discharge and water table to be anti-clockwise in the riparian zone and clockwise in the hillslope. In general, the riparian zone has a larger drainage- and contributing area than the hillslope (Camporese et al., 2014). The storage in the riparian zone is more persistent and stays wet long after rainfall events and during streamflow recession because of redistribution from upslope water. The riparian zone also usually responds faster to precipitation, because of higher antecedent wetness and shallower water tables (Camporese et al., 2014). On the other hand, Penna et al. (2011) observed opposite directions of the loops, i.e. during rainfall events with dry antecedent conditions, discharge responded and peaked earlier than hillslope soil moisture. For events with wet antecedent conditions, streamflow lagged soil moisture.

2.2 Landslides and their causes

The following sections briefly discusses landslide theory, including types of landslides, static conditions that form the basis of a landslide occurrence and some triggering factors with emphasis put on the hydrological triggering factors.

2.2.1 Types of landslides

The term “landslide” refers to any downward movement of slope-forming materials composed of natural rocks, soil, artificial fill, or combinations of these materials (Sidle et al., 2013a). The various types of landslides can be differentiated by many parameters including type of mass movement, type of material, water content, velocity, volume etc. A widely used classification scheme, developed by Varnes (1978), distinguished by the type of mass movement (falls, topples, slides, spreads, and flows) (Figure 2) and the type of material (bedrock, coarse soil and fine soils). Coarse soils refer to soil containing more than

20 % gravel and coarse sizes (Varnes, 1978). The "Varnes Classification System" is used as a basis for several new classification systems, including the version recently proposed by Hungr et al. (2014) and given in Table 1. Here, the rows represent the type of movement and the columns represent the type of material (Hungr et al., 2014).

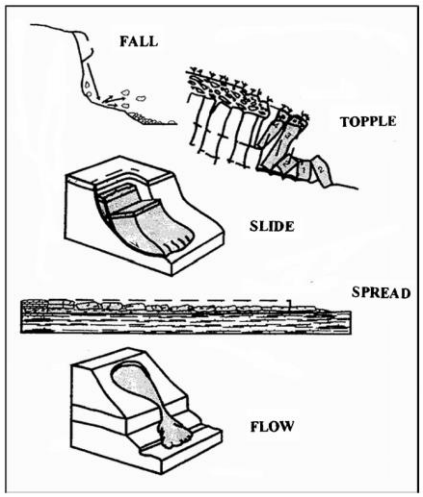

Figure 2) Illustration of the types of movement (from Hungr et al., 2014).

Table 1) A summary of the proposed new version of the Varnes classification system (from Hungr et al. 2014).

Type of movement	Rock	Soil
Fall	1. *Rock/ice* fall[a]	2. *Boulder/debris/silt* fall[a]
Topple	3. Rock block topple[a]	5. *Gravel/sand/silt* topple[a]
	4. Rock flexural topple	
Slide	6. Rock rotational slide	11. *Clay/silt* rotational slide
	7. Rock planar slide[a]	12. *Clay/silt* planar slide
	8. Rock wedge slide[a]	13. *Gravel/sand/debris* slide[a]
	9. Rock compound slide	14. *Clay/silt* compound slide
	10. Rock irregular slide[a]	
Spread	15. Rock slope spread	16. *Sand/silt* liquefaction spread[a]
		17. Sensitive clay spread[a]
Flow	18. *Rock/ice* avalanche[a]	19. *Sand/silt/debris* dry flow
		20. *Sand/silt/debris* flowslide[a]
		21. Sensitive clay flowslide[a]
		22. Debris flow[a]
		23. Mud flow[a]
		24. Debris flood
		25. Debris avalanche[a]
		26. Earthflow
		27. Peat flow
Slope deformation	28. Mountain slope deformation	30. Soil slope deformation
	29. Rock slope deformation	31. Soil creep
		32. Solifluction

In Norway, the most frequent landslides in soils are found in Table 1 as type 11, 12, 13, 21, 22, 24 and 25. In addition it is possible to observe landslides in filling and cuts along linear infrastructure (e.g. roads and railways) (NVE, 2011b). Classification of landslides in Norway are commonly based on the type of material; rock, debris, clay and snow (NVE, 2011a; NVE, 2011b). An example of a classification is presented in Figure 3 (NGI, 1979; NGI, 1977; Veidirektorated, 2014). Here, the landslides are divided based on the proportion between snow, soil/rock and water.

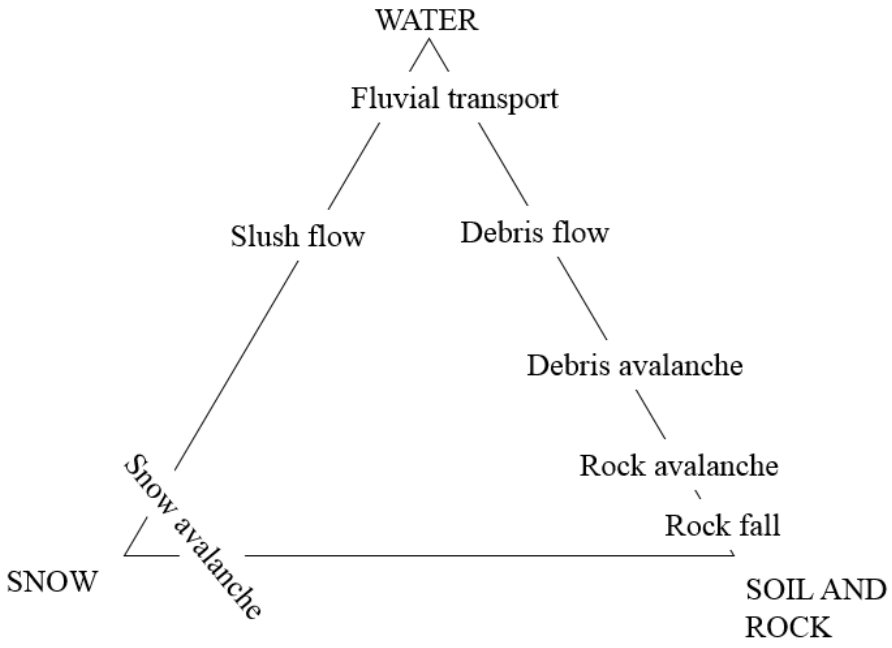

Figure 3) Landslide classification based on type of material (modified from NGI (1977), NGI (1979) and Veidirektoratet, 2014).

In this study, only debris avalanches and debris flows are included (Figure 4), which are classified as flows in soil (no. 22 and 25 in Table 1). Debris avalanches are very rapid to extremely rapid movements of partially or completely saturated debris on steep slopes outside of an established channel. They occur at various parts of the slope and rarely at the same location due to depletion of materials (Hungr et al., 2014). Debris flows are very rapid to extremely rapid, flood-like movement of completely saturated non-plastic debris in an established channel. They often occur simultaneously with floods, starting as debris slides, debris avalanches or rock falls. They could also often occur when erosion along the stream removes support from the base of the slope (Hungr et al., 2014). Both debris avalanches and debris flows are usually caused by intense/prolonged rainfall or heavy snowmelt (NVE,

2011b). The transition between the two types is smooth and they have many similar features which often make it hard to distinguish between them (NVE, 2011b; Hungr et al., 2014). A summary of a comparison between the two types is given Table 2.

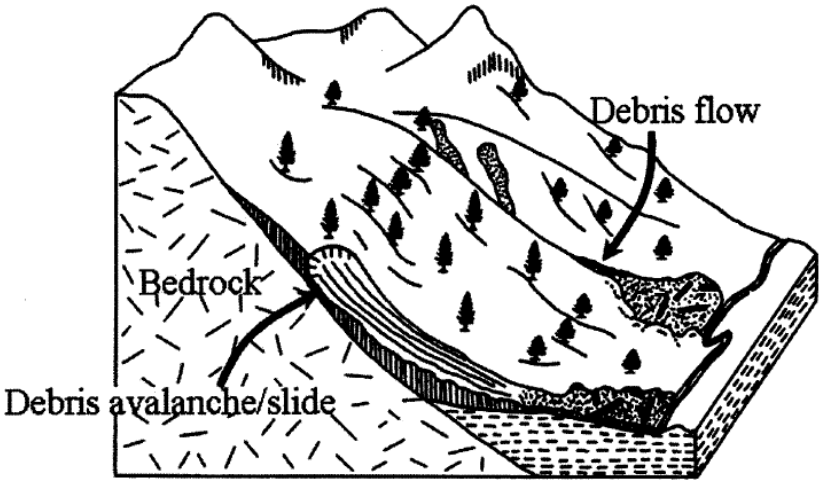

Figure 4) Illustration of a debris avalanche on a steep hillslope where thin soils are underlain by relatively impermeable bedrock (to the left). On the right side is the lower extent of a debris flow that was triggered by landslides; the debris flow extends into a headwater channel (Sidle et al., 2013b)

Table 2) Information about debris avalanches and debris flows (from NVE, 2011b).

Type	Conditions at the location of landslide	Triggering mechanisms
Debris avalanche	• Steep, soil covered slopes (> 25-30 º) • No established channel • Partially or completely saturated	• Intense/prolonged rainfall and/or snowmelt • Points or cracks in saturated soils
Debris flow	• Steep, flooding rivers and streams eroding soil cover • Established channel, often where there is not a permanent flow of water • Completely saturated	• Floods caused by intense rainfall and/or snowmelt or dam breakage • Intense erosion together with a large discharge • Soils added by debris slide, debris avalanches and rockfall

2.2.2 Static conditions

The static conditions form the basis for the occurrence of a landslide at any location. They are assumed to be constant over time, however some of them can change due to human activity or other impacts. The static conditions include the shape of terrain and slope angle, soil type and thickness, layering and grain size distribution, vegetation, and hydrological properties (e.g. maximum storage capacity) (NVE, 2014c). Generally, in order to generate a landslide the slopes must be above 20º-25º and there must be enough loose soil present (Hungr et al., 2014)

2.2.3 Triggering factors

Landslides occur in a variety of landscapes across the world triggered by weather, earthquakes, volcanic activity, and human activity (NVE, 2014c). Earthquakes and volcanic activity will not be described in this thesis as they are not very relevant for landslide occurrences in Norway.

2.2.3.1 Groundwater and precipitation

The most important triggering factor for landslides in soil is considered to be water (Wieczorek and Glade, 2005; Sidle et al., 2013c). Water affects the slope stability by decreasing the suction, increasing pore-water pressure, seepage erosion etc. Infiltration of water to the soil, by extreme rainfall or rapid snowmelt, causes a sudden rise of the water table and an increase in water-pressure. This results in a reduced effective stress between the individual soil grains, which reduces the resistance to shear and in turn weakens the slope. In addition, the load of water causes a downward driving force of the soil column (Wieczorek and Glade, 2005; Sidle et al., 2013c). The groundwater level varies with precipitation and evapotranspiration, rendering wetting and drying cycles, which can be considered cyclic loads. During continuously repetitive cycles the slope experiences accumulated plastic deformation and damage, causing unstable slopes. In these cases, even small rainfalls of short duration can trigger landslides (Xu et al., 2010).

The intensity and duration of rainfalls are also closely related to the occurrence of landslides as it directly affects the groundwater and impacts the seepage characteristics of the slope (Sidle et al., 2013c). Heavy rainfall raises the groundwater table within a hillslope and leads to instability. Rainfall of low intensity and long duration commonly leads to greater depths of the sliding plane, triggering larger landslides (Wu et al., 2015). Finally, the occurrence of overland flow (described in section 2.1.1) causes an increased soil erosion and a reduced slope stability, possibly triggering landslides (Xu et al., 2010).

2.2.3.2 Freezing of water in soil and soil frost

Freezing of water in soil is a common triggering factor in Norway during winter and spring (Colleuille et al., 2009). When water freezes it expands about 10 % possibly causing displacement within the soil. This phenomenon is especially important during spring when repetitive cycles of snowmelt and water freeze are common. When water freezes in fissures and cracks, an additional downslope pressure is exerted that may trigger landslides. Soil frost is another common triggering factor that may prevent water from infiltrating into the ground, causing locally increased soil water content and pore water pressure. Soil frost may act as a sliding layer, similar to hard, impermeable bedrock. During spring and summer when top soil is reheated, the top soil layer may experience high pore-water pressure when rain and/or snowmelt infiltrate the unfrozen parts. This causes high pore-water pressure which increases the potential for a landslide to occur (Colleuille et al., 2009; Boje, 2011)

2.2.3.3 Human activity

Human activities, such as deforestation, construction and road work can change the natural drainage of the slope or slope gradient, making it more prone to landslides (NVE, 2014c). In Norway, bad maintenance of culverts diverting water under roads and railways commonly triggers landslides. As water accumulates, caused by leaves, branches, rocks and ice preventing water from flowing through the culverts, the pressure on the culverts increase, possibly causing it to break and trigger landslides. This problem has often been observed at several Norwegian forest roads (Fergus et al., 2011). Another common problem related to human activities in Norway is clear cutting in steep, wooded slopes (NVE, 2014a).

3 Study area

The area of study is confined to Southern Norway (Figure 5) that can be divided into four main physiographic and geomorphological regions; East (Reg.1), South (Reg.2), West (Reg.3) and Central (Reg.4) (NVE, 2014a).

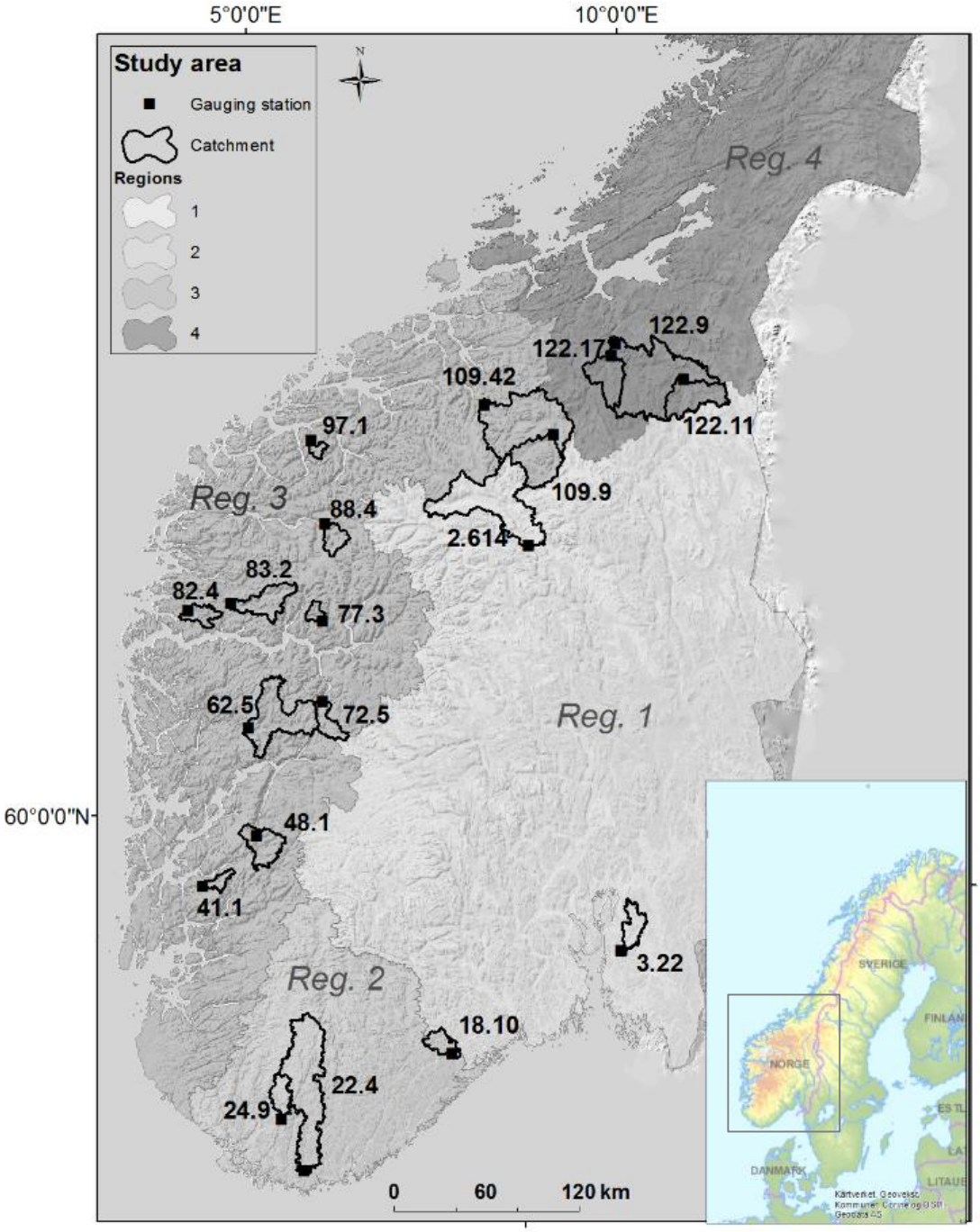

Figure 5) A map of the study area, Southern Norway. The 19 catchments, indicated with catchment number (see Table 3) are located in four regions. The gauging stations associated with the catchments are indicated.

3.1 Physiography and geology

In general, the landscape in South Norway ranges from mountains to low-lying areas and fjords. In Reg.1 and 2. the landscape is mostly hilly, characterized by forest, farmlands and gentle valleys. There is a spatial variation in the direction of the valleys with a northwest-southeast direction in the western part and a north-south direction in the eastern part. Around the Oslofjord, where the valleys congregate, there is a large area of lowland. The largest lake, Mjøsa, the largest river, Glomma, and the two longest valleys, Østerdalen and Gudbrandsdalen, are located in Reg.1 (NVE, 2014a). Reg.3 is characterized by steep mountains and deep fjords reaching more than 200 km inland in to the glaciers. Reg.4 consists of less steep landscape with rounded hills and mountains, and larger areas of lowlands (NVE, 2014a). A soil cover map of South Norway is shown in Figure 6 (www.ngu.no). Reg.1 is mainly covered by moraine deposits. The soil layer in Reg. 2, 3 and 3 is shallower. In general, larger areas of valley-sides and floors are covered by continuous till deposits. Avalanche deposits is mainly found in the western and northern parts of the study area.

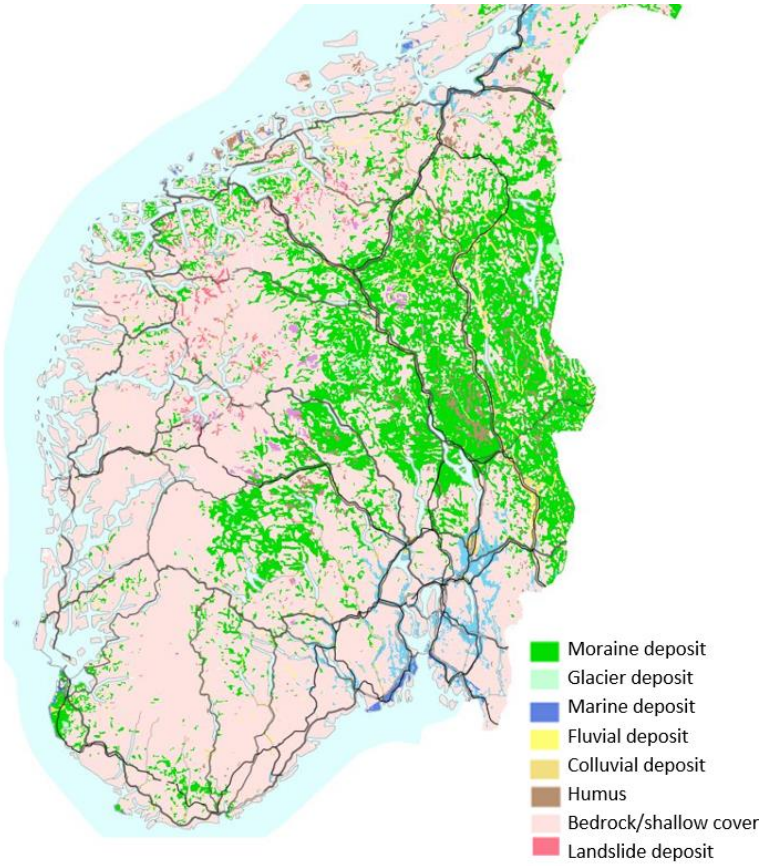

Figure 6) Soil cover map of South Norway. From Geological Survey of Norway (2016).

3.2 Climate

Due to the varied and complex topography, there are large local climate gradients in South Norway. The spatial distribution of precipitation is presented in Figure 7a (www.senorge.no). Reg.1 and 4, and most of Reg. 2, experiences a continental climate, with less precipitation (Stalsberg et al., 2012; NVE, 2014a). Along the west coast in Reg.3 the North Atlantic current forces warm, moist air across the coastal mountains causing high amounts of precipitation. In this area, the wettest parts of Norway are found from Hardangerfjorden to the Møre area, with a normal annual precipitation above 4000 mm. Contrary, the lowest normal annual precipitation, below 300 mm, are found inland (Reg.1) in Oppland municipality (NVE, 2014a). Figure 7b presents the spatial distribution of the normal annual runoff, which follows that of normal annual precipitation (www.senorge.no). The highest runoff is found in the western parts, with a discharge of more than 4000 mm pr. year. In Reg.1, the lowest runoff is found with a runoff below 200 mm pr. year. The spatial distribution of temperatures follows that of topography, with the highest values found along the coast in the western and southern parts.

3.3 Hydrological regimes

The varied topography, geology and climate result in different hydrological regimes. In Reg.1, 2 and 4 the rivers are long with gentle slopes. In Reg.3 the rivers are relatively short and steep (NVE, 2014a). Air temperature is the main controlling factor on the snow season and the snowpack volume, thus the temperature regimes causes differences in the regional importance of snowmelt as a runoff generation process (Vormoor et al., 2015). Within the study area, roughly two basic patterns in runoff regimes are found (Vormoor et al., 2015). Reg.1, 2 and 3 are characterized by prominent spring flows during spring and summer, mainly due to snowmelt. The runoff is also large during autumn. During winter, snow accumulation causes dominant low water flow. Reg.3 experience prominent high flows during autumn, winter and spring, mainly due to the influence of precipitation falling as rain due to warmer winters. Numerous variations reflecting local climate as well as transitional, mixed regimes do, however, exist (NVE, 2014a; Vormoor et al., 2015).

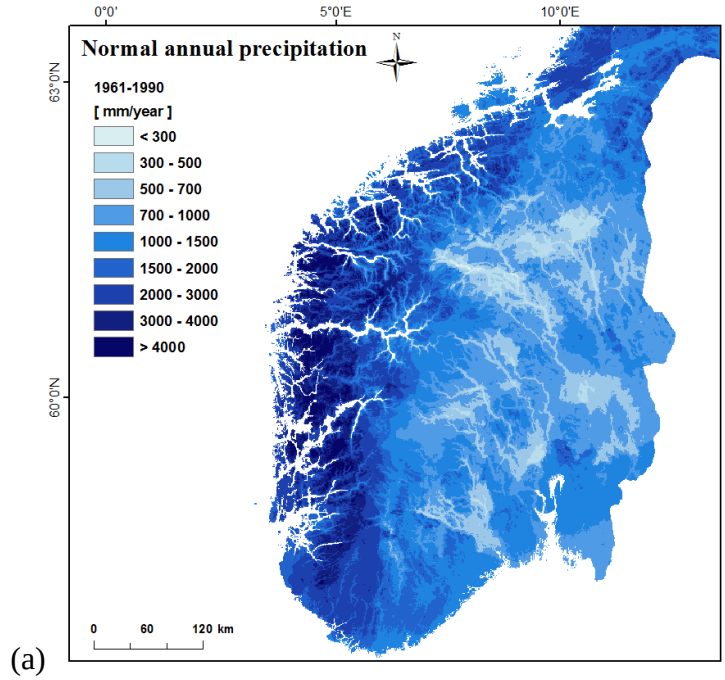

(a)

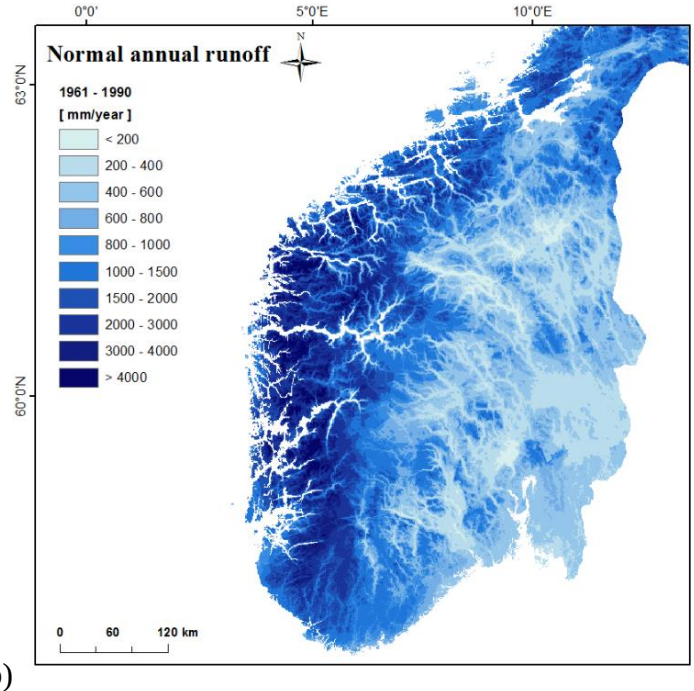

(b)

Figure 7) Spatial distribution of normal annual precipitation (a) and normal annual runoff (b) from 1961 to 1990 for Southern Norway. From www.senorge.no.

3.4 Studied catchments

Within the study area, 19 catchments are selected from NVEs database Hydra II. The size of the catchments vary from 89 km^2 in catchment 97.1 to 3086 km^2 in catchment 122.9. It should be notet that catchment 122.9 and 109.42 include smaller catchments (122.11 and

122.17, and 109.9, respectively) which is refleceted in the information given in Table 3. In the landslide analysis in this thesis, however, they are treated as separate catchments (as presented in Figure 5). The lowest mean elevations are found in the southern parts of South Norway, while the highest mean elevtions are found in west (Reg.3). The steepest mean slopes are also found in the western parts, with two catchments, 77.3 and 97.1, associated with particularly steep slopes (49 ° and 59 °, respectively). In contary, the mean slope in catchment 3.22 is only 3 °. For catchment 122.17, the mean slope is not found (noted NA). The maximum storage capasity, *M,* range from 38 mm in catchment 122.9 to 266 mm in catchment 83.2. The catchment characteristics describing the hillslope is derived by the distributions of distances from points in the catchment to the nearest river reach (see section 5.1.3).

Table 3) Catchment characteristics derived from NVEs database Hydra II and GIS analysis. M is total storage capacity [mm]. The hillslope characteristics in DDD is represented by the mean distance ($\bar{d}$) and maximum distance (d_{max}) from points in the catchment to the nearest river reach (see section 5.1.3)

Catchment		Reg.	Area [km^2]	MAD [m3/s]	Mean elevation [m.a.s.l.]	Mean slope [°]	M [mm]	*Hillslope DD* $\bar{d}$ [m]	*Hillslope DD* d_{max} [m]
2.614	*Rosten*	1	1834	33	1187	8	46	413	1500
3.22	*Høgfoss*	1	299	3	153	3	56	212	1200
18.10	*Gjerstad*	2	236	7	314	23	40	223	1000
22.4	*Kjølemo*	2	1758	84	560	24	64	167	1500
24.9	*Tingvatn*	2	272	16	589	27	85	161	700
41.1	*Stordalsvatn*	3	131	14	684	36	164	151	960
48.1	*Sandvenvatn*	3	470	38	1091	36	94	275	1480
62.5	*Bulken*	3	1092	69	868	32	100	190	1200
72.5	*Brekke Bru*	3	268	17	1272	37	103	255	1500
77.3	*Sogndalsvatn*	3	111	8	1002	49	93	301	1500
82.4	*Nautsundvatn*	3	219	19	464	34	80	191	990
83.2	*Viksvatn*	3	508	45	841	39	266	222	1640
88.4	*Lovatn*	3	235	18	1339	35	256	339	2000
97.1	*Fetvatn*	3	89	8	592	57	75	330	1500
109.42	*Elverhøy*	3	2437	72	1217	10	46	362	1500
109.9	*Risefoss*	3	745	17	1347	22	58	406	1500
122.9	*Gaulfoss*	4	3086	80	734	7	38	181	1200
122.11	*Eggafoss*	4	654	18	843	29	45	172	1000
122.17	*Hugdal Bru*	4	546	12	623	NA	44	213	1500

4 Data

This chapter presents the landslide data, including information about the Norwegian landslide database, and the model data, including hydro-meteorological input data. Groundwater level observations are also presented.

4.1 Landslide data

The landslide data has been extracted from the Norwegian landslide database (www.skrednett.no). A total of 76 landslide events have been selected (Figure 8). The landslide events include debris avalanches, debris flows and unspecified landslides in soil, i.e. either debris avalanches or debris flows.

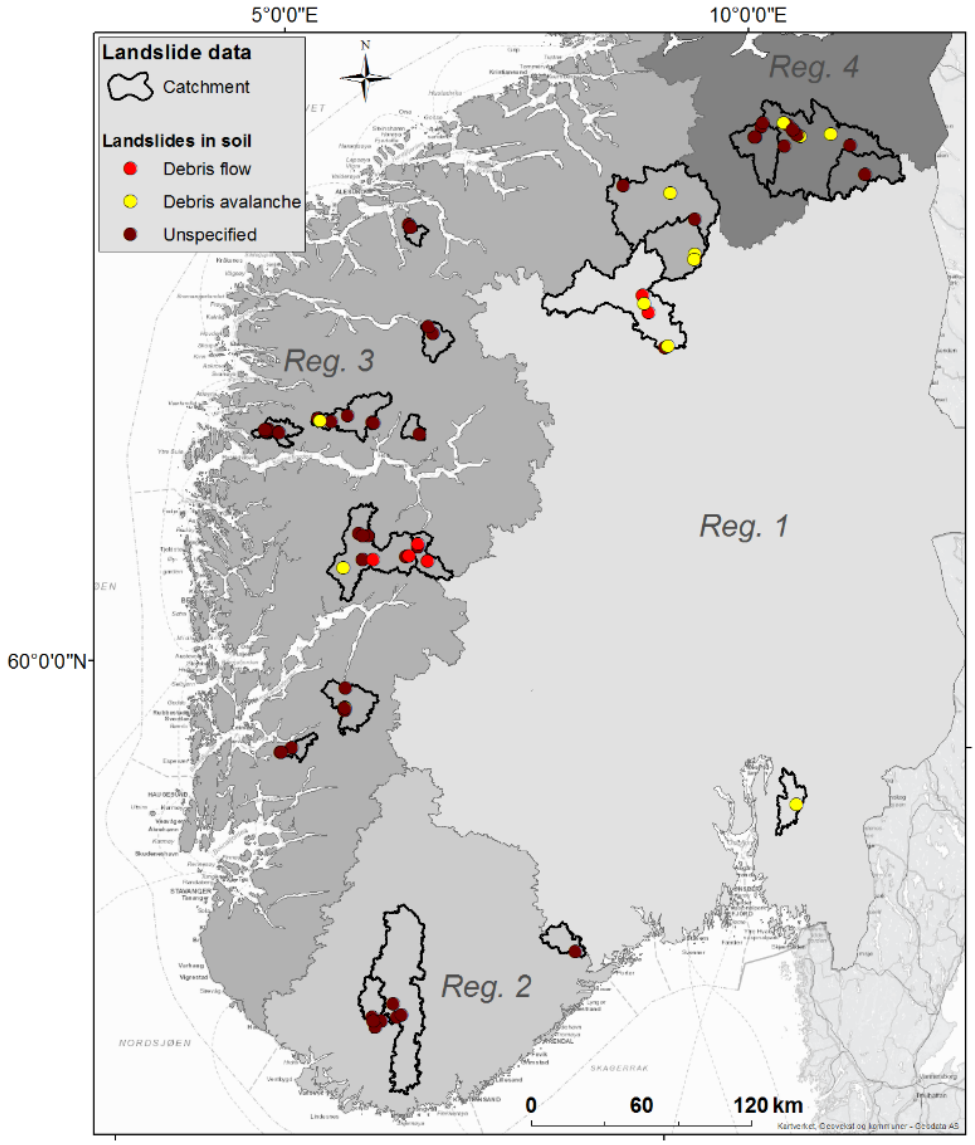

Figure 8) Spatial distribution of landslide events within the selected catchments.

The number of landslide events pr. catchment range from one event (catchments 3.22, 18.10 and 77.3), to ten events (catchment 122.9). The landslides are recorded within the period of 17th of March 1990 and 29th of October 2014. For several days there are more than one landslide event registered within one catchment, and in several catchments. A complete list of all landslide events can be found in Appendix I.

The Norwegian landslide database

The Norwegian landslide database is found online at www.skrednett.no. The database includes all types of mass movements, e.g. rockfalls, debris avalanches, debris flows, slush flows and snow avalanches (NVE, 2012). There are more than 50 000 landslide events registered until present time. The landslide events are represented as points placed where the landslide events hit the road or railway, or where the landslide caused damage or loss of life. The point of initiation is unknown. To some degree, the type of landslide, data, time of day, volume and damages are also registered (NVE, 2012).

The landslide database is a unique national collection, providing a good overview of landslide events (NVE, 2012). The database has, however, its weaknesses and limitations. In general, the process of registration of landslide events is time consuming, always affected by subjectivity and the reliability of the landslide registrations is often difficult to evaluate/determine. The information about the landslide events often lack data (such as date, time of day, volume etc.) making it difficult to relate the landslide events to triggering factors or to analyze the vulnerability. Further, the database is not complete in that not all landslide events occurring in Norway are registered. The landslide events are only registered when infrastructure, such as road or railway, have been hit or when the landslides affected humans. For this reason a control quality is required before any analyses is performed (NVE, 2012).

4.2 Model input data

Daily resolution of precipitation, temperature and discharge are obtained from a meteorological grid of resolution 1 km x 1 km (www.met.no). The data are for the period 01.09.1985 to 31.12.2014. The grid includes areal averages of precipitation and temperature values for ten elevation zones. The daily input data are from 06:00 am to 06:00 am, associated with the date from 00:00 to 06:00 am (Figure 9).

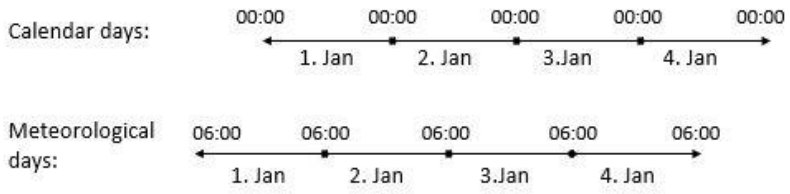

Figure 9) Illustration of calendar days (00:00-00:00) and meteorological data (06:00-06:00)

Model performance relies on optimal input data and a data quality check has been performed. The input data (precipitation, temperature and discharge) was checked for gaps and missing data and if necessary, replaced with data collected from NVEs database Hydra II. In cases where there was only a few consecutive time steps of missing data and no data was available in Hydra II, the missing data was substituted using interpolation of the observed data the day before and the day after. All input data are provided by NVE.

4.3 Groundwater observations

Times series of storage in the study catchments are not available. Measurements from groundwater wells [m below surface] are available, however, only for a few study catchments. Data from three groundwater wells, two in Sogndalsvatn (77.3) and one in Rosten (2.614) were collected from Hydra II. In Sogndalsvatn, well 1 is situated at the bottom of a hillslope, about 50 meters from the river and well 2 in situated at a higher part of the hillslope, about 100 meters from the river. Due to bad measurements, only data from 1.1.2014 to 31.12.2014 will be used. In Rosten, the groundwater well is located about 100 m from the river and at 566 m.a.s.l. The correlation between storage fluctuations simulated by the DDD and observed groundwater level fluctuations has previously been measured. In Grosettjern, Skaugen and Onof (2014) found a correlation of 0.71 (Table 4), while a correlation of 0.62 was found in Sula (Weltzien, 2015). The groundwater observations are provided by NVE.

Table 4) Correlation from two previous studies between fluctuations in storage simulated by the DDD model and observed groundwater levels (Skaugen and Onof, 2014; Weltzien, 2015).

Studies	**Correlation**
Skaugen and Onof (2014)	0.71
Weltzien (2015)	0.62

5 Method

5.1 DDD model

The DDD model (Skaugen and Onof, 2014; Skaugen and Mengistu, 2015) is a parameter-parsimonious rainfall- runoff model that currently runs operationally at daily and three hourly time steps at the flood and landslide forecasting service at NVE together with the HBV model (Bergström, 1995; Sælthun, 1996). At present, the model is only used for flood predictions, not for landslides. The model is written in the programming language R (www.r-project.org). The input is precipitation [mm] and air temperature [ºC], while observed discharge [m3/s] is used as evaluation data. A summarization of the structure of the DDD model is given below. For a full description see Skaugen and Onof (2014) and Skaugen and Mengistu (2015).

Model parameters

Most of the parameters in DDD model are derived using a Geographical Information (GIS) and measurements, thus introducing only 10 calibrated parameters compared to 18 in the HBV model. The parameters derived using GIS include hypsographic curve, catchment area and the distance distributions of soils, bogs, glacier and river. The GIS analyses are carried out using the national 25 m x 25 m resolution digital elevation model (DEM) (www.statkart.no). Recession data, mean annual runoff and spatial variability of precipitation are used to derive parameters including, amongst others, the mean of subsurface water reservoir and shape and scale parameter of gamma distributed recession characteristics (see the following sections). Other parameters have fixed values obtained through experience in calibrating DDD for gauged catchments in Norway. A few parameters are also set a fixed value that are within the recommended range for the HBV model (Sælthun, 1996). The model parameters with comments and methods of estimation are found in Appendix II.

5.1.1 General model structure

The DDD model can be structured in three main subroutines: subsurface module, runoff dynamics, including hillslope routing and river routing, and the snow routine. Catchments are divided into 10 elevation zones with equal area. For each elevation zone, the precipitation and temperature is extracted directly from gridded data sets of resolution 1x1

km. This allows us to obtain reasonable simulated values of discharge without the need for a calibration correction of the lapse rates of precipitation and temperature. Only a general up-down adjustment of precipitation is calibrated. Four types of landscape and vegetation are included in the model; soil, bogs, glacier and river.

Here follows a detailed description of the updated subsurface module (Skaugen and Mengistu, 2015), runoff dynamics, i.e. hillslope- and river routing, and the snow module.

5.1.2 Subsurface module

The subsurface has a 2D representation in that it calculates the saturated and unsaturated soil moisture along a hillslope representing the entire catchment in question. The model estimates the capacity of the subsurface reservoir at different levels of saturation and predicts overland flow. Recently, a new formulation of the subsurface has been presented (Skaugen and Mengistu, 2015), where the parameters are derived solely from observed recession data and the mean annual runoff, thus introducing no additional calibration parameters in the subsurface module. An illustration of the subsurface reservoir is presented in Figure 10.

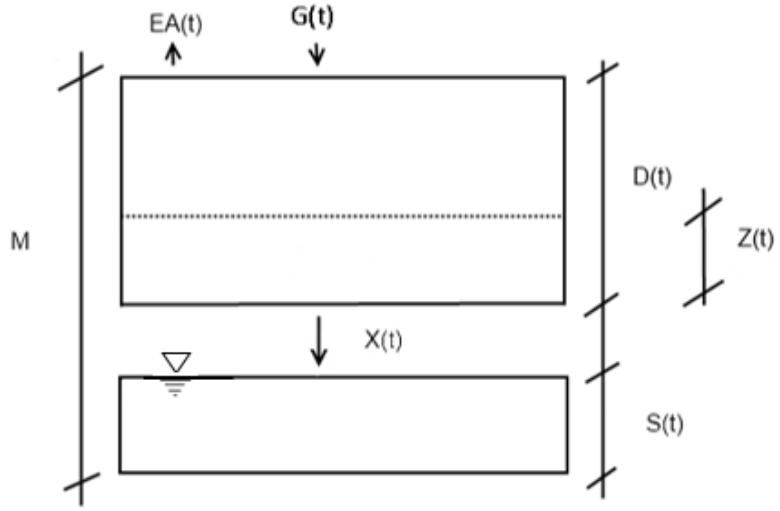

Figure 10) Illustration of the subsurface water reservoir M of the DDD model. G(t) represents the input of rain and snowmelt. The total storage capacity M is divided between a saturated zone S and an unsaturated zone D. The actual soil moisture in D is Z. The ratio (G(t)+Z(t))/D(t) controls the release of excess water to S and hence to runoff. (From Skaugen and Onof, 2014)

The groundwater reservoir is parameterized by its mean catchment scale storage, m_s, which is assumed equal to the water in the soils at steady state. In the subsurface module the total volume capacity of the subsurface storage is specified by the parameter, *M* [mm], which is

shared between a saturated zone, *S* [mm], and an unsaturated zone, *D* [mm]. Note that both *S* and *D* are states and change with time, but the sum is will always be *M*. The input, *G* [mm], which is added to *D*, is a sum of precipitation and snowmelt, *P* [mm] and *sm* [mm], respectively. The actual water content in *D* is called *Z* [mm] and is referred to as the volumetric water content. After time, *t*, the volumetric water content is evaluated and the subsurface are updated depending on whether the volumetric water content exceeds a field capacity threshold, *R*, of 30 % of *D(t)*. If so, the excess water, *X(t)* [mm], is added to the *S(t)*.

Actual evapotranspiration, *Ea(t)*, drawn from *Z*, is a function of potential evapotranspiration, *Ep* [mm day^{-1}], and the level of storage. Potential evapotranspiration is estimated using a degree-day factor, θ_{cea} [mm ^{o}C^{-1} day^{-1}], which for positive temperatures (*T*) is positive and for negative temperatures zero. *Q (t)* is runoff and the equations for the runoff dynamics are given in section 5.1.3. To summarize:

Input: $$G(t) = P(t) + sm(t) \quad (1)$$

Potential evapotranspiration: $$Ep(t) = \theta cea \times T(t) \quad (2)$$

Evapotranspiration: $$Ea(t) = Ep(t) \times \frac{S(t)+Z(t)}{M} \quad (3)$$

Excess water: $$X(t) = Max\left\{\frac{G(t)+Z(t)}{D(t)} - R, 0\right\} D(t). \quad (4)$$

Groundwater: $$\frac{dS}{dt} = X(t) - Q(t). \quad (5)$$

Soil water content: $$\frac{dZ}{dt} = G(t) - X(t) - Ea(t). \quad (6)$$

Soil water zone: $$\frac{dD}{dt} = -\frac{dS}{dt}. \quad (7)$$

The variability of the hydrograph is found to be largely controlled by M, with an increased amplitude of the hydrograph associated with smaller storage capacity and vice versa. In order to solve the non-observability of fluctuations of catchment-scale storage, the catchment-scale storage is assumed to be related to recession and its distribution. The distribution of storage is thus considered a scaled version of that of recession. The subsurface reservoir increases non-linearly according to the shape of the distribution of

recessions. The total storage capacity, *M*, which is derived using observed recession data and the mean annual runoff, is divided into *i* storage levels, all assigned different wave velocities, or celerities [ms^{-1}] (See Skaugen and Onof, 2014).

5.1.3 Runoff dynamics

The runoff dynamics, i.e. hillslope- and river routing, are completely parameterized from observed catchment features derived using GIS and runoff recession. The distance distributions (Figure 11) express the areal fraction of the catchment as a function of distance from the river network. The distance from points in the catchment to the nearest river is found to be exponentially distributed,

$$f(d) = \gamma\, e^{-\gamma\, d}. \qquad (8)$$

The parameter γ equals:

$$\gamma = 1/\bar{d} \qquad (9)$$

where $\bar{d}$ is the mean distance, which differs from catchment to catchment.

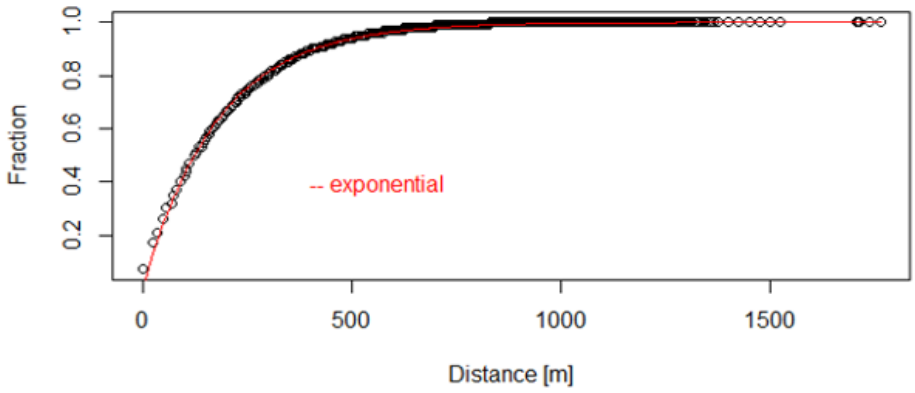

Figure 11) The empirical cumulative distribution function of distances between points in the catchment to the nearest river reach (circles)in catchment 62.5, Bulken. The solid line represents an exponential distribution function fitted to the data. The mean distance is $\bar{d}$=190.2 m and the maximum distance is d_{max} = 1500.0 m

The distance distribution can be visualized in a different way (Figure 12) with the areas for each distance interval, Δ*d*, plotted against the distance to the river network. The ratio between the areas is constant, κ, and can be related to γ as:

$$\gamma = -log(\kappa) \,/\, \Delta d \qquad (10)$$

The water (i.e. rainfall or snowmelt) added to the catchment is transported through the soils to the river network by waves of celerities, *v*, determined by the saturated storage, *S(t)*, in the catchment. The distance travelled by water, Δ*d*, during a suitable time step, Δ*t*, is:

$$\Delta d = v\Delta t \qquad (11)$$

and by rearranging and combining Eq. 9, Eq. 10 and Eq. 11, the celerity can be formulated as:

$$v = \frac{-log(\kappa)\bar{d}}{\Delta t}. \qquad (12)$$

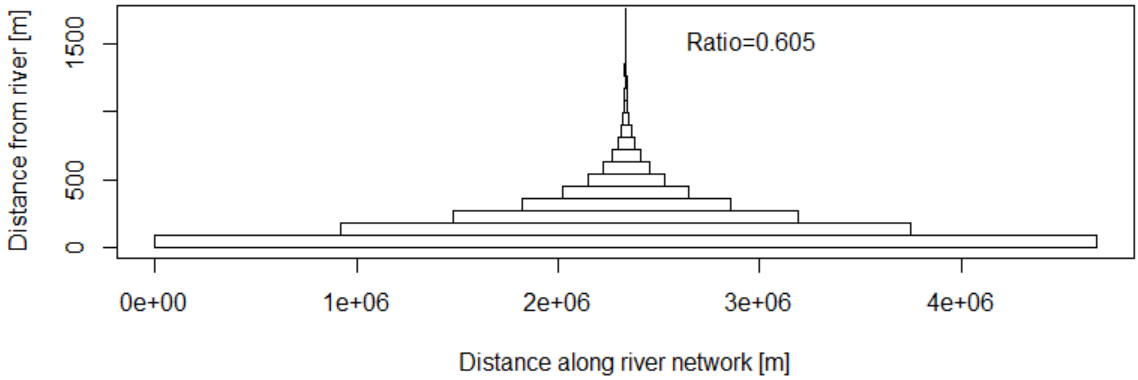

Figure 12) Catchment area as a function of distance from the river network for the same catchment as in Figure 11 (62.5, Bulken). The ratio ,κ, between the consecutive areas is shown as "Ratio".

The celerities, v_i, associated with the different storage levels, *i*, are determined by the actual storage, S(t), and estimated using the exponential recession with parameter Λ, in $Q(t) = Q_0\,\Lambda e^{-\Lambda(t-t_0)}$, where Q_0 is the peak discharge immediately before recession starts. The parameter Λ,

$$\Lambda(t) = log\big(Q(t)\big) - log\big(Q(t+\Delta t)\big), \qquad (13)$$

is the slope per Δt of the recession and is related to the constant κ as:

$$\Lambda = -log(\kappa). \qquad (14)$$

From Eq. 12 and Eq. 14 the celerity, *v*, can also be written as a function of Λ as:

$$v = \frac{\Lambda\,\bar{d}}{\Delta t}. \qquad (15)$$

The storage levels, *i*, of M are divided corresponding to the quantiles of the distribution of Λ under the assumption that higher storage is related to higher values of Λ. Each individual storage level *i* has a unit hydrograph (UH) with the parameter λ_i, estimated such that the

runoff from several storage levels will give a UH equal to the exponential UH with parameter Λ_i, i.e.

$$\Lambda_i e^{-\Lambda_i(t-t_0)} = \omega_1\lambda_1 e^{-\lambda_1(t-t_0)} + \omega_2\lambda_2 e^{-\lambda_2(t-t_0)} + \cdots + \omega_i\lambda_i e^{-\lambda_i(t-t_0)} \quad (16)$$

where Λ_i is the recession characteristic for the sum of storage levels up to *i*, i.e. $\Lambda_1 = f(\lambda_1)$, $\Lambda_2 = f(\lambda_1, \lambda_2)$ etc., and ω_i are the weights associated with the discharge from each level estimated by

$$\omega_i = \frac{\Lambda_i}{\sum_{k=1}^{i}\Lambda_k}. \quad (17)$$

The celerity for each storage level is

$$v_i = \frac{\lambda_i \bar{d}}{\Delta t} \quad (18)$$

As mentioned in section 5.1.2 ,the shape of the distribution of *S* is assumed to be equal to that of recession, *Λ*. The distributions of *Λ*, and thus *S*, are modelled as a two-parameter gamma distribution:

$$f(\Lambda) = \frac{1}{\beta^{\delta}\Gamma(\delta)}\Lambda^{\delta-1}\exp\left(-\left(\frac{\Lambda}{\beta}\right), \ \delta > 0, \beta > 0, \right. \quad (19)$$

where δ and β are shape and scale parameters respectively and estimated from observed Λs (Eq. 13) and

$$f(S) = \frac{1}{\eta^{\delta}\Gamma(\delta)}S^{\delta-1}\exp\left(-\left(\frac{S}{\eta}\right)\right) \quad (20)$$

Where η is the scale parameter:

$$\eta = \beta/c \quad (21)$$

and c is a constant and equal to

$$c = \bar{\Lambda}/m_s \quad (22)$$

$\bar{\Lambda}$ is the mean value of Λ and estimated from the parameters of the fitted gamma distribution and representing the mean recession characteristic. The parameter δ is the same for the two distributions since the distribution of *S* is a scaled version of *Λ*.

In the DDD model, overland flow occurs when *S* = *M*, i.e. when the subsurface is completely saturated. Overland flow is then the excess water *X*(*Δt*) which is assigned to a saturation

level not included in *M*. The celerity for this level of saturation is derived from the 99 % quantile of the exponential distribution fitted to λ.

5.1.4 Snow routine

In the snow routine, snowmelt is calculated using a degree-day model. The amount of snowmelt is a linear function of the difference between the calibrated threshold temperature for melting and actual air temperature, *Ta*.

$$sm = CX \times (Ta - TS)\ [mm] \qquad (23)$$

where *CX* is the degree-day factor and *TS* is the threshold temperature when snowmelt starts. A two-parameter gamma distribution is used to model both the spatial distribution of accumulated snow water equivalent (SWE) and the melting:

$$f_{\nu_o \alpha_o}(y) = \frac{1}{\Gamma(\nu_o)} {\alpha_o}^{\nu_o} y^{\nu_o - 1} e^{-\alpha_o y} \qquad (24)$$

where Γ is the gamma function, shape, ν_o, and scale, α_o, are parameters and *y* is a random variable.

The shape, ν_o and scale, α_o, parameters are estimated from observed spatial variability of precipitation. The spatial probability density functions (PDF) of accumulation or melt events differ in shape according to intensity. For a detailed description of the snow routine in DDD see Skaugen and Randen (2013) and Skaugen and Weltzien (2015).

5.2 Distribution of storage along the hillslope

In the DDD model, the 2-D state of the subsurface can be assessed at any point in the simulated time series by simple statements in the model code. One can also assess the 2-D states at any point of the hillslope by creating additional code to be included in the model code. In this thesis, additional R-code assessing the hillslope at each 100 m interval, i.e. Δd = 100m, from the river to the top of the hillslope was created. The purpose of this section is to explain how the temporal and spatial distribution of the subsurface in the DDD model allows the subsurface state to be assessed at any points along the hillslope. First, a brief summary of the subsurface and the runoff dynamics in the DDD model is given.

The DDD model determines the distribution of distances from a point in the catchment to its nearest river reach by creating equidistant buffers around the river network (Figure 13). The areas of the equidistant buffers decrease with increasing distant from the river reach

(white to black color) and thus, the equidistant buffer adjacent to the river reach represents the largest area. This is equivalent to the catchment areas representing the distance distribution in Figure 12. For a given distance interval, here Δd = 100, the equidistant buffer adjacent to the river reach represents the same catchment area as the catchment area at the bottom, i.e. the largest box, in Figure 12. The area of the equidistant buffer furthest away from the river reach is the same as the catchment area at the top, i.e. the smallest box, in Figure 12.

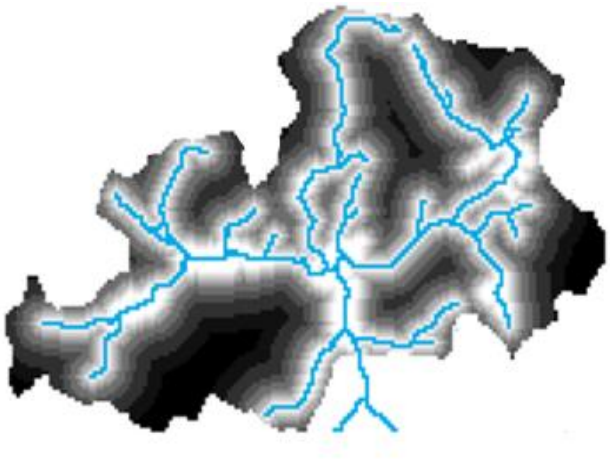

Figure 13) Equidistant buffers created around the river network to determine the distance distribution in the DDD model, i.e. the distance from points in the catchment to the nearest river reach (Ivar Peereboom, NVE).

Figure 14a shows a snapshot of how the storage is modelled by the DDD. The catchment is represented as one hillslope where the x-axis shows the distance from the river to the top of the hillslope. The y-axis shows the different storage levels, i, where level i=1-4 represents the total volume capacity, M, and level i=5 represents overland flow. The wetting up of a catchment occurs from the riparian zone outwards and up the hillslope. In Figure 14b, the same figure is illustrated in 3-D with the distance along the river reach added as a third axis. The red, solid lines represent Δd where three intervals of the hillslope, used in this analysis, are noted. The intervals are referred to as the lower-, middle- and upper hillslope, or points of the hillslope.

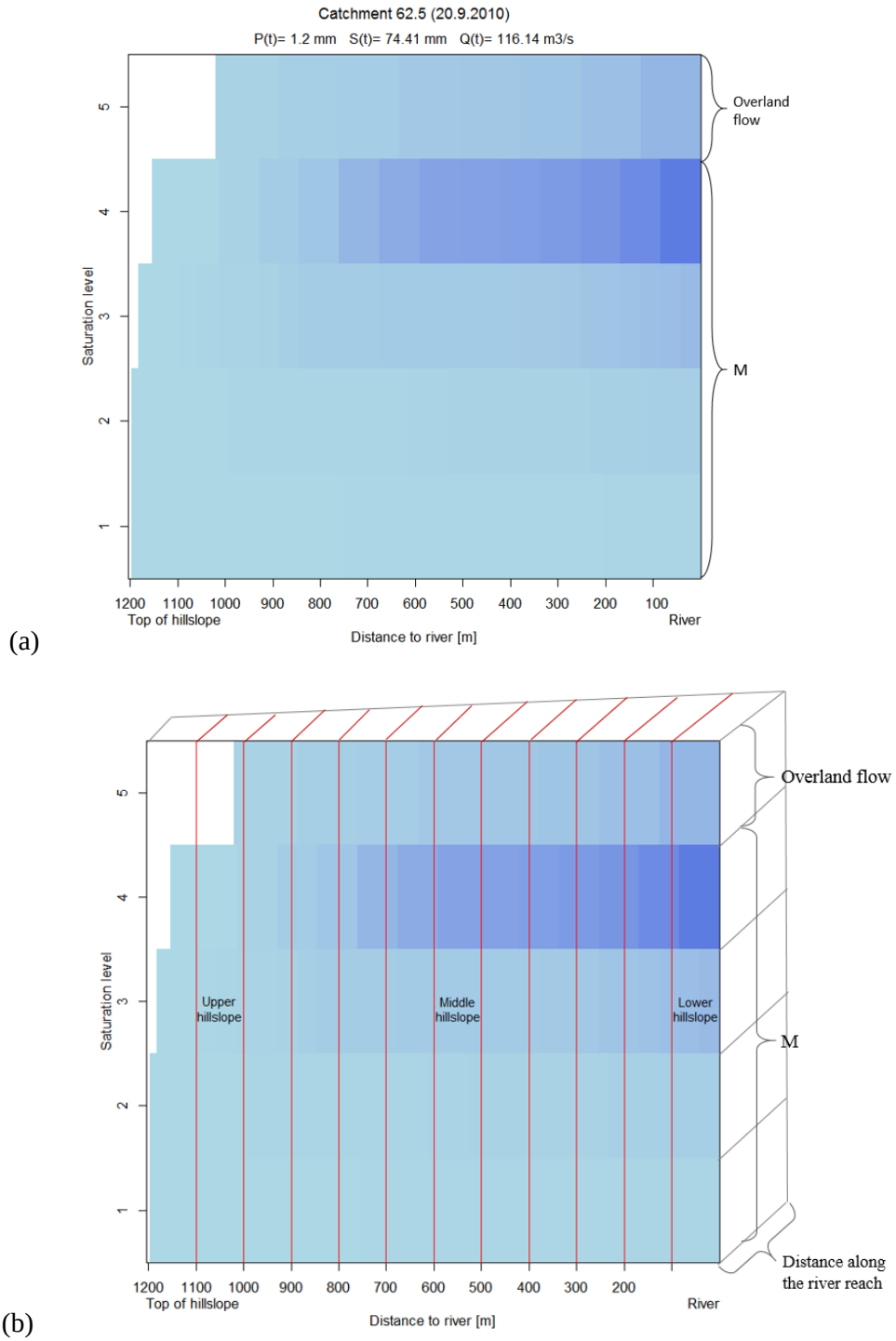

Figure 14) Snapshot of the storage of the DDD where the catchment is represented as one hillslope. a) The x-axis shows the distance from the river to the top of the hillslope. The y-axis shows the storage levels where 1-4 represents the total storage capacity and level 5 represents overland flow. The outline of boxes (especially seen in the higher storage levels) represents an area according to the distance distribution and the associated celerity that will drain pr. time interval. The darker the blue color, the more water is present in the box. In b) the same as in a) is illustrated in 3-D with the distance along the river reach added as a third axis. The solid, red lines represents the distance interval, Δd = 100m. The three points of the hillslope (lower-, middle-, and upper hillslope) used in the landslide analysis are marked.

As described in section 5.2.1, each storage level has a UH and is associated with a celerity, v_i. Thus, each storage level is associated with a unique representation of the catchment areas as a function of distance from the river (Figure 15). In Figure 14, this is represented by the outline of boxes, especially seen in the higher storage levels. Each box represents an area according to the distance distribution and the associated celerity that will drain pr. time interval. The higher the celerities, the more of the catchment area is drained pr. time unit, represented by the widths of the boxes. Because the water flows faster on the surface than in the subsurface, the largest boxes are found in storage level 5 (overland flow). In *M*, the width of the boxes decreases downward due to decreasing celerity, i.e. less water drained pr. time interval. The darker the blue color, the more water is present in the box.

The number of intervals, *j*, from the river reach to the top of the hillslope is equal to $d_{max}/\Delta d$. Figure 14a and b can be seen together with the equidistant buffers (Figure 13) and with the catchment area as a function of distance from river reach (Figure 12). For a given interval length, the interval adjacent to the river (marked "lower hillslope") in Figure 14b represents the same area as the equidistant buffer area adjacent to the river in Figure 13 and the area represented by the box at the bottom in Figure 12.

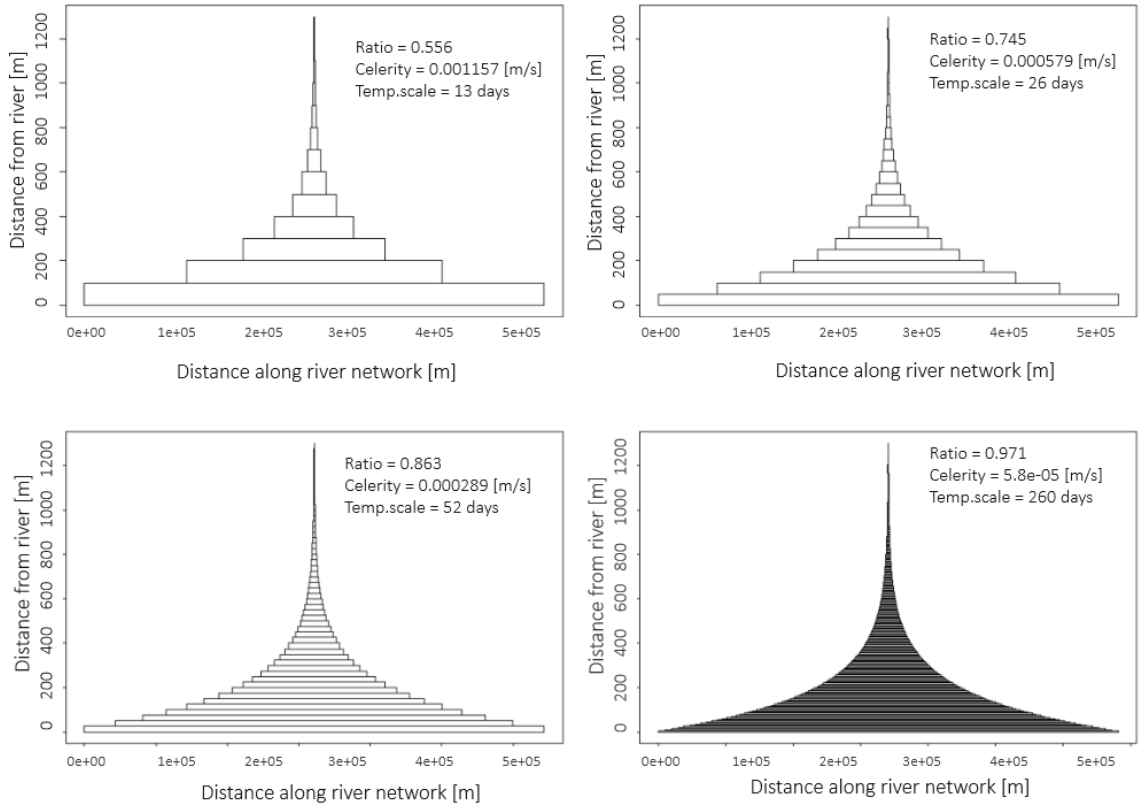

Figure 15) Catchment area as a function of distance from the river network representing the four storage levels in M: level 4 (top left), level 3 (top right), level 2(bottom left), and level 1 (bottom right).

The fact that the width of the boxes increase with increasing storage level means that within a Δd, the number of boxes included from each storage level varies, with the highest number of boxes included from storage level 1. For example, let us say that one box in storage level 4 represents 100 m. Then, within the 100 m, storage level 3, 2 and 1 might for example be represented by 1.5 boxes, 4 boxes and 10 boxes, respectively. In other words, for Δd = 100m, the water present in storage level 4 is drained after one time step, while the water present in storage level 1 is drained after 10 time steps. Thus, the storage within each Δd is found by integrating across the vertical layers in *M*. Integration across storage level 1-5 gives the total amount of water present within each Δd.

The sum of all storage values at each interval is equal to the total storage in the catchment:

$$S(t) = \sum_1^j S_j\,(t) \qquad (25)$$

where S_j is the storage at each interval and j=$d_{max}/\Delta d$ is the total number of intervals.

Any input, *U*, is distributed in time along the hillslope by a UH. For a UH with ratio of e.g. 0.75, the immediate area upstream is only 0.75 the size of the adjacent area downstream and thus receive 0.75 the amount of rainfall. For a hillslope divided into *j* intervals the storage due to *U* at each interval will be

$$S_j = U * \frac{a_j}{A} \qquad (26)$$

where a_j is the area associated with each interval and *A* is the total catchment area.

Note that S_j does not express the local depth of water, but rather a scaled value. The depth of water [mm] at each area interval can be calculated by

$$U = S_j * \frac{A}{a_j} \qquad (27)$$

where *U* not only refers to the input at present time but also depends on the input from all previous time steps upslope.

The storage values at the lower, middle and upper hillslope (S_{lower}, S_{middle} *and* S_{upper}, respectively) are not recalculated by Eq. 29 and thus expressed as scaled values throughout this thesis. The scaled storage values are thus combinations of the scaled input at the present time and the scaled water redistributed from upslope (from all previous time steps). The lower hillslope always represents the first 100 m from the river network, i.e. 0-100 m from the river. The distance from the river to the middle hillslope and to the top hillslope vary with catchment, as the maximum distance, d_{max}, vary. The upper hillslope is chosen to

represent the distance interval second furthest away from the river. This is because the distance interval furthest away from the river represents a very small area. There is no maximum storage capacity defined for each Δd. Therefore, the maximum storage capacity at each point of the hillslope in each catchment is considered to be the highest simulated value, $S_{j\_max,}$ at each point of the hillslope in each catchment. The S_{j_max} only occur once during the entire calibration and validation period.

5.3 Model calibration and validation

The model input data is divided about half into a calibration- and a validation period. For all catchments, except 122.9 (Gaulfoss) and 122.17 (Eggafoss), the validation period is from 1st of September 1985 to 31st of August 2000, and the calibration period from 1st of September 2000 to 31st of December 2014 (Table 5).

The model runs automatically with the calibration program MCMC (Markov chain Monte Carlo) (Soetart and Petzholdt, 2010). The MCMC seeks to minimize the differences between the modeled and observed runoff values. The Nash-Sutcliffe model efficiency coefficients (NS) (Nash and Sutcliffe, 1970) is used as the goodness-of-fit measure. The NS range between -∞ and 1, with zero indicating equal skill to that of the mean annual discharge (MAD) and one means a perfect simulation, i.e. equal values.

The NS equation is as follows:

$$NS = 1 - \frac{\sum_{t=1}^{n}(Q_t^{obs} - Q_t^{sim})^2}{\sum_{t=1}^{n}(Q_t^{obs} - Q_{mean}^{obs})^2} \qquad (28)$$

where n is the number of time steps, Q_t^{obs} and Q_t^{sim} are the observed- and simulated discharge at time t, respectively, and Q_{mean}^{obs} is the mean observed discharge.

The mean and standard deviation of NS using ten different parameter sets is used to evaluate the model. In order to take into account the equifinality associated with the nature of the model the parameter sets are associated with the quantiles (100, 97, 95, 92, 90, 87, 85, 82, 80 and 78 %) of distribution of NS from the MCMC calibration are used to evaluate the model. This will also prevent an optimum, which might be optimal for the wrong reasons.

Table 5) Calibration and validation period for the 19 catchments.

Catchment	Calibration period	Validation period
2.614, 3.22, 18.10, 22.4, 24.9, 41.1, 48.1, 62.5, 72.5, 77.3, 82.4, 83.2, 88.4, 97.1, 109.9, 109.42, 122.11	01.09.2000 -31.12.2014	01.09.1985 - 31.08.2000
122.9	01.09.2002 - 31.12.2014	31.09.1988 -31.08.2002
122.17	01.09.2007 - 19.09.2014	01.09.1985 - 31.12.2000

5.4 Selection of landslide data

A total of 76 landslide events have been used in this study(Figure 8), selected using ArcMap. When selecting the landslides the following restrictions were made; 1) all debris avalanches, debris flows and unspecified landslides in soil, 2) landslides situated within a DDD (HBV) catchment and 3) landslides occurring within the period 1st of September 1985 to 31st of December 2014. Only landslides with known time of occurrence were selected. In particular those registered as "exact time", "within a few hours", "within a day" in the "column of uncertainty". When more than one landslide occurred in the same catchment at the same day but at different locations, the landslide events were grouped to one event as they are associated with the same hydro-meteorological event. The precipitation and temperature a few days prior to the landslide events were studied and the landslides occurring when there was little or no precipitation were removed. These registrations are most likely rockfalls, i.e. incorrect registrations, or landslides occurring as a result of snowmelt (not the focus in this study).

When looking at the model input data (precipitation and temperature) associated with the chosen landslide events, the DDD model was found to experience some problems modelling the precipitation input at temperatures around 0-1° C. As described in section 5.1, the precipitation is simulated as either rain or snow based on a threshold temperature. In reality, precipitation commonly falls as snow in the higher, colder parts of the catchment and rain in the lower parts (Engen-Skaugen et al., 2007). This have resulted in some errors in the simulated values of snow reservoir- and storage, which can be seen as an increase in the snow reservoir instead of an increase in storage. During winter and colder periods, this is, obviously, a common scenario. However, when a landslide is recorded under such circumstances, either the simulation is correct and the landslide is a misregistration (most

likely a rockfall), or there is an error in the simulation. In the latter case, some or all of the precipitation should be modelled as rainfall, thus increasing the level of storage. The landslide events recorded under such circumstances were removed.

In order to get the best possible dataset of landslide events for the analysis, the final list of the selected landslide events was controlled by looking at aerial photos, maps of topography and when available, orthophotos taken before and after the landslide events was studied to identify landslide features The landslide events believed to be misregistrations were therefore removed.

5.5 Qualitative landslide investigation

The main objectives of this study are achieved through the sub-objectives listed at the end of chapter 1, which involves exploring the simulated results of the DDD model in various ways at a window of time surrounding the landslide events. As a reminder, the main objectives are to 1) determine if the DDD model has any capacity to predict the hydrological conditions triggering landslides and 2) investigate how hysteresis is represented in the model and how it relates to landslide occurrences. The procedures associated with the sub-objectives are described in the following sections.

5.5.1 Storage as an indicator for landslide occurrence.

Water in soil is considered the main factor for triggering landslides (described in section 2.2.3) and thus the motivation for looking at the saturated storage values, *S(t)* simulated by the DDD model as an indicator for landslide occurrences. The storage values were evaluated in terms of saturation (% of maximum storage capacity, *M*). Due to the shift in meteorological days and landslide days, i.e. calendar days, the storage values were investigated the day of the landslide events (*D_Landslide*), as well as the day prior to the landslide events (*D-1_Landslide*). The distribution of the saturations found for the 76 landslide events were calculated, including the maximum and minimum saturation, median and mean, and 1st and 3rd quantile. The 1st and 3rd quantile gives the saturation level of which ¾ and ¼ of the landslide events are above, respectively.

5.5.2 Temporal dynamics of saturation for landslide events

Landslides often occur during heavy rainfall, caused by a rapid rise in groundwater level, or when the soil experiences prolonged high saturation due to the succession of medium rainstorms (see section 2.2). Based on this, the temporal dynamics of saturation at the time surrounding the landslide events were investigated. The landslides were evaluated in terms of the behavior of saturation up to the events; a sharp gradient in saturation, a prolonged high saturation or both. The landslide with no such dynamical indicators are said to have "no indications for landslide occurrence". A prolonged high saturation was initially determined to be three or more consecutive days of completely saturated conditions (S=M). However, the soil was also said to experience prolonged high saturated if there were some days with almost completely saturated conditions during a longer period of completely saturated conditions. The investigation of the temporal dynamics of saturation was performed by visual inspection of bar plots of saturation 20 days prior to the landslide events (and 10 days following).

Finally, for the landslide events found with no indications for landslide occurrence the simulated discharge (Q_{sim}) were checked against observed discharge (Q_{obs}) to see if there were large deviation possibly indicating errors in the simulated storage.

5.5.3 Landslide occurrences and overland flow

Overland flow is simulated when the subsurface is completely saturated. Based on the knowledge that landslides typically occur under completely saturated conditions, the simulation of overland flow [mm] by the DDD was investigated for the *D_Landslide* and *D-1_Landslide*. Note that overland flow is the water found in storage level 5 in Figure 14. The "total water" [mm] or "storage/saturation including overland flow" is the water in storage level 1-5. The temporal dynamics of saturation including overland flow (in % of *M)* was investigated to see it the landslides were characterized by a peak in the values of overland flow. Since the values are given in percent of maximum storage capacity, *M*, the values above 100 % indicate the presence of overland flow.

5.5.4 Indications for landslides in the characteristics of the subsurface along the hillslope

The three points of the hillslope (lower, middle and upper) were investigated in similarity to the entire catchment, described in the sections above. However, as described in section 5.2, the storages at the three points of the hillslope are scaled values and there is no defined maximum storage capacity for each point. Thus, for each catchment, the level of saturations at each point were determined based on the maximum simulated value associated with each point in each catchment (S_{lower_max}, S_{middle_max} and S_{upper_max}).

5.5.5 Hysteresis and landslide occurrences

Based on the knowledge that landslides are closely related to hydrological responses, the simulated storage-discharge hysteresis represented by the DDD model at the time surrounding the landslide events were investigated. The storage [mm] and the discharge [mm/day] were plotted in a suitable window of time surrounding the landslide events. The hysteresis were evaluated in terms of the direction of the loops (Figure 1). The hysteresis were investigated at both catchment scale (S-Q), as well as at the three points of the hillslope (S_{lower}-Q, S_{middle}-Q and S_{upper}-Q). Finally, the landslides were evaluated in terms of where they occurred on the hysteretic loop; during the recharge (rising limb), on the top or during the recession (falling limb).

6 Results

In the following, the model performance and model validation by groundwater measurements are presented. The successive sections present the simulation results, i.e. the results of the qualitative landslide investigation (section 5.5). First, the results of the characteristics of the subsurface (sections 5.5.1-5.5.3) are presented for the entire catchment. A separate section with the results for the hillslope follows. In the last part of this chapter, the results of the storage-discharge hysteresis is presented, including how hysteresis is represented in the DDD model, at catchment scale as well as at hillslope scale, and finally how the landslide occurrences are related to hysteresis.

6.1 Model calibration and validation results

The Nash-Sutcliffe model efficiency coefficients for the calibration period (*NS Cal.*) and for the validation period (*NS Val.*) are seen in Table 6. The standard deviations (brackets), indicate the spread of the *NS* from ten runs and thus the uncertainty of the model.

Table 6) Performance of the Distance Distribution Dynamics measured by the Nash-Sutcliffe criterion for the 19 catchment. The bracketed numbers indicate standard deviation of NS from ten runs.

Catchment		*NS Cal.*	*NS Val.*
2.614	*Rosten*	0.85 (0.005)	0.85 (0.015)
3.22	*Høgfoss*	0.71 (0.001)	0.62 (0.014)
18.10	*Gjerstad*	0.82 (0.006)	0.76 (0.010)
22.4	*Kjølemo*	0.74 (0.003)	0.71 (0.003)
24.9	*Tingvatn*	0.88 (0.005)	0.79 (0.006)
41.1	*Stordalsvatn*	0.79 (0.006)	0.78 (0.028)
48.1	*Sandvenvatn*	0.84 (0.006)	0.80 (0.012)
62.5	*Bulken*	0.86 (0.005)	0.86 (0.017)
72.5	*Brekke*	0.81 (0.003)	0.73 (0.008)
77.3	*Sogndalsvatn*	0.82 (0.004)	0.78 (0.004)
82.4	*Nautsundvatn*	0.86 (0.005)	0.85 (0.011)
83.2	*Viksvatn*	0.81 (0.008)	0.80 (0.009)
88.4	*Lovatn*	0.90 (0.003)	0.89 (0.004)
97.1	*Fetvatn*	0.65 (0.003)	0.63 (0.007)
109.42	*Elverhøy*	0.71 (0.004)	0.74 (0.006)
109.9	*Risefoss*	0.78 (0.005)	0.78 (0.008)
122.11	*Eggafoss*	0.78 (0.005)	0.80 (0.009)
122.17	*Hugdal Bru*	0.70 (0.012)	0.78 (0.022)
122.9	*Gaulfoss*	0.82 (0.005)	0.83 (0.006)
	MEAN	**0.80 (0.005)**	**0.78 (0.010)**

The overall calibration results range from 0.65 to 0.90, with a mean of 0.80. More than half of the catchments have *NS Cal*. equal to or above 0.80. The validation results gave, for many catchments, relatively similar values as the calibration results with a mean *NS* of 0.78. Eight catchments have *NS. Val* equal to or above 0.80. The standard deviations are lower for the calibration period than the validation period.

6.2 Validation of DDD model by comparing fluctuations of the simulated storage and groundwater observations

The DDD model is validated by comparing the simulated storage [mm] (catchment value) to observed groundwater levels [m below ground]. Since the measuring units are different, the values cannot be compared directly and therefore, the fluctuations of the simulated storage is compared with the fluctuations of the observed groundwater levels. The results of the correlation is presented in Table 7. Even though the groundwater levels not necessarily represents the fluctuation of the entire catchments, the results from catchment 2.614 in Table 7 suggest that the simulated storage and groundwater level coincide. In catchment 77.3, the correlation is zero. However, the correlation is found to be not significant with a p-value above 0.3. A correlation is said to be significant if the p-value is below 0.05.

Table 7) Correlation between fluctuations of simulated storage and observed groundwater level

	Correlation
Catchment 2.614	0.79
Catchment 77.3	0.05

In Figure 16a, simulated storage fluctuations at the lower, middle and upper hillslope is presented. In Figure 16b, groundwater fluctuations at the two wells situated at two points of a hillslope (referred to as lower and upper well) in catchment 77.3 is presented. Note that the lower and upper well are located closer to each other (about 50), than the distance between the lower, middle and upper hillslope in DDD model. By visual inspection, it is clear that the fluctuations vary along the hillslope, especially seen in Figure 16a between the lower hillslope and the two other points of the hillslope. The coefficient of variation (*cv*), i.e. the dispersion of the data around the mean, for the observed groundwater levels is

found to be 0.188 and 0.438 for the lower and upper well, respectively. For the simulated storage values along the hillslope in DDD model, the *cv* shows the same pattern of increasing *cv* upslope with 0.512, 0.459 and 0.785 for the lower, middle and upper hillslope, respectively. An increasing *cv* upslope is found for all 19 catchments included in this analysis.

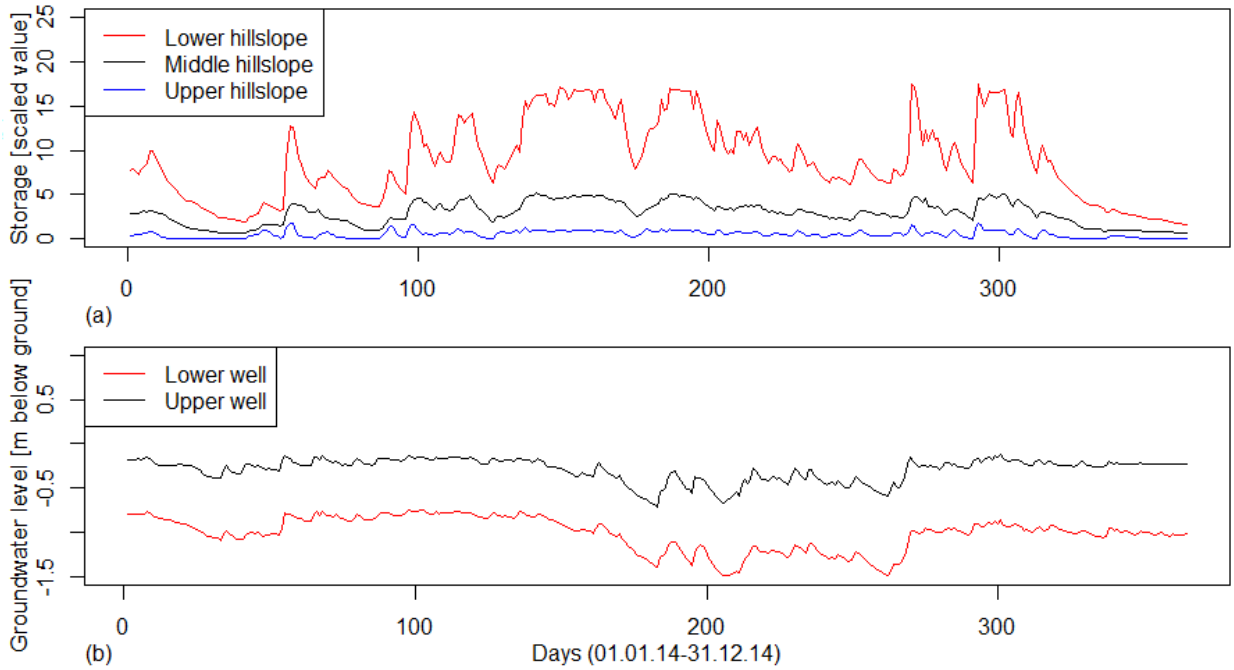

Figure 16) Fluctuations in catchment 77.3 for a) simulated storage for the lower, middle and upper hillslope, and b) observed groundwater level at two wells located in a slope (lower and upper).

6.3 Storage as an indicator of landslide occurrence

This section presents the results of the simulated, storage values (catchment values) found with the 76 landslide events. The storage was investigated the day of the landslide events (*D_Landslide*) and the day prior to the landslide event (*D-1_Landslide*).

In Table 8, the number of landslide events associated with completely saturated conditions are given. As many as 53 landslide events (70 %) occur during completely saturated conditions ($S_{D\_Landslide} = M$). Of these, the soil reach completely saturated conditions the same day as the landslide event for eight events (i.e., $S_{D\text{-}1\_Landslide} < M$ *and* $S_{D\_Landslide} = M$). Thus, 45 events occur at least one day after the soil reach complete saturation ($S_{D\text{-}1\_Landslide}$

$=M$ *and* $S_{D\_Landslide} = M$). 70 % of the landslide events are also associated with completely saturated conditions the day prior to the events ($S_{D\text{-}1\_Landslide} = M$), meaning that eight landslide events that occur under partially saturated conditions are associated with completely saturated conditions the day prior to the landslide (i.e., $S_{D\text{-}1\_Landslide} = M$ *and* $S_{D\_Landslide} < M$).

Table 8) The number of landslide events associated with completely saturated conditions (S=M) and partially saturated conditions (S<M).

	Number of landslide events	
	Saturated conditions	**Partially saturated conditions**
D-1_Landslide	53 events (70 %)	23 events (30 %)
D_Landslide	53 events (70 %)	23 events (30 %)

In Table 9, a summary of the distribution of saturation (given in percent of maximum storage capacity, *M*) is presented. The summary shows that the majority of the landslide events occur for very high storage values. Only a few landslide events occur for relatively low storage values, with the minimum saturation found at 69 %. The 1st quantile tells us that 75 % of the landslide events are associated with storage values higher than 94.5 % of *M*.

Of the 23 landslide events occurring under partially saturated conditions, 12 events occur for saturations above 90 %, in which four events occur for saturations above 95 %. The landslide events are also associated with high storage values the day prior to the landslide, only slightly lower than for *D_Landslide*.

Table 9) A summary of the distribution of storage in percent of maximum storage capacity, M.

	Distribution of storage [% of *M*]					
	Min.	**1st Quant.**	**Median**	**Mean**	**3rd Quant.**	**Max.**
D-1_Landslide	47.5	93.0	100.0	94.5	100.0	100.0
D_Landslide	69.0	94.5	100.0	97.0	100.0	100.0

6.4 Temporal dynamics of saturation for landslide events

This section presents the results of the temporal dynamics of saturation (catchment values) at the time surrounding the landslide events.

The majority of the landslide events are characterized by either a sharp gradient in saturation (37 events), a prolonged high saturation (16 events) or both (17 events) (Table 10). This means that more than 90 % of the landslide events have indications for landslide occurrence in the temporal dynamics of saturation. Only eight landslides are found with no dynamical indications, in which three events occur during completely saturated conditions. Keep in mind that a prolonged high saturation refers to three or more consecutive days of completely saturated conditions. An event can therefore occur during completely saturated conditions without being associated with a prolonged high saturation.

Table 10) The temporal dynamics of saturation associated with the 76 landslide events.

	Number of landslide events
Sharp gradient	37 events
Prolonged high saturation	16 events
Both the above	17 events
Neither the above	6 events

Examples of the temporal dynamics of saturation for four landslides occurring during completely saturated conditions is presented in Figure 17. The events are characterized by a sharp gradient in saturation (a), a prolonged high saturation (b), both (c) and no indication (d). The landslide found with no indications occur after a gradually increase in storage one day after completely saturated conditions are reached. In Appendix III, the temporal dynamics of saturation for all landslide events are presented.

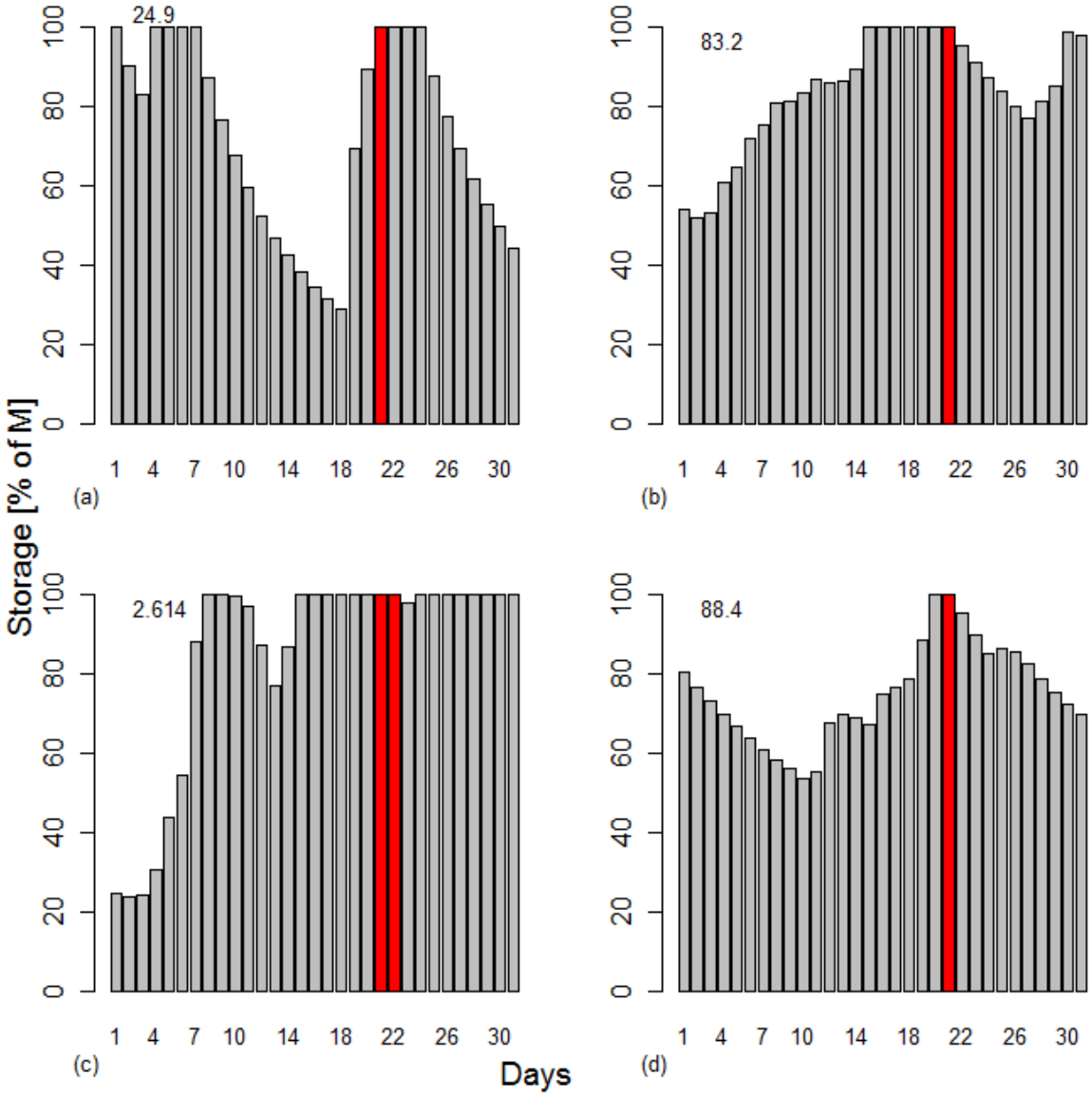

Figure 17) Bar plots of the temporal distribution of for four landslide events occurring during completely saturated conditions. a) a sharp gradient (04.10.04), b)prolonged high saturation(14.11.05), c) both a sharp gradient and a prolonged high saturation(22-23.05.13) and d) no indicators (only found with completely saturated conditions)(28.10.14). The red bars represent the day(s) of the landslide event(s).

In Table 11, the results of the temporal dynamics of saturation for the 23 landslides occurring under partially saturated conditions are given (presented in Table 8). These events are especially interesting since they are not indicated by the storage values, i.e. do not occur during completely saturated conditions. Note that landslides occurring under partially saturated conditions can be associated with a prolonged high saturation if they occur shortly after a period of consecutive days of completely saturated conditions. Table 11 shows that 15 events are found with a sharp gradient in saturation, while three events occur shortly after a period of prolonged high saturation. Finally, four events have no such characteristics.

Table 11) The temporal dynamics of saturation found for the 23 landslide events occurring under partially saturated conditions.

	Number of landslide events
Sharp gradient	15 events
Prolonged high saturation	3 events
Both the above	1 event
Neither the above	4 events

In Figure 18, the temporal dynamics of saturation for four landslide events occurring under partially saturated conditions are presented. The events are found with a sharp gradient (a), a prolonged high saturation (b), both (c) and no indications (d). The events in Figure 18a and c occur for relatively very high storage values (about 90 % of *M*). In Figure 18b, the event also occurs one day after the soil was completely saturated. The event found without any indication for landslide occurrence (Figure 18d) occurs during a gradually increasing storage at a saturation level of about 80 %.

When it comes to the four landslide events found without any dynamical indicators, one occurs during saturation of 98.5 % of *M* and are therefore considered indicated by the storage value. For the remaining three events, the simulated and observed discharge (Q_{sim} and Q_{obs}) at the time surrounding the landslide events were compared to see if there were any large deviations indicating possible simulation errors. All three landslide events occur for relatively low discharge values compared to the discharge values before and/or after the event (Figure 19). Two of the landslide events occurred in April (a and c) and one occurred in September (b). The largest deviation seems to be in Figure 19a with the largest deviation in the days prior to the landslide event. For the two landslide events in Figure 19b and Figure 19c, the simulated and observed discharges appears to be roughly the same.

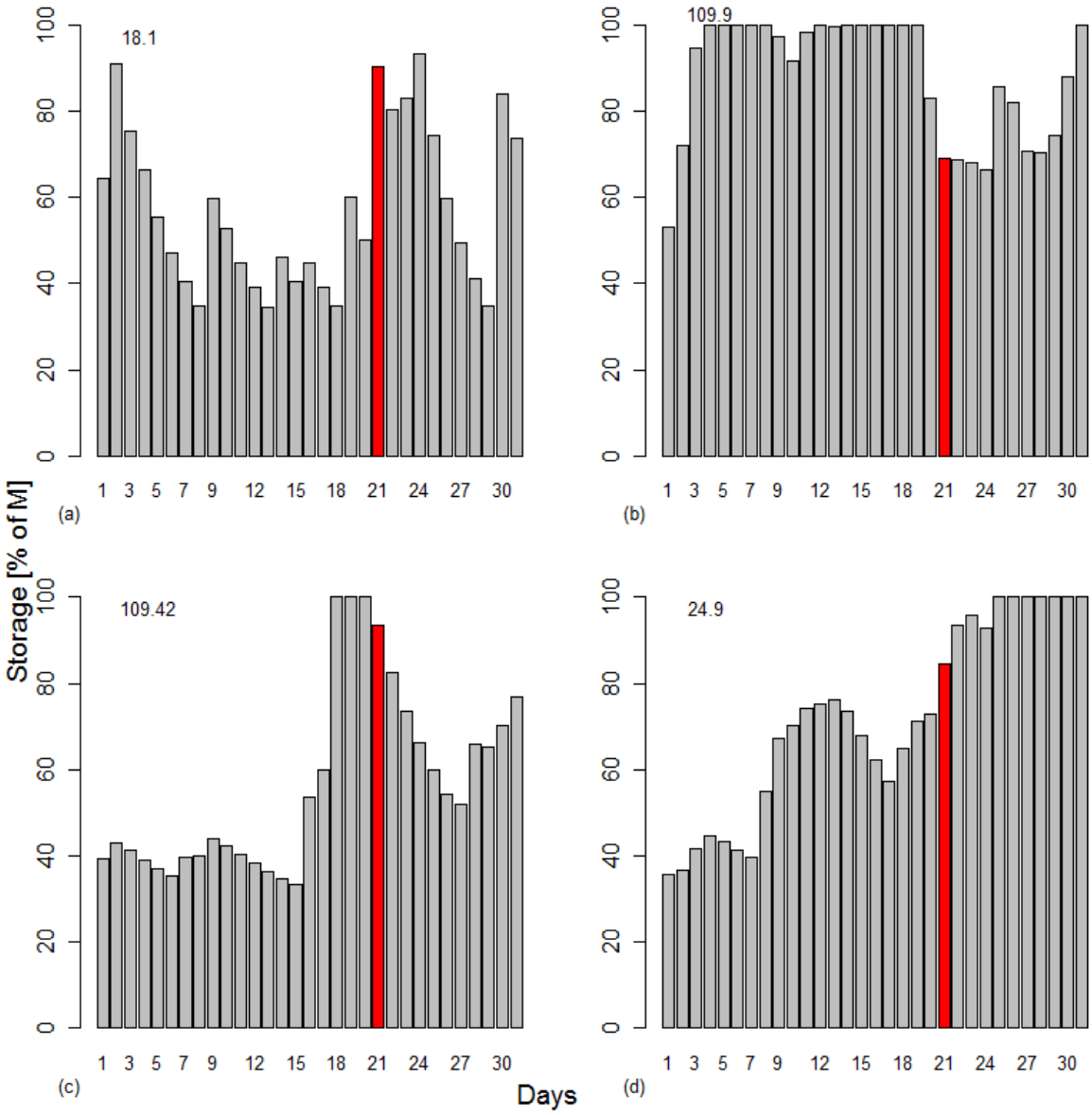

Figure 18) Bar plots of the temporal distribution of saturation for four landslide events occurring under partially completely saturated conditions. a) a sharp gradient (26.08.11), b) following a prolonged high saturation (04.06.13), c) both a sharp gradient and a prolonged high saturation (16.08.03) and d) no indicators (25.04.06). The red bars represent the day of the landslide event.

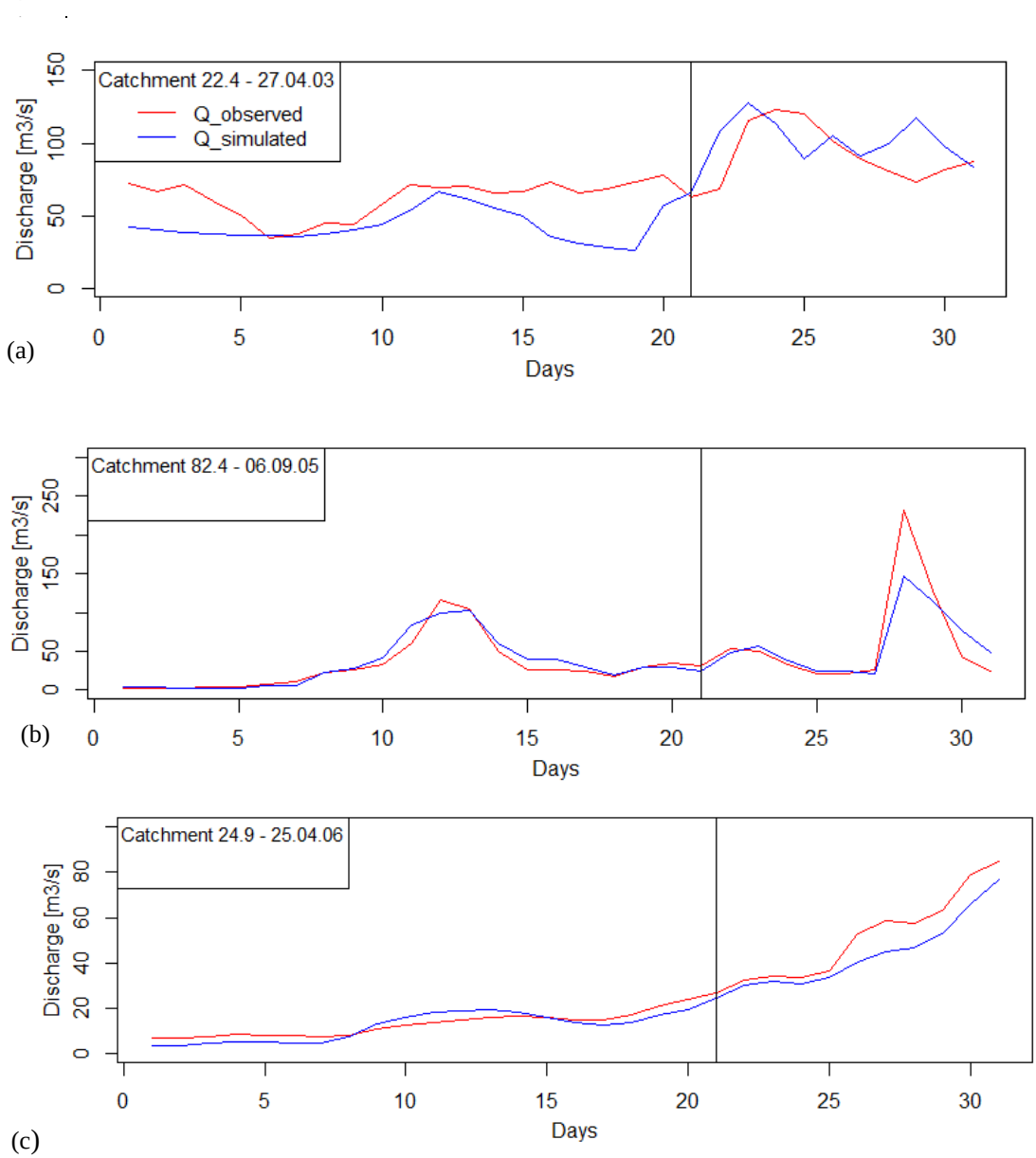

Figure 19) Observed discharge and simulated discharge for the four landslide events found with no indication for landslide occurrence. a) catchment 22.4, b) catchment 82.4 and d) catchment 24.9. The black, vertical lines (at day 21) indicate the day of the landslide event.

6.5 Landslide occurrences and overland flow

The simulation of overland flow (catchment values) found for the landslide events is presented in this section, together with the temporal dynamics of saturation including overland flow.

Overland flow is simulated for 66 landslide events (Table 12), which means that only ten events occur without. For the day prior to the landslide events, 59 landslides are found with overland flow. All landslide events occurring during completely saturated conditions are found with overland flow. The highest values of overland flow are, in most cases, found in

the western catchments with the highest simulated overland flow of 174 mm in addition to *M*. The lowest values are found for the landslide events occurring under partially saturated conditions, with the lowest value of 2 mm.

Table 12) The occurrence of overland flow for the 76 landslide events for the day prior to the landslide and the day of the landslide.

	Number of landslide events
D-1_Landslide	59 events (79 %)
D_Landslide	66 events (87 %)

Temporal dynamics of saturation including overland flow

The temporal dynamics of saturation including overland flow is investigated due to the fact that many landslide events are associated with prolonged high saturations and it is difficult to say why these landslides are triggered those exact days (see section 6.4). By including simulated overland flow to the saturation levels, one hopes to find indications for landslide occurrence in the temporal dynamics, for example that the landslides occur the day with the highest amount water present in the catchment, i.e. the highest values of overland flow.

In Table 10 and Table 11 we found that 30 landslide events have a prolonged high saturation and occur for completely saturated conditions. Out of these, 21 landslide events show a distinct peak when including overland flow to the saturation levels (Table 13). Note that in order for the landslides to be associated with a distinct peak they must occur directly at the peak or right before or after the peak. Examples of landslides occurring at the peak are illustrated in Figure 20a and b. These two events are the same as presented in Figure 17b and c. Nine landslide events does not occur at a peak, in which four occur for relatively high values and close to the peak. These four are said to be slightly indicated. An example is given in Figure 20c where the event occurs at high values, three days after the peak. Finally, five events are found with no dynamical indicators in the temporal dynamics of saturation including overland flow. An example is found in Figure 20d. The plots for all landslide events are found in Appendix IV.

Table 13) The temporal dynamics of saturation including overland flow for 30 events occurring for S=M and prolonged high saturation (see section 6.4).

	Number of landslide events

A distinct peak	21 events
Slightly indicated	5 events
No indications	4 events

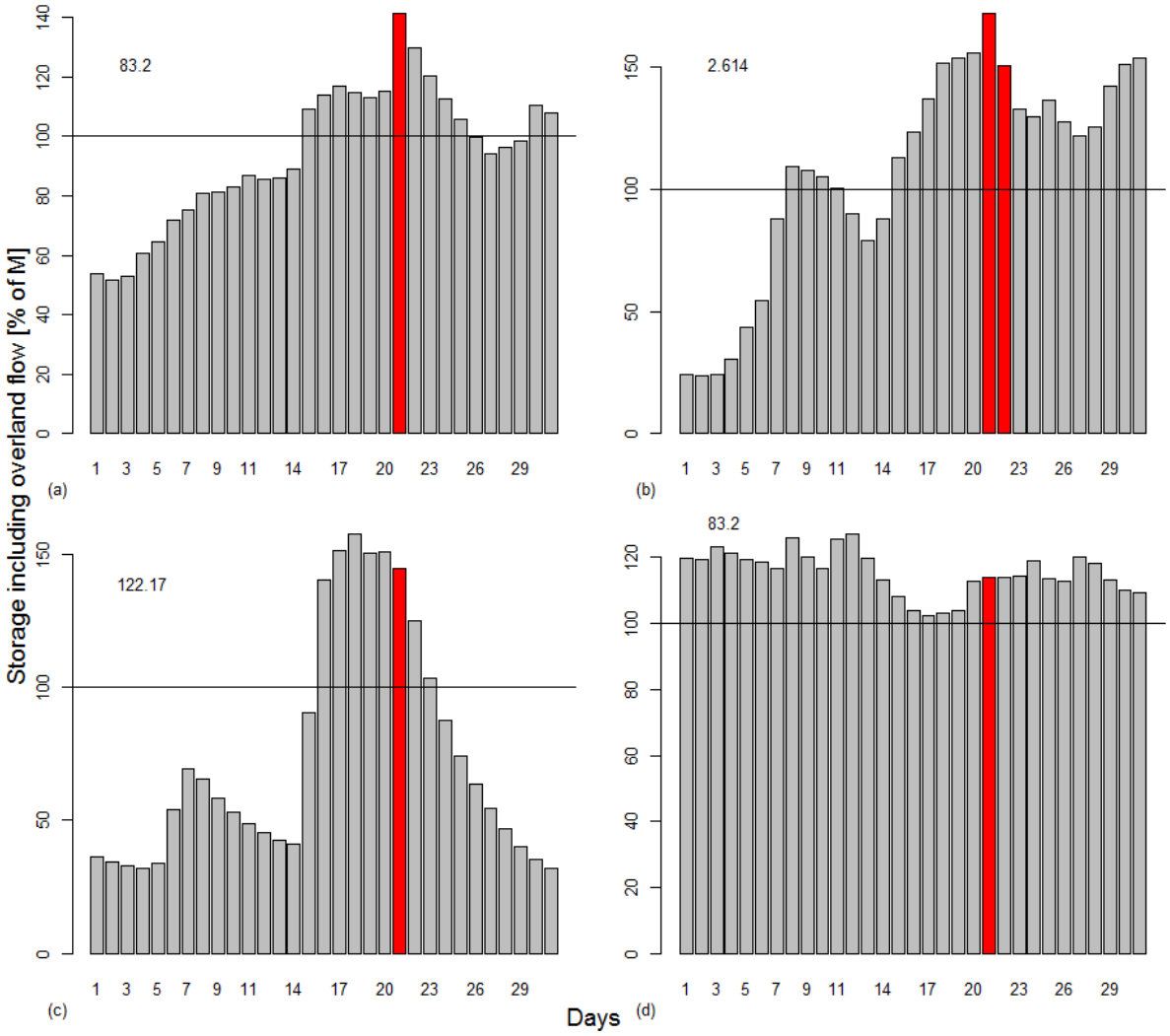

Figure 20) Bar plots of the temporal distribution of saturation for landslide events associated with prolonged high saturation. The landslide events are indicated by a) a distinct peak (14.11.05), b) a distinct peak (22-23.05.13), c) slightly indicated (08.05.95) and d) no indicators (29.06.99). The black horizontal line indicates maximum storage capacity (S=M). The red bars represent the day(s) of the landslide event(s).

6.6 Indications for landslides in the characteristics of the subsurface along the hillslope

In this section, the results for the lower, middle and upper hillslope are presented. This includes the storage, the temporal dynamics of storage and overland flow simulated at each point of the hillslope for the landslide events.

6.6.1 Spatial distribution of storage along the hillslope

A summary of the distribution of storage (scaled values, see section 5.2) along the hillslope is presented in Table 14. Note that the storage values in this section are given in percent of the maximum, scaled, simulated storage value at each point of the hillslope (S_{j_max}) for each catchment.

Table 14) A summary of the distribution of storage (scaled values) associated with the three points of the hillslope; lower, middle and upper. The storage values are given in % of the maximum simulated storage value at each point of the hillslope(S_{j_max}) for each catchment.

		Distribution of storage associated with the landslide events [% of S_{j_max}, for each catchment]					
		Min.	1st Quant.	Median	Mean	3rd Quant.	Max.
Lower hillslope	$D\text{-}1_{Landslide}$	37.0	80.0	88.5	84.5	91.0	98.5
	$D_{Landslide}$	63.0	81.0	80.0	85.5	91.0	96.5
Middle hillslope	$D\text{-}1_{Landslide}$	30.0	75.0	80.0	79.0	87.0	100.0
	$D_{Landslide}$	55.0	77.0	82.0	82.0	88.5	100.0
Upper hillslope	$D_{Landslide\text{-}1}$	18.0	36.0	42.0	43.0	52.0	68.0
	$D_{Landslide}$	13.0	31.0	39.5	42.5	52.0	74.0

The results show relatively high storage values at the lower and middle hillslope. At the upper hillslope the values are lower. Landslide occurrences during maximum simulated storage ($S_j=S_{j\_max}$ = 100 %) are only found at the middle hillslope and only for one landslide event. This result is, however, a bit misleading since we found in the previous results (Table 8) that 70 % of the landslide events occur under completely saturated conditions (i.e. $S=M$ and $\sum S_j=M$). What we can see from the results in Table 14, however, is that the distribution of storage along the hillslope vary. Thus, for any given storage value, S (catchment value),

the storage can be distributed differently along the hillslope. Since the $\sum_1^j S_j\ (t) \leq M$, more water at lower parts of the hillslope corresponds to a less water in the higher parts of the hillslope, and vice versa.

6.6.2 Temporal dynamics of storage along the hillslope

The temporal dynamics of scaled storages at the points of hillslope are, for the majority of the events, found to be similar and sometimes almost identical to the entire catchment. This is especially seen at the lower and middle hillslope. Examples of two landslide events are presented in Figure 21 a and b, where the lower and middle hillslope are very similar to the entire catchment (presented in Figure 17a and b, respectively). The upper hillslopes are also similar, especially the event in Figure 21a, however, the changes appears more variable. The higher peaks and lower "valleys " are mainly seen due to the low values of storage (due to the low associated areas). The event seen in Figure 21b occurs after six days of prolonged maximum saturated at catchment scale. At the lower hillslope, the storage during these six days are found to decrease, while at the middle hillslope the same days are found with an increasing storage. Because of this, the landslide is characterized by a peak in storage at the middle hillslope. In fact, 26 landslide events are found with a peak in storage at the middle hillslope, exclusively. This event is also a good illustration of different distributions of storage found for a given storage value (here S=M) mentioned in the previous section. In this case, the water is more evenly distributed along the hillslope with more water at the middle hillslope, relative to S_{middle_max}, and thus less water at the lower hillslope, relative to S_{lower_max}. Remember, always $S_{lower} > S_{middle} > S_{upper}$ due to the associated areas.

The black bars in Figure 21a indicate the maximum scaled storage value at the lower hillslope. Note that this value is not S_{lower_max} but only the highest value within the 31 days surrounding the landslide event. The black bars at the middle and upper hillslope represent the corresponding storage values. This is a good illustration of a situation where a more water is found at the lower part of the hillslope and thus, less water at the middle hillslope. The storage values at the upper hillslope does not necessarily follow this pattern, in fact quite rare.

Figure 21 also shows that even though the two landslide events occur during completely saturated conditions, neither of them are associated with completely saturated conditions at the lower, middle or upper hillslope (Table 14) because there are other days with higher storage values.

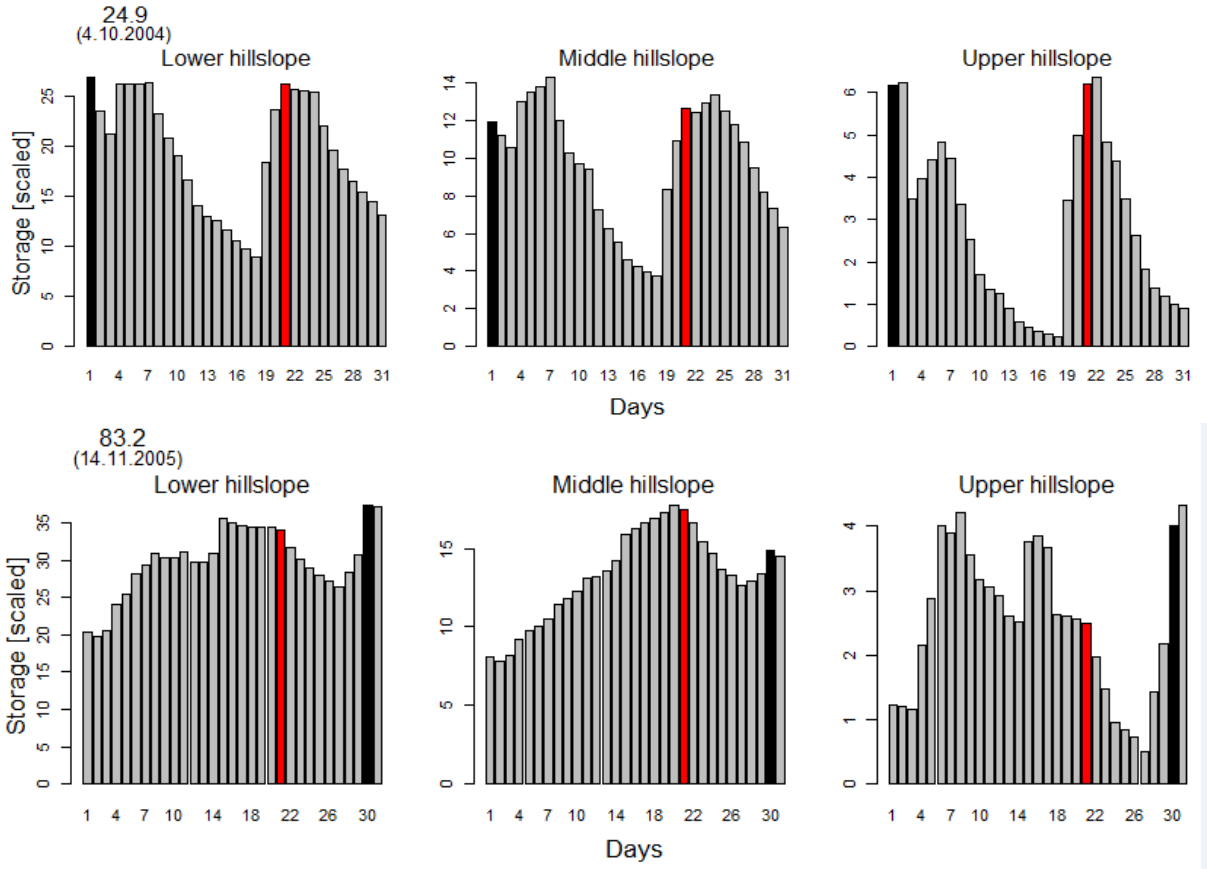

Figure 21) Bar plots of the temporal dynamics of storage (scaled) at the lower, middle and upper hillslope at the time surrounding two landslide event. The red bars represent the day of the landslide event. The black bars indicate the maximum scaled storage value at the lower hillslope found within the 31 days surrounding the landslide event and the corresponding storage values at the middle and upper hillslope.

6.6.3 Landslide occurrences and the occurrence of overland flow along the hillslope

In Table 15, the simulation of overland flow at the three points of the hillslope are presented. The lower hillslope is identical to that of the entire catchment (Table 12) with 59 events (*D-1_Landslide*) and 66 events (*D_Landslide*). Only one landslide event occurs with overland flow at the lower hillslope, exclusively. The number of landslide events found with overland flow decrease with increasing distance from river reach.

Table 15) Overland flow at the lower, middle and upper point of hillslope.

	The number of landslide events		
	Lower hillslope	**Middle hillslope**	**Upper hillslope**
D-1_Landslide	59 events (79 %)	58 events (76 %)	58 events (76 %)
D_Landslide	66 events (87 %)	65 events (86 %)	59 events (79 %)

6.7 Hysteresis in the DDD model

In this section, the representation of the simulated storage-discharge hysteresis in DDD model associated with the landslide events is presented, first for the entire catchment and then for the three points of the hillslope. The connection between landslide occurrences and hysteresis follows.

Clearly, the relationship between storage and discharge, represented by DDD model, is not a one-to-one relationship (Figure 22). Thus, any given value of storage is associated with several values of discharge and vice versa. In Figure 22a, the storage and discharge relationship found for the entire calibration and validation period in one catchment is presented. The same is presented in Figure 22b only with overland flow included in the storage values. The number of active storage levels, i.e. which storage levels contain water, is to some extent seen in the plot. This is especially seen for storage level 1 (from S = 0 to about 15%) and storage level 1 and 2 (from S of about 15 – 25 %) since they are associated with a smaller range of discharge values and also there are few/no outliers. When storage level 3 and 4 is active, the range of discharge is larger and there are more outliers. The storage seems to range from about 25 – 55 % and 55 % - 100 %, respectively. This means that when water is added to storage level 4 the level of saturation is minimum 55 %. Overland flow is the values above 100 %. The range of S and Q and also how clear the sections are, vary between catchments.

The storage-discharge relationships (without overland flow) at the three points of the hillslope are shown in Figure 23. Note the different storage values (scaled values). The discharge, *Q*, is equal. The lower and middle hillslope are very similar to that of the entire catchment. At the upper hillslope, the relationship between discharge and storage looks very scattered, with a higher frequency of lower storage values. It can also be seen that the highest values of discharge is not associated with the highest values of storage.

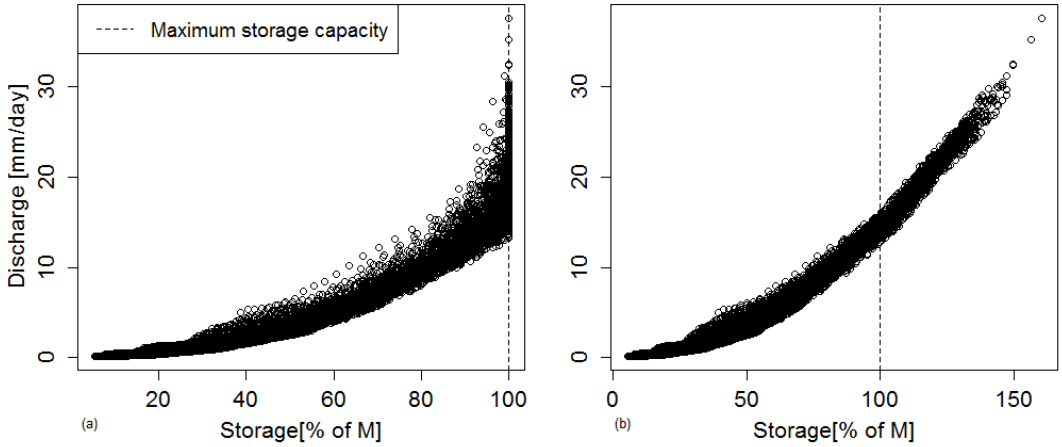

Figure 22) The storage-discharge relationship for a) all storage values and b) all storage values including overland flow. The data is from the calibration- and validation period in catchment 88.4. The stippled, vertical line indicates the maximum storage capacity.

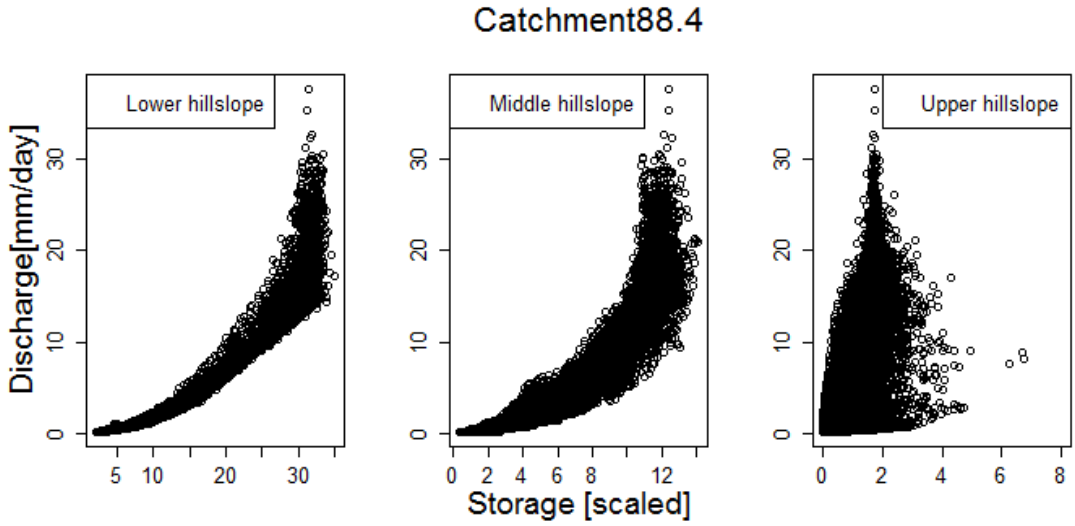

Figure 23) The storage-discharge relationship in catchment 88.4 at the lower hillslope (left), middle hillslope and upper hillslope (right).

6.7.1 Representation of the hysteresis in DDD model

The hysteretic relationships between simulated storage [mm] (catchment value) and discharge [mm/day] represented by DDD model ware found to vary in scale, shape and direction, often showing complex patterns. The hysteretic loops were evaluated in terms of the direction of the loop, i.e. anti-clockwise or clockwise, where an anti-clockwise loop refers to a higher storage on the rising limb than on the recession for a given discharge and vice versa. Half of the landslide events have anti-clockwise loops (Table 16), while only 14 events are associated with clockwise loops. In general, the scale of the hysteretic loops

ranges from highly non-linear relationships to displaying almost linear one-to-one relationships. Four events are almost linear. Finally, about 25 % of the landslide events are found to display "non-classifiable", complex patterns. Hysteresis for all landslide events are found in Appendix X. A typical example of a landslide found with an anti-clockwise hysteretic loop is presented in Figure 24b with associated precipitation in Figure 24a. In Figure 24c overland flow is included in the storage values.

Table 16) The number of landslides with clockwise-, anti-clockwise-, almost linear- or complex storage-discharge hysteresis.

	Number of landslide events
Clockwise loops	14 events (18 %)
Anti-clockwise loops	38 events (50 %)
Almost linear	6 events (7 %)
Complex hysteresis	17 events (24 %)

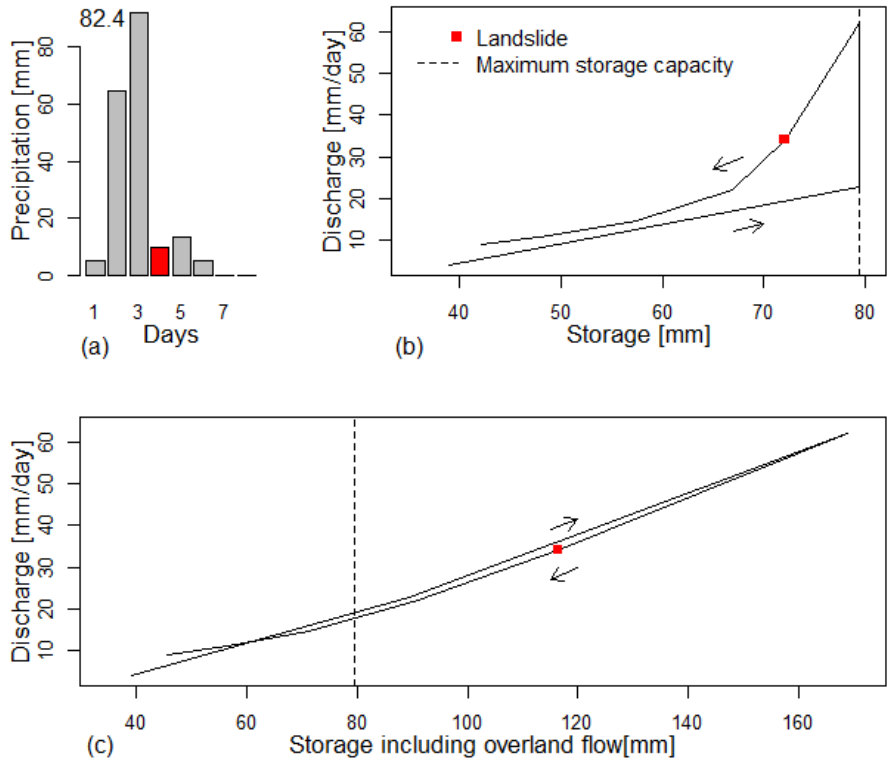

Figure 24) An example of hysteresis(anti-clockwise) associated with the landslide event, 21.03.14 in catchment 82.4. a) Bar plot of precipitation, b) anti-clockwise hysteresis in the storage-discharge relationship and c) the hysteretic relationship in the storage including overland flow- discharge relationship. The stippled, vertical line indicates the maximum storage capacity, M. The arrows denote the direction of the loops The day of the landslide event is indicated in red.

The hysteresis in Figure 24 illustrates a common behavior where the storage reaches maximum capacity before the discharge peaks causing the loop to follow the maximum storage while the discharge continues to increase, i.e. the discharge lags storage. This is the case for more than 60 % of the landslide events and the case for most of the landslide events associated with anti-clockwise loops. In fact, in all hysteretic loops with an anti-clockwise direction, the storage reaches maximum capacity. Only a few clockwise loops are found at maximum storage values. When including overland flow to the storage values (Figure 24c) the hysteretic loops becomes narrow, often exhibiting almost a linear relationships. The storage including overland flow and discharge peaks simultaneously for the majority of the events. For some landslide events, the direction of the loop changes when including overland flow as seen in Figure 24c, however, the plots are usually very narrow.

6.7.2 Representation of hysteresis along the hillslope

The hysteresis at the lower, middle and upper hillslope are also found to vary in scale, shape and direction. The results of the hysteresis, evaluated in terms of the direction, is presented in Table 17. The lower and upper hillslope have a higher frequency of anti-clockwise loops. At the middle hillslope, on the other hand, clockwise hysteretic loops occurs more frequent. An example of hysteresis at the lower, middle and upper hillslope for one landslide event (the same event as presented for the entire catchment in Figure 24) is presented in Figure 25. This plot shows a typical scenario where anti-clockwise loops are found at the lower and upper hillslope, while the middle hillslope shows a clockwise loop. At the middle and upper hillslope, the loops are almost linear at the time of the landslide event.

Table 17) The number of landslides with clockwise-, anti-clockwise-, almost linear- or complex storage-discharge hysteresis at the lower, middle and upper point of the hillslope.

	Number of landslide events		
	Lower hillslope	**Middle hillslope**	**Upper hillslope**
Clockwise hysteretic loop	11 events	46 events	11 events
Anti-clockwise hysteretic loop	54 events	23 events	57 events
Almost linear	3 events	3 events	4 events
Complex hysteresis	8 events	4 events	4 events

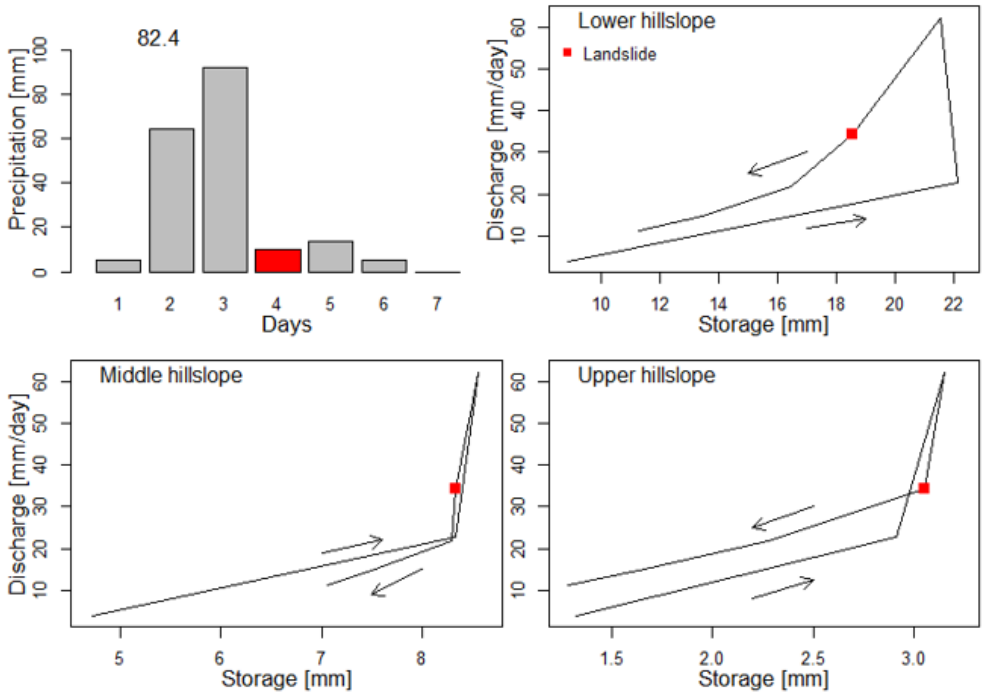

Figure 25) Bar plot of precipitation and simulated storage-discharge hysteresis for the landslide 21.03.2014 in catchment 82.4 at the lower- (top right), middle- (bottom left) and upper hillslope (bottom right). The arrows denote the direction of the loops. The day of the landslides are indicated in red.

6.7.3 Landslide occurrences and hysteresis

The landslide events were investigated in terms of where they occurred on the hysteretic loop; during recharge, at the top of the loop or during recession. This investigation was only performed at catchment scale. The result, presented in Table 18, shows that the landslides are evenly distributed on the hysteretic loop with 19 landslide events occurring during recharge, 25 at the top and 26 during recession. Most of the landslide events that are associated with the recharge or recession occur one day prior to or following the peak. Finally, the hysteresis for six landslide events were too complex to determine the position. It should be noted that recharge and recession are also found during maximum storage values depending on whether the discharge is increasing or decreasing.

In Figure 26, examples of landslides occurring during recharge (a), at the top of the loop (a and b) and during recession(c) is presented. Both of these landslide events occur under completely saturated conditions. The landslides in Figure 26a occur after a one day of heavy rain, while the events in Figure 26b are associated with a large rainfall event lasting for more than three days.

Table 18) The number of landslide events occurring during recharge (i.e. rising limb), at the top or during the recession (i.e. falling limb) of the hysteretic curve.

	Number of landslide events
Recharge	19
Top	25
Recession	26
Not possible to determine	6

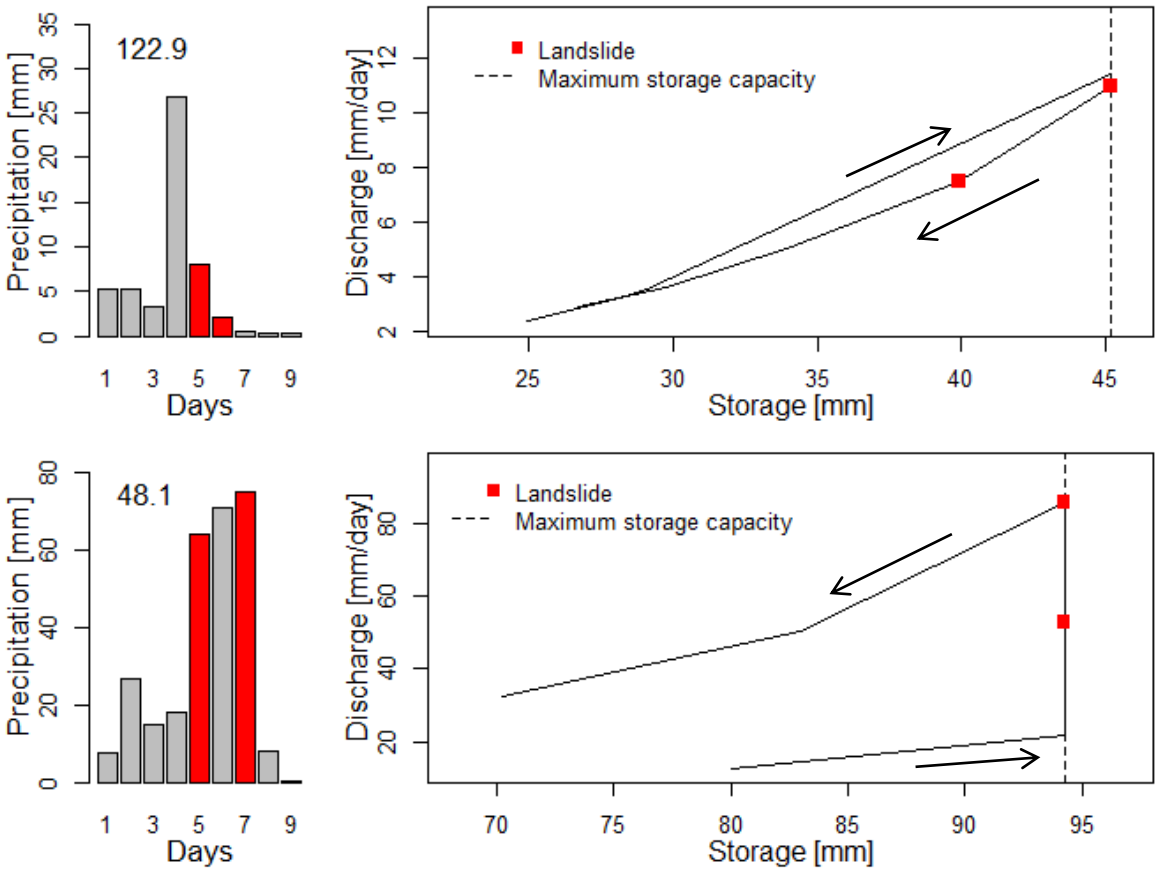

Figure 26) Bar plot of precipitation and simulated storage-discharge hysteresis for a) two landslide events in catchment 122.9 occurring 22-23.6.2014 and b) two landslide events in catchment 48.1 occurring the 26-28.10.2014. The arrows indicate the direction of the loop. The day of the landslide events are indicated in red.

7 Discussion

The chapter will first address the issue of landslide data quality, model performance and limitations and uncertainties related to the model. The following sections discuss of the characteristics of the subsurface associated with the landslide events, i.e. the saturated storage, the temporal dynamics of saturation and overland flow (presented in sections 6.3-6.6). The results of the entire catchment will be addressed first, followed by the results for the three points of the hillslope. The last section addresses how hysteresis, the nonlinear loop-like behavior common in many natural systems, is represented by the DDD model at the time surrounding the landslide events. First the results at catchment scale is discussed, followed by the results at the three points of the hillslope. The last part of this sections deals with how the occurrence of landslides can be related to hysteresis.

7.1 Landslide data quality

The landslide events are collected from the Norwegian landslide database. Within the database, there are weaknesses and limitations that may have impacted the result of the landslide analysis. A main uncertainty is related to the type of landslide registered in the database. Since this study only focuses on debris avalanches and debris flows, misregistrations in the database (e.g. rockfalls registered as debris avalanches) would affect the results because these types commonly are associated with different hydrological conditions. Even though the number of misregistrations were reduced (described in section 5.4) there are still uncertainties related to whether all misregistrations were detected. In addition, the majority of the landslide events in the database, and thus most of the landslides included in this analysis, are registered as unspecified landslides in soil making it impossible to separate debris avalanches and debris flows in the analysis. Other uncertainties relates to the missing information in the landslide database of the timing, i.e. time of day, and point of initiation. The lack of the timing is especially problematic due to the fact that the hydrological data and the landslide data do not coincide (i.e. the landslide data is registered from 00:00 to 00:00 and the hydrological data is registered from 06:00 to 06:00). The landslides may have occurred between 00:00 and 06:00 and are therefore associated with the hydrological data from the wrong day. The lack of points of initiation is problematic, especially in analysis involving the hydrological conditions at points. Finally, there are uncertainties related to lack of registrations since landslides are only recorded where damages on infrastructures are registered. Norway consists of mountainous areas and there

are large areas with few roads, railways and houses. Therefore, it is reasonable to assume that there are more landslide occurrences than what is registered in the landslide database, which limits the landslide analysis to investigate only a subset of landslide events.

7.2 Model performance

The meteorological data used as input in this analysis is the best available dataset, interpolated from the observation network of the Norwegian Meteorological Institute (met.no). The length of the complete input data of 25 years (1985-2014) is well within the range of what is necessary and sufficient for a reliable calibration. According to the Nash-Sutcliffe model efficiency all catchments meet the criterion for the acceptable performance of NS > 0.6 (Patil and Stieglitz, 2014). The structure of DDD model is thus considered to be suitable for simulations of hydrological conditions at catchment scale.

Validation of DDD model by comparing fluctuations of the simulated storage and groundwater observations

Fluctuations in the storage values [mm] simulated by DDD model were compared with fluctuations of the observed groundwater levels [m below ground] in order to validate the model. The results of the correlation in catchment 2.614 in this study, as well as results of correlation found in two other studies (Skaugen and Onof, 2014; Weltzien, 2015) indicate that the storage levels experiences similar variations as the observed groundwater tables. The poor correlation found in catchment 77.3 was not significant. The coefficient of variation also shows that the variation increase upslope in correspondence with the groundwater measurements. It is important to keep in mind that the storage values in the DDD represent the entire catchment, while the groundwater level observations are point observation and might not represent the entire catchment. Groundwater level fluctuations vary with location of the borehole relative to the river (Myrabø, 1997), i.e. at the hillslope or adjacent to the river and also with catchment topography and porosity.

7.3 Model uncertainties and limitations

All hydrological models are simplifications of the real world and are therefore bound to be associated with uncertainties (Quinn et al., 1991). The uncertainties arise from several sources, mainly associated with the natural variability related to the hydro-meteorological input data, model parameters and the model itself, which in turn will affect the result.

In general, model performance relies on the quality of the data it is based on (Kirchner, 2009), which in this case includes the observational data used as input (precipitation and temperature) and evaluation (discharge). Rainfall measurements, which is very often considered to be the main driving force of many hydrological models, is especially related to large uncertainties due to the difficulties in measurements. The most significant errors found for accumulation of rainfall in buckets include losses due to wind, evaporation and splashing (Habib et al., 2001). The wind-induced undercatch is considered the largest component of error.

Other uncertainties arise from the model parameters and the model itself. In the case of the DDD model, most of the parameters are derived from maps and measurements, introducing few calibration parameters. The reduced number of calibration parameters reduces the uncertainty and provides a more realistic representation of the subsurface hydrology, compared to models with a higher number of calibration parameters (Skaugen and Onof, 2014). The fact that the model has a 2D representation of the subsurface (with length, y, and depth, z) provides us with spatial information of groundwater dynamics. The model is therefore assumed to give a more realistic representation of the wetting and drainage of the subsurface compared to typical conceptual, 1D- rainfall-runoff models (Beven, 2006). However, the model assumes homogenous conditions at equal distances from the river. This is not realistic seen as there could be local areas of complete saturation occurring at local low points in the hillslope or hollows in the subsurface, which is difficult to model (Anderson and Burt, 1977; Weill et al., 2013). This also applies to the assumption of a homogenous storage conditions along the hillslope. Other assumptions and simplifications that might lead to some errors in the estimated output include the a subsurface that is assumed to be connected at all times. Hydrological connectivity, i.e. the connection (or dis-connection) of flow pathways between different parts of the catchment, is considered to be a dominant control of subsurface flow and discharge (Haught and van Meerveld, 2011).

There is also a very simple parameterization applied for the percolation of water from the unsaturated to the saturated reservoirs in DDD model. Measurements from the unsaturated zone are probably needed in order to improve the process of percolation. This should be investigated in future research.

Finally, the model was found to experience some problems related to the simulation of precipitation. The DDD model does not take advantage of spatially distributed meteorology and precipitation is therefore simulated as either rain or snow. This is not a realistic representation of nature as precipitation may fall as rain in the lower parts of the catchment and snow in the higher parts. Storage, and thus discharge, responds to the rate of precipitation and thus, errors in the simulations will in turn affect the results of the storage and thus the results of the landslide analysis.

7.4 Storage as an indicator for landslide occurrences

The results found that the majority of the landslide events occurred for very high storage levels, often at maximum storage values, which corresponds well with what we know about hydrological conditions triggering landslides (described in section 2.2.3.1). The fact that eight landslide events occurred during partially saturated conditions but were found with completely saturated conditions the day prior to the landslide suggests that the landslides occurred between 00:00-06:00. This means that they should have been associated with the meteorological data the previous day. If this is the case as much as 88 % of the landslides would have been found with completely saturated conditions. This is, however, only speculations and not possible to investigate further due to uncertainties related to the timing (i.e. time of day) for the landslide events. Of the 23 landslides that occurred under partially saturated conditions, eight events occurred during winter and spring (December through May). Based on the discovery of errors in the simulated precipitation during periods of T = 0-1 °C, it is reasonable to assume that some of these events are affected by such simulation errors. Even though the landslide data have been checked for these errors (described in section 5.4), they are only checked for a shorter period up to the landslide events. Possible simulation errors in the time prior to the checked period could also cause errors in the storage values, i.e. lower storage values, at the time of the landslide events as the storage values might be “lagging”. There is also the possibility that the landslides are caused by other processes not included in this analysis, such as snowmelt, water freezing, soil frost

condition or human activity. Finally, the landslide events could also be misregistrations in the landslide database.

7.5 Temporal dynamics of saturation for landslide events

Infiltration of water to the soil by extreme rainfall or rapid snowmelt causes a sudden rise of the water table and an increase in water-pressure, possibly triggering landslides (Wieczorek and Glade, 2005). This corresponds well with the findings in this study that 70 % of the landslide events were characterized by a sharp gradient in saturation (Table 10). That almost half of the landslide events also occurred during prolonged high saturations suggests that the soil can be completely saturated without triggering landslides. Thus, the timing of the landslide occurrences seems to be linked to additional input of rainfall, which in the DDD model is simulated as overland flow. It is therefore likely to assume that there are some indications for landslide occurrences in the values of overland flow, however, this is discussed in the next section (7.6). In Norway, periods of prolonged high saturations, especially in the eastern parts, are related to spring melt season or caused by long time infiltration of successive medium rainfall events (Jaedicke and Kleven, 2008; NVE, 2014b). Landslide events occurring during such conditions are documented and an example is the landslide event occurring 22th May 2013 (and 23th) during a major spring flood referred to as "Pinseflommen in 2013" (NVE, 2014b) (See Figure 17c). The western parts of Norway experiences rainfall events of higher intensity, have steeper slopes and shallower soil cover which causes a more rapid wetting and drainage of the soil. Based on this, it is likely to assume that periods of prolonged high saturation occurs less frequently in the western parts than in the eastern parts (NVE, 2014b). The fact that a high number of landslide events were associated with a prolonged high saturation in some of the western catchments, especially 83.2 and 88.4 (Appendix II), suggest that the estimated maximum storage capacity, *M*, might be too low for some catchments. This is, however, beyond the scope of this study, but is definitely something that should be investigated in the future.

From the results in section 6.3 and 6.4, it is clear that only four landslide events were found without any dynamical indicators for landslide events (Table 11), in which one event occurred during saturations of 98.5%. Thus, three events had no indications for landslide occurrence. Of these events, one occurred in April and it was speculated in the section 7.1 whether these winter/spring events were associated with errors in the simulated storage values. By visual inspection of the deviations in the simulated- and observed discharge

(*Qsim* and *Qobs*, respectively) this seems to be the case for this event (Figure 19a) since *Qsim* is lower than the *Qobs* suggesting that the precipitation might be simulated as snow. Thus, when disregarding the landslide possibly associated with errors in the simulated storage, only two events were found without any dynamical indicators in the subsurface representation in the DDD model. One could ask if these events are correct registration (i.e. debris flows or debris avalanches) triggered during unusual conditions, or if they are misregistrations in the database or caused by something else than hydrological conditions.

7.6 Landslide occurrences and overland flow

Based on the findings that maximum storage values were frequently simulated by DDD model at the time surrounding the landslide events, overland flow was expected to be simulated for many landslides events. Clearly, this was the case as 87 % of the landslide events found with overland flow (Table 12). It is, however, uncertainties related to whether the overland flow simulated by DDD model reflects what is observed in nature. There are no available measurements of overland flow and it is therefore not possible to evaluate the simulated overland flow values. On the other hand, numerous studies have documented that overland flow is related to the occurrence of rainfall-induced landslides (Jaedicke and Kleven, 2008; Yu Luo et al, 2012) supporting the results of this study. Overland flow increases soil erosion, as well as reduces the slope stability, which are factors controlling the landslide occurrence. Overland flow is considered important in landslide hazard assessments (Yu Luo et al, 2012) and hence should be included when investigating and predicting landslides.

The inclusion of overland flow to the storage values gave noticeable improvements in terms of finding indications for landslide occurrence in the temporal dynamics of saturation (Table 13). This indicates that the timing of the landslide events are linked to additional input of rainfall, which is simulated as overland flow in DDD model. The landslide event occurring during “Pinseflommen” (22 May 2013), mentioned in the previous section, is a good example. The event occurred after prolonged high saturation, triggered by additional input (NVE, 2014b), which seems to be exactly the case simulated by DDD model and illustrated in Figure 20b.

7.7 Indications for landslides in the characteristics of the subsurface along the hillslope

The main purpose of investigating the storage (scaled) at different points along the hillslope was to see if the landslide events could be characterized by the spatially varying storage. One hoped to be able to link the saturation at the different points of the hillslope to the occurrence of landslide events. However, the analysis was limited due to the lack of information related to the starting points of the landslides in the database. There are methods to determine the points where the landslides most likely were triggered, however, these processes are time consuming, often problematic, and therefore not carried out in this thesis. There are also some difficulties arising from the storage values at each interval and due to the fact that the maximum storage capacity at each interval is not defined (described in section 5.2). This makes it more challenging to interpret the results of the saturation and compare across catchments.

However, it is clear that the storage has a distribution that varies along the hillslope and with time. This means that the for a given storage (e.g. $S=M$), S can be distributed differently along the hillslope and thus the proportions of water at the lower, middle and upper hillslope vary (Table 14). Keep in mind that the storage values always decrease with increasing distance from river due to the associated areas (see section 5.2). Since the sum of storage at all points of the hillslope are equal to or less than M, very high simulated storage values at the lower hillslope are associated with lower values at the middle hillslope (Figure 21). Very high simulated storage values at middle hillslope are associated with a more evenly distributed storage along the hillslope. Because the scaled storage values at the upper hillslope always accounts for a small proportion of the total storage, the storage values at the upper hillslope can be high or low (relative to the other storage values at the upper hillslope) independent of the distribution of storage at the lower and middle hillslope. The temporal dynamics of saturation in the hillslope indicate that the behavior at the lower hillslope reflects that of the entire catchment.

It is interesting to see that quite a few landslides were characterized by a peak in storage at the middle hillslope but not at the lower and upper hillslope, or at catchment scale. This was often seen for the events that occurred during prolonged high saturations at catchment scale, suggesting that landslides may occur when a higher proportion of water is found at the middle hillslope (i.e. more evenly distributed storage). However, the lack of initial points of initiation for the landslides makes it impossible to know whether they occurred below, at

or above the middle hillslope. For further investigation, the starting points of the landslide events (i.e., in what distance from the river) must be determined.

7.8 Hysteresis

The non-single valued relationship between storage and discharge in the DDD model comes from exponential UHs of different temporal scale (Skaugen and Mengistu, 2015). The storage-discharge curve represented by DDD model is found to resemble what is found in some other studies, including the one illustrated by Sloan (2000) (Figure 27).

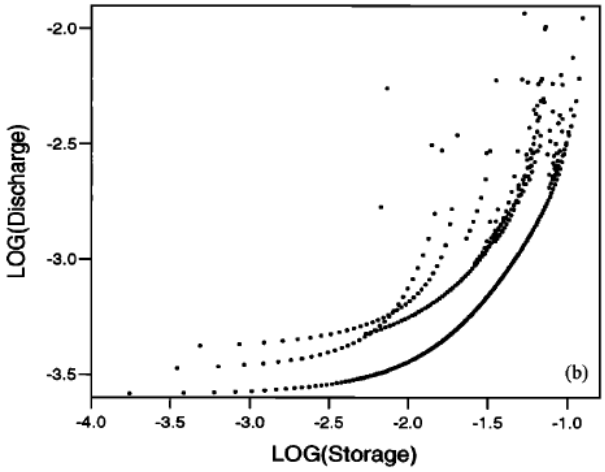

Figure 27) Storage and discharge relationship plotted on log-log scales (Sloan, 2000).

The non-single valued relationship between storage and discharge lead to the investigation of hysteresis and clearly, the structure of the DDD model allows addressing the important issue of the relationship between discharge and the volume of water stored in the subsurface reservoir. Thus, the model has shown to be able to reproduce the nonlinear, hysteretic relationship in storage and discharge observed in the field and documented for a long array of experimental catchments (Myrabø, 1997; McGlynn and McDonnell, 2003; Allen et al., 2010; Penna et al., 2011; Weill et al., 2013; Davies and Beven, 2015). These studies also report variation in the hysteretic loops (i.e. loops of varying direction, shape and scale) supporting the results of this work. However, if the causes of the hysteresis and its various loops found in the DDD model coincide with the causes of hysteresis documented elsewhere is discussed in the following section.

Hysteresis are complex processes, controlled by many factors, which in turn makes it difficult to distinguish between the different factors and their effects. The complexity is probably a main reason for the different hysteresis documented in the literature (see section 2.1.3). In addition, the hysteresis found for the landslide events in this thesis are not the best representation of hysteresis, since they are influenced by additional input. An ideal representation would be a storage-discharge hysteresis associated with a period of one significant rainfall event followed by several days of no input (i.e. no rain nor snowmelt). In this case, one would be able to see how the catchment responds to input and more importantly, how the water drains without the influence of additional input. The additional input, particularly input during recession, found for the landslide events in this thesis is assumed to affect the results in this analysis, however, it is not clear to what extent.

In this thesis, the hysteretic loops were evaluated in terms of the direction of the hysteretic loops. The main controlling factors are considered to be the relationship between the amount of water present in the subsurface (including water added from input and redistributed from upslope) and the amount of water drained. Amongst researchers there is a general agreement that hysteresis is mainly controlled by moisture degree, moisture input, hydrological connectivity and catchment characteristics such as topography, area, soil type etc. (Penna et al., 2011; Davies and Beven, 2015). Obviously, the variables which are not included in the DDD model, such as hydrological connectivity, is not relevant for explaining the hysteresis found in the DDD model. On the other hand, the movement of water through the catchment in the DDD model, which in turn effects the amount of water present and drained, is determined by the level of saturation, thus different celerities, and by the distance distribution, which take into consideration many of the factors just mentioned such as length, slope, area etc. (Skaugen and Onof, 2014). In addition, it also, to some extent, includes soil type since the type of soil is assumed to be reflected by the river density in the catchment (which again is described by distance distribution). On the other hand, the fact that the hysteretic loops found in this work vary with direction within each catchment (i.e. similar catchment characteristics gives varying directions) indicates that catchment characteristics, such as area and slope, have minor effects on the direction of the loops. Thus, the main controlling factors found in this study and documented in literature coincide to some extent.

In general, the change in storage simulated by the DDD model is a result of the amount of water added (from redistribution from upslope and input, i.e. rainfall or snowmelt) and the

amount of water drained pr. time step. The amount of water redistributed from upslope and drained pr. time step depends on the antecedent wetness, i.e. level of saturation. The level of saturation controls the size of the area drained pr. time step (determined by the celerities (see section 5.1.3) and the amount of water within the drained area (represented by the width of the boxes and the shades of blue, Figure 14), respectively. Also, how the storage and the discharge responds to precipitation varies depending on the antecedent wetness. During dry moisture conditions, there is little water drained from the subsurface pr. time unit and almost all input is stored in the subsurface. The effect of input on discharge is marginal. During wet conditions more water is drained pr. time unit from the subsurface, as a higher level of saturation is associated with a higher celerity, and the precipitation has a greater impact on the discharge. Another important factor is overland flow, which will strongly affect both the magnitude and the timing of discharge peak. This helps explain the almost linear relationships arising when adding overland flow to the values of storage (Figure 24). It also suggest that the for high amounts of overland flow the overland flow becomes too dominant and the effect of hysteresis vanishes.

The directions of the hysteretic loops comes from the changes within each variable, i.e. dS/dt and dQ/dt. In the DDD model, the dynamics of discharge are modelled using linear storages arranged in parallel, which causes the recession of Q to be exponential (with different shape and scale parameters) (Skaugen and Mengistu, 2015). Investigations of the storage values show that the recession of S is also exponential, with a much smoother curve (Figure 28). In Figure 28, discharge and storage for one significant rainfall event without any additional influence of input is presented. In this case, the storage reaches its maximum capacity causing the discharge to experience a further increase, i.e. discharge lags storage. The storage values are higher during recharge (blue numbers) than during recession (red numbers) for a given discharge (equal discharge values are indicated by equal numbers), which corresponds to an anti-clockwise hysteresis. Based on the fact that the maximum storage capacity is reached for the majority of the landslide events and that anti-clockwise loops are found more frequently, it is reasonable to assume that the changes in storage and discharge related to the landslide events resembles that in Figure 28, obviously at different scales.

Numerical effects could have impacted the hysteresis due to the fact that in a discretization, discharge is averaged over a time interval, while state of the subsurface is calculated at the

end on the time step. This could cause the storage to be higher during recession than during recharge for a given Q, however, this effect is considered to be very small.

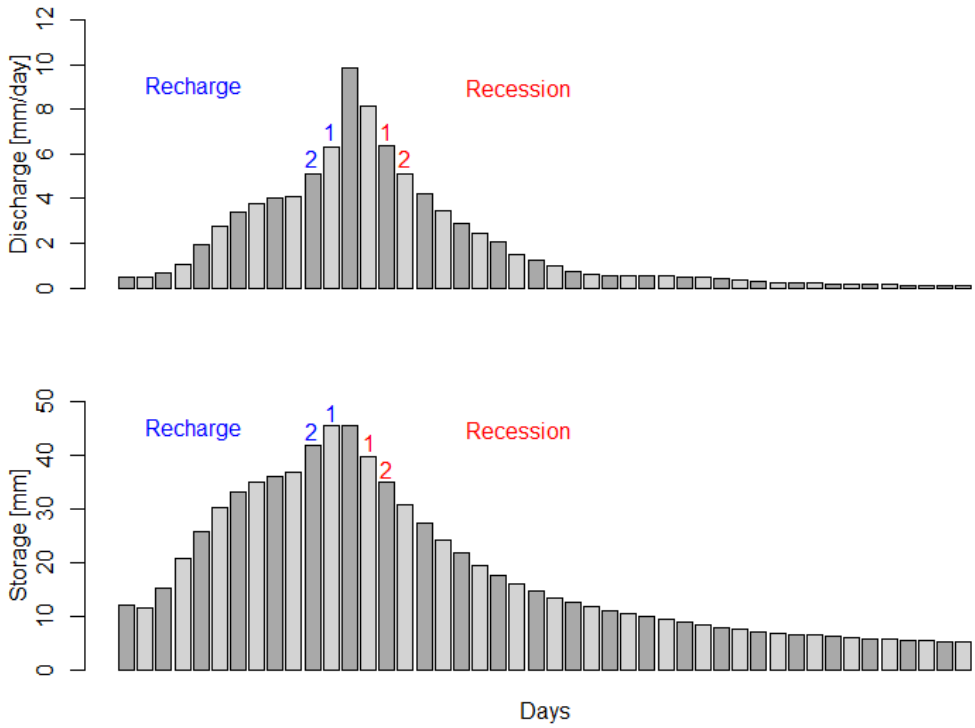

Figure 28) Bar plot of the recharge and recession of discharge (above) and storage (below) illustrated for one rainfall event. Equal numbers in the plot of discharge indicate equal discharge value during recharge (blue) and recession (red). In the plot of storage, the same numbers indicate the storage values associated with the discharge value which shows a higher storage during recharge than recession for a given discharge.

7.8.1 Hysteresis at the hillslope

Hysteretic loops are found to vary with location and several studies have identified anti-clockwise loops at lower parts of the hillslope and clockwise loops at higher parts of the hillslope (e.g. Myrabø, 1997 and Kendall et al.,1999), thus supporting the main results of this study (when disregarding the upper hillslope) (see Table 17). In literature, the main explanatory factors for the direction of the loops are antecedent wetness and hydrological connectivity (see section 2.1.3). In the case of DDD model, the different directions are introduced by the dynamics of the subsurface along the hillslope. This means that the explanations of hysteresis along the hillslope is similar to that of the entire catchment, apart

from the fact that it only involves the changes of storage at each individual point along hillslope (dS_j/dt).

The fact that hysteresis vary along the hillslope is not surprising seen as the behavior of storage along the hillslope vary (see sections 6.6 and 7.7). When it comes to the different directions of hysteresis at the lower and middle hillslope, Figure 21 is a good illustration of the different behavior at the two points which causes the different direction of the loops. The lower hillslope experiences a larger effect of antecedent moisture, due to redistribution from upslope and thus, the ratio of water between the lower hillslope and the immediately adjacent area upslope (seen by the color of blue in the snapshot of the subsurface presented in Figure 14) is larger than the ratio of water between the area of the middle hillslope and the adjacent area upslope. Thus, often, more water drain from the lower hillslope than what is added from upslope, compared to the water added and drained at the middle hillslope. The changes in storage at the middle hillslope seems to be more stable, requiring less input in order for the storage to remain stable or increase (which is seen in Figure 21). At the upper hillslope, storage is not affected by water from upslope, thus solely affected by input (rainfall or snowmelt) and the water drained pr. time unit. It should be noted that the storage values at the upper hillslopes are very low, due to the low associated areas, and even small errors in the simulated values can change the direction of the loops.

7.8.2 Landslide occurrences and hysteresis

The fact that the DDD model was able to represent hysteresis lead to the investigation of whether the landslide occurrences could be associated with any particular position on the hysteretic loops, i.e. if they occurred during recharge or recession, or at the top of the curve. No similar studies are found in literature. The results indicate that there is little connection between landslide occurrences and hysteresis (see Table 18), aside from the obvious fact that most landslides occur at high levels of both storage and discharge. Following the results of section 6.3 that the majority of the landslides occur at maximum storage capacity, this leads to the assumption that the landslides are more related to storage (and precipitation) than discharge. There are, however, large uncertainties related to the results, especially regarding the uncertainty in the timing of the landslide occurrences. The distribution is no longer even. This is, however, only speculations. Secondly, seen as the landslides usually occur just a few hours following a significant rainfall event, daily resolution does not give satisfactory results, and hourly- or 3 hourly-resolution should be used. Hourly resolution of

input may allow for a better correlation between landslides and hysteresis, however only if the registration of timing of the landslide events improves.

7.9 General recommendations and future work

This study, which is the first in exploring the representation of the subsurface in the DDD model in relation to landslide occurrence and the first assessing points of the hillslope, highlighted some limitations within the spatial characters of the model. For future analysis using the DDD model there are several aspects that needs to be considered. Firstly, the model should take advantage of the distributed meteorology. General model improvements should include the percolation of water from the unsaturated to the saturated reservoir. Finally, the 2D representation of the hillslope has the potential to be used in relation to landslide occurrence, however, only if the registration of landslide events improves, starting with initial points of the landslide events. Future studies of hysteresis represented by the DDD model should include a more detailed study of the changes within storage and discharge, *dS/dt and dQ/dt,* at different levels of saturation, preferably without the influence of additional input.

8 Conclusion

In this thesis, a parameter-parsimonious rainfall-runoff model, DDD (Distance Distribution Dynamics), is used to simulate the hydrological conditions for rainfall induced landslide events. The aims were to 1) determine if the model has any capacity to predict the hydrological conditions triggering landslides and 2) investigate storage-discharge hysteresis, represented by DDD model and to see how landslides relate to hysteresis. A total of 76 landslide events have been explored by investigating the simulated storage before and during the landslide events for the entire catchment, as well as for three points of the hillslope; lower, middle and upper hillslope.

Evaluated for the entire catchment, 70 % of the landslides occurred during completely saturated conditions and more than 90 % of the events were characterized by a sharp gradient and/or a prolonged high saturation. Following this conclusion, the DDD model has capacity to predict the hydrological conditions triggering landslides. The simulation of overland flow proved to be relevant for the landslides, found for 87 % of the landslide events. The inclusion of overland flow to the saturation values gave noticeable improvements in terms of indicating the landslide events occurring during prolonged high saturation, suggesting that landslides often are triggered by additional input of rainfall. This results propose that overland flow should be considered in landslide assessments using the DDD model. The results for the hillslope showed that the storage has a distribution that varies along the hillslope and with time. The 2D representation of the hillslope has the potential to be used in landslide investigation, however, only if the registration of landslide events improves, starting with landslide initiation points.

Regarding the hysteresis, the result have demonstrated that model is able to represent the storage-discharge hysteresis observed in field and documented in the literature for a wide array of experiments, both at catchment scale and at points along the hillslope. The hysteresis is closely linked to the flow of water through the catchment, mainly introduced by different unit hydrographs, saturations and moisture input. However, hysteresis are complex processes and there are still many aspects which are not known, suggesting that further exploration of the changes in storage and discharge, *dS/dt and dQ/dt,* would be useful. In terms of relating the landslide occurrences with the hysteretic loops, the results indicate that there are too large uncertainties related to the timing of the landslides. In addition, hourly precipitation would most likely allow for a better correlation between landslide occurrence and hysteresis.

9 References

ALLEN, D. M., WHITFIELD, P. H. & WERNER, A. 2010. Groundwater level responses in temperate mountainous terrain: regime classification, and linkages to climate and streamflow. *Hydrological Processes,* 24**,** 3392-3412.

ANDERSON, M. G. & BURT, T. P. 1977. Automatic monitoring of soil moisture conditions in a hillslope spur and hollow. *Journal of Hydrology,* 33**,** 27-36.

BERGSTRÖM, S. 1995. The HBV Model. *In:* SINGH, V. J. (ed.) *Computer Models of Watershed Hydrology.* Colorado, United States of America: Water Resources Publications.

BEVEN, K. 2006. Searching for the Holy Grail of scientific hydrology: Qt=(S, R, Δt)A as closure. *Hydrol. Earth Syst. Sci.,* 10**,** 609-618.

BEVEN, K. & GERMANN, P. 1982. Macropores and water flow in soils. *Water Resources Research,* 18**,** 1311-1325.

BOJE, S. N. 2011. Modeling of soil water conditions as an indicator for predicting landslides in Norway. MSc/MA Dissertation. University of Oslo, Dep. of Geoscience.

BOJE, S. N., COLLEUILLE, H., CEPEDA, J. & DEVOLI, G. 2014. Landslide thresholds at regional scale for the early warning system in Norway. Proceedings 3rd World Landslide Forum 3, 2-6 June 2014, Beijing.

CAMPORESE, M., PENNA, D., BORGA, M. & PANICONI, C. 2014. A field and modeling study of nonlinear storage-discharge dynamics for an Alpine headwater catchment. *Water Resources Research,* 50**,** 806-822.

COLLEUILLE, H., BELDRING, S. & HAUGEN, L. E. 2009. From monitoring to simulation and forecasting of soil frost [in Norwegian]. *Frost i Jord 2009.* 110: 7-17: The Norwegian Public Roads Administration. Oslo.

DAVIES, J. A. C. & BEVEN, K. 2015. Hysteresis and scale in catchment storage, flow and transport. *Hydrological Processes,* 29**,** 3604-3615.

DETTY, J. M. & MCGUIRE, K. J. 2010. Topographic controls on shallow groundwater dynamics: implications of hydrologic connectivity between hillslopes and riparian zones in a till mantled catchment. *Hydrological Processes,* 24**,** 2222-2236.

DEVOLI, G., KLEIVANE, I., SUND, M., ORTHE, N.-K., EKKER, R., JOHNSEN, R. & COLLEUILLE, H. 2014. Landslide early warning system and web tool for real-time scenarios and for distribution of warning messages in Norway. Proceeding IAEG 2014, 15-19 September, Torino, Italy.

DYRRDAL, A., ISAKSEN, K., HYGEN, H. & MEYER, N. 2012. Changes in meteorological variables that can trigger natural hazards in Norway. *Climate Research,* 55**,** 153-165.

EBEL, B. A., LOAGUE, K. & BORJA, R. I. 2010. The impacts of hysteresis on variably saturated hydrologic response and slope failure. *Environmental Earth Sciences,* 61**,** 1215-1225.

ENGEN-SKAUGEN, T., BENESTAD, R. & ROALD, L. A. 2007. Empirically downscaling of runoff in Norway; Is it feasible? : Norwegian Meteorological Institute. Report no. 15-2007; Oslo; 54 pp.

FANNIN, R. J. & JAAKKOLA, J. 1999. Hydrological response of hillslope soils above a debris-slide headscarp. *Canadian Geotechnical Journal,* 36**,** 1111-1122.

FERGUS, T., HØYDAL, Ø. A., JOHNSRUD, T.-E., SANDERSEN, F. & SCHANCHE, S. 2011. Skogsveger og skredfare - veileder. *Landbruks- og matdepartementet*.

FUHRMANN, C. M., KONRAD, C. E. & BAND, L. E. 2008. Climatological Perspectives on the Rainfall Characteristics Associated with Landslides in Western North Carolina. *Physical Geography,* 29**,** 289-305.

Geological Survey of Norway. 2016. The national dataase of soils of Norway. Retrieved 02.05.2016. Available at: www.ngu.no/kart/losmasse

HABIB, E., KRAJEWSKI, W. & KRUGER, A. 2001. Sampling Errors of Tipping-Bucket Rain Gauge Measurements. *Journal of Hydrologic Engineering,* 6**,** 159-166.

HAUGHT, D. R. W. & VAN MEERVELD, H. J. 2011. Spatial variation in transient water table responses: differences between an upper and lower hillslope zone. *Hydrological Processes,* 25**,** 3866-3877.

HENNRICH, K. & CROZIER, M. J. 2004. A hillslope hydrology approach for catchment-scale slope stability analysis. *Earth Surface Processes and Landforms,* 29**,** 599-610.

HUNGR, O., LEROUEIL, S. & PICARELLI, L. 2014. The Varnes classification of landslide types, an update. *Landslides,* 11**,** 167-194.

JAEDICKE, C. & KLEVEN, A. 2008. Long-term precipitation and slide activity in south-eastern Norway, autumn 2000. *Hydrological Processes,* 22**,** 495-505.

KENDALL, K. A., SHANLEY, J. B. & MCDONNELL, J. J. 1999. A hydrometric and geochemical approach to test the transmissivity feedback hypothesis during snowmelt. *Journal of Hydrology,* 219**,** 188-205.

KIRCHNER, J. W. 2009. Catchments as simple dynamical systems: Catchment characterization, rainfall-runoff modeling, and doing hydrology backward. *Water Resources Research,* 45.

KIRKBY, M. 1988. Hillslope runoff processes and models. *Journal of Hydrology,* 100**,** 315-340.

LEHMANN, P., HINZ, C., MCGRATH, G., TROMP-VAN MEERVELD, H. J. & MCDONNELL, J. J. 2007. Rainfall threshold for hillslope outflow: an emergent property of flow pathway connectivity. *Hydrol. Earth Syst. Sci.,* 11**,** 1047-1063.

LIED, K. 2014. Innledning og historikk. *SKRED: skredfare og sikringstiltak - pratiske erfaringer og teoretiske prinsipper.* NGI and Universitetsforlaget.

MCGLYNN, B. L. & MCDONNELL, J. J. 2003. Quantifying the relative contributions of riparian and hillslope zones to catchment runoff. *Water Resources Research,* 39**,** n/a-n/a.

MYRABØ, S. 1997. Temporal and spatial scale of response area and groundwater variation in Till. *Hydrological Processes,* 11**,** 1861-1880.

NASH, J. E. & SUTCLIFFE, J. V. 1970. River flow forecasting through conceptual models part I — A discussion of principles. *Journal of Hydrology,* 10**,** 282-290.

NGI 1977. Prøveprosjekt for vedrørende kartlegging av skred. 284.

NGI 1979. Skredfarevurdering. NGI Årsberetning for 1978 og 1979. Rapport skrevet for Norges byggforskningsinstitutt, NBI byggforskserie som Byggedetaljer. A511.202.

NORBIATO, D. & BORGA, M. 2008. Analysis of hysteretic behaviour of a hillslope-storage kinematic wave model for subsurface flow. *Advances in Water Resources,* 31**,** 118-131.

NVE 2008. Faktaark: Jordskred og flomskred. *Norwegian Water Resources and Energy Directorate,* 8 pp.

NVE 2011a. Plan for skredfarekartlegging. Status og prioriteringer innen oversiktskartlegging og detaljert skredfarekartlegging i NVEs regi. Oslo, Norway: The Norwegian Water Resources and Energy Directorate. NVE Report no. 14 /2011; Oslo.

NVE 2011b. Plan for skredfarekartlegging - Delrapport jordskred og flomskred.: Norwegian Water Resources and Energy Directorate. NVE Report no. 16/2011; Oslo.

NVE 2012. Registrering av skredhendelser: status og fremtidige behov: Internt notat. Oslo: The Norwegian Water Resources and Energy Directorate

NVE 2014a. Preliminary regionalization and susceptibility analysis for landslide early warning purposes in Norway. The Norwegian Water Resources and Energy Directorate. Report no. 37-2014; Oslo; 52pp.

NVE 2014b. Jord- og sørpeskred i Sør-Norge, mai 2013. . The Norwegian Water Resources and Energy Directorate. NVE Report no. 52/2014; Oslo; 38pp.

NVE 2014c. Regional varsling av jordskredfare: analyse av historiske jordskred, flomskred og sørpeskred i Gudbrandsdalen og Ottadalen. The Norwegian Water Resources and Energy Directorate . NVE report no. 44/2014; Oslo; 63pp.

NVE 2015. The national database of avalanches and rock falls of Norway. Assessed 15.10.2015. Available at: www.skrednett.no

PATIL, S. & STIEGLITZ, M. 2014. Modelling daily streamflow at ungauged catchments: what information is necessary? *Hydrological Processes,* 28**,** 1159-1169.

PENNA, D., TROMP-VAN MEERVELD, H. J., GOBBI, A., BORGA, M. & DALLA FONTANA, G. 2011. The influence of soil moisture on threshold runoff generation processes in an alpine headwater catchment. *Hydrology and Earth System Sciences,* 15**,** 689-702.

QUINN, P., BEVEN, K., CHEVALLIER, P. & PLANCHON, O. 1991. The prediction of hillslope flow paths for distributed hydrological modelling using digital terrain models. *Hydrological Processes,* 5**,** 59-79.

RADATZ, T. F., THOMPSON, A. M. & MADISON, F. W. 2013. Soil moisture and rainfall intensity thresholds for runoff generation in southwestern Wisconsin agricultural watersheds. *Hydrological Processes,* 27**,** 3521-3534.

SeNorge.no. 2016. Weather, water, snow and climate in Norway. Retrieved 12.03.2016. Available from: www.senorge.no

SENEVIRATNE, S. I., NICHOLLS, N., EASTERLING, D., C.M., G., KANAE, S., KOSSIN, J., LUO, Y., MARENGO, J., MCINNES, K., RAHIMI, M., REICHSTEIN, M., SORTEBERG, A., VERA, C. & ZHANG, X. 2012. Changes in climate extremes and their impacts on the natural physical environment. In: Managing the Risks of Extreme Events and Disasters to Advance Climate Change Adaptation *In:* C.B. FIELD, V. B., T.F. STOCKER, D. QIN, D.J. DOKKEN, K.L EBI, M.D. MAESTRANDREA, K.J. MACH, G.-K. PLATTNER, S.K. ALLEN, M. TIGNOR, AND O.M. MIDGLEY (ed.) *A Special Report of Working Groups I and II of the Intergovernmental Panel on Climate Change (IPCC).* Cambridge University Press, Cambridge, UK, and New York, NY, USA.

SIDLE, R. C., OCHIAI, H., SIDLE, R. C. & OCHIAI, H. 2013a. Introduction and Overview of Landslide Problems. *Landslides: Processes, Prediction, and Land Use.* American Geophysical Union.

SIDLE, R. C., OCHIAI, H., SIDLE, R. C. & OCHIAI, H. 2013b. Characteristics of Various Types of Landslides. *Landslides: Processes, Prediction, and Land Use.* American Geophysical Union.

SIDLE, R. C., OCHIAI, H., SIDLE, R. C. & OCHIAI, H. 2013c. Natural Factors Influencing Landslides. *Landslides: Processes, Prediction, and Land Use.* American Geophysical Union.

SKAUGEN, T. & MENGISTU, Z. 2015. Estimating catchment scale groundwater dynamics from recession analysis - enhanced constraining if hydrological models *Hydrol. Earth Syst. Sci.,* 19**,** 43.

SKAUGEN, T. & ONOF, C. 2014. A rainfall-runoff model parameterized from GIS and runoff data. *Hydrological Processes,* 28**,** 4529-4542.

SKAUGEN, T. & RANDEN, F. 2013. Modeling the spatial distribution of snow water equivalent, taking into account changes in snow covered area. *Annals of Glaciology***,** 54(62).

SKAUGEN, T. & WELTZIEN, I. 2015. Implementing a calibration free procedure for the spatial distribution of snow water equivalent in a parsimonious rainfall runoff model. In prep.

SLOAN, W. T. 2000. A physics-based function for modeling transient groundwater discharge at the watershed scale. *Water Resources Research,* 36**,** 225-241.

SOETART, K. & PETZHOLDT, T. 2010. Inverse modelling, sensitivity and Monte Carlo analysis in R using package FME. *Journal of Statistical Software,* 33**,** 1-28.

SPENCE, C. 2010. A Paradigm Shift in Hydrology: Storage Thresholds Across Scales Influence Catchment Runoff Generation. *Geography Compass,* 4**,** 819-833.

STALSBERG, K., FISCHER, L., RUBENSDOTTER, L. & SLETTEN, K. 2012. Approaches to shallow landslide and debris flow - assessments in Norway. . *Landslides and Engineered Slopes: Protecting Society through Improved Understanding - Eberhardt et al. (eds) © 2012,* Taylor & Francis Group, London, ISBN 978-0-415-62123-6.

SÆLTHUN, N. R. 1996. The 'Nordic' HBV Model. Description and Documentation of the Model Version. Developed for the Project Climate Change and Energy Production. *The Norwegian Water Resources and Energy Directorate. ,* Publication no. 7 - 1996: Oslo; 26 pp.

VARNES, D. 1978. Slope movement types and processes. In: Schuster RL, Krizek RJ (eds)Landslides, analysis and control, special report 176:. *Transportation research board, National Academy of Science***,** 11-13.

VEIDIREKTORATED 2014. Flom- og sørpeskred. Veiledning. Håndboka V139. www.vegvesenet.no.

VISINTIN, A. 2006. Quasilinear parabolic P.D.E.s with discontinuous hysteresis. *Annali di Matematica Pura ed Applicata,* 185**,** 487-519.

VORMOOR, K., LAWRENCE, D., HEISTERMANN, M. & BRONSTERT, A. 2015. Climate change impacts on the seasonality and generation processes of floods – projections and uncertainties for catchments with mixed snowmelt/rainfall regimes. *Hydrol. Earth Syst. Sci.,* 19**,** 913-931.

WEILL, S., ALTISSIMO, M., CASSIANI, G., DEIANA, R., MARANI, M. & PUTTI, M. 2013. Saturated area dynamics and streamflow generation from coupled surface–subsurface simulations and field observations. *Advances in Water Resources,* 59**,** 196-208.

WELTZIEN, I. 2015. Parsimonious snow modelling for application in hydrological models Calibration free methods for estimating spatial distribution and melt of snow. MSc/MA Dissertation. University of Oslo, Dep. of Geoscience.

WIECZOREK, G. & GLADE, T. 2005. Climatic factors influencing occurrence of debris flows. *Debris-flow Hazards and Related Phenomena.* Springer Berlin Heidelberg.

WU, L. Z., HUANG, R. Q., XU, Q., ZHANG, L. M. & LI, H. L. 2015. Analysis of physical testing of rainfall-induced soil slope failures. *Environmental Earth Sciences,* 73**,** 8519-8531.

XU, Q., LU, Y., YIN, H. & LI, Z. 2010. Shakedown analysis of a slope with cyclic groundwater level. *International Journal for Numerical and Analytical Methods in Geomechanics,* 34**,** 517-531.

ZEHE, E., ELSENBEER, H., LINDENMAIER, F., SCHULZ, K. & BLÖSCHL, G. 2007. Patterns of predictability in hydrological threshold systems. *Water Resources Research,* 43**,** n/a-n/a.

ZEHE, E., GRAEFF, T., MORGNER, M., BAUER, A. & BRONSTERT, A. 2010. Plot and field scale soil moisture dynamics and subsurface wetness control on runoff generation in a headwater in the Ore Mountains. *Hydrol. Earth Syst. Sci.,* 14**,** 873-889.

ZHOU, Y., DONG, D., LIU, J. & LI, W. 2013. Upgrading a regional groundwater level monitoring network for Beijing Plain, China. *Geoscience Frontiers,* 4**,** 127-138.

ZUECCO, G., PENNA, D., BORGA, M. & VAN MEERVELD, H. J. 2015. A versatile index to characterize hysteresis between hydrological variables at the runoff event timescale. *Hydrological Processes***,** n/a-n/a.

Appendix I – Landslide data

Table 19) Information of the landslide events.

Catchment	Date of landslide occurrence	Number of landslides	Type of landslide	Storage [% of *M*]		Storage including overland flow [% of *M*]		Temporal dynamics of saturation	Hysteresis	Position of landslide occurrence
				D-1_landslide	*D_Landslide*	*D-1_landslide*	*D_Landslide*			
2.614	30.04.00	1	Debris flow	73.8	93.4	73.8	93.4	Sharp gradient	Anti-clockwise	Recharge
	10.06.11	4	Debris flow/ Unspecified	100	100	173.2	186.7	Prolonged high sat.	Anti-clockwise	Top
	26.07.11	1	Debris flow	85.3	78.4	85.3	78.4	Sharp gradient	Linear	Recession
	22.05.13	3	Debris avalanche	100	100	155.9	172.1	Both	Anti-clockwise	Top
	23.05.13	3	Debris flow/ avalanche	100	100	172.1	150.5	Both	Anti-clockwise	Recession
3.22	16.01.08	1	Debris avalanche	100	100	122.8	142.5	Sharp gradient	Complex	Top
18.1	26.08.11	1	Unspecified	50	90.4	50	90.4	Sharp gradient	Almost linear	Top
22.4	27.04.03	1	Unspecified	76.7	81.5	76.7	81.5	Neither	Complex	Recharge
	29.08.06	1	Unspecified	100	95.3	152.9	136.7	Sharp gradient	Complex	Recession
	30.12.13	1	Unspecified	93.3	100	178.7	231.3	Prolonged high sat.	Complex	Top
	04.10.04	1	Unspecified	89.2	100	89.2	174.6	Sharp gradient	Anti-clockwise	Recharge
	25.04.06	2	Unspecified	72.9	84.4	72.9	84.4	Neither	Anti-clockwise	Recharge
	02.01.14	1	Unspecified	100	100	167.8	178.2	Prolonged high sat.	Clockwise	Recharge
	08.04.14	1	Unspecified	100	100	108.8	115.3	Sharp gradient	Anti-clockwise	Top
41.1	17.04.10	1	Unspecified	70.6	84.4	70.6	84.4	Sharp gradient	Clockwise	Recharge
	22.03.11	3	Unspecified	100	100	116.3	120.3	Sharp gradient	Clockwise	Recharge

Table 22 continues

41.1	06.04.11	2	Unspecified	100	100	123.7	134.5	Both	Complex	Top
48.1	15.08.00	1	Unspecified	100	100	135.8	120.9	Neither	Clockwise	Recession
	15.07.14	1	Unspecified	100	100	122.6	118.1	Prolonged high sat.	Anti-clockwise	Recession
	26.10.14	1	Unspecified	100	100	122.5	194.7	Both	Anti-clockwise	Recharge
	28.10.14	2	Debris avalanche	100	100	248.2	284.5	Both	Anti-clockwise	Top
62.5	23.04.96	1	Debris flow	100	100	132.2	128.9	Both	Anti-clockwise	Recession
	30.10.01	2	Unspecified	100	100	109.9	117.5	Sharp gradient	Anti-clockwise	Recharge
	13.05.02	1	Unspecified	93.1	90.5	121.5	110.9	Prolonged high sat.	Complex	Recession
	15.12.04	1	Unspecified	100	100	138.1	124	Sharp gradient	Clockwise	Recession
	12.01.05	1	Unspecified	100	100	109.1	121.2	Both	Anti-clockwise	Top
	14.09.05	1	Debris flow	100	100	150.7	158.7	Sharp gradient	Anti-clockwise	Top
	14.11.05	1	Debris flow	100	100	129	169.4	Prolonged high sat.	Anti-clockwise	Top
	28.10.07	1	Unspecified	76.8	100	76.8	133.8	Sharp gradient	Complex	Complex
	14.09.10	1	Unspecified	78.2	100	78.2	106.1	Sharp gradient	Anti-clockwise	Recharge
72.5	15.06.95	1	Unspecified	100	100	110.9	109.4	Prolonged high sat.	Anti-clockwise	Recession
	08.06.96	1	Debris flow	100	100	114.7	129.6	Sharp gradient	Anti-clockwise	Top
	14.09.05	2	Debris flow	89.8	100	89.8	104.9	Prolonged high sat.	Linear	Top
77.3	22.07.10	1	Unspecified	100	89	167.9	132	Sharp gradient	Anti-clockwise	Recession
82.4	17.01.03	1	Unspecified	100	100	172.7	205.5	Both	Anti-clockwise	Top
	06.09.05	1	Unspecified	80.1	73.8	80.1	73.8	Neither	Anti-clockwise	Recharge
	14.11.05	2	Unspecified	100	100	183.1	210.6	Prolonged high sat.	Anti-clockwise	Top
	25.04.06	1	Unspecified	82.6	92	82.6	92	Sharp gradient	Linear	Recharge
	26.04.06	1	Unspecified	92	100	92	105.9	Sharp gradient	Linear	Top
	21.03.14	1	Unspecified	100	90.7	212.3	146.4	Sharp gradient	Anti-clockwise	Recession
	27.10.14	1	Unspecified	100	100	153.8	201.3	Both	Anti-clockwise	Recharge

Table 22 continues

83.2	27.10.95	1	Unspecified	100	100	170.8	164.7	Prolonged high sat.	Anti-clockwise	Recession
	29.06.99	1	Unspecified	100	100	112.7	113.9	Prolonged high sat.	Anti-clockwise	Recharge
	14.11.05	1	Unspecified	100	100	115.3	141.4	Prolonged high sat.	Anti-clockwise	Top
	29.11.11	1	Unspecified	100	100	105.3	129.3	Prolonged high sat.	Anti-clockwise	Top
	05.09.12	1	Unspecified	100	100	102.5	102.8	Neither	Clockwise	Recession
	16.11.13	1	Debris avalanche	96.1	100	96.1	110.7	Sharp gradient	Anti-clockwise	Top
88.4	13.09.97	1	Unspecified	91.5	91.7	98.9	98.1	Prolonged high sat.	Complex	Complex
	14.08.03	1	Unspecified	100	100	115.9	123.9	Prolonged high sat.	Complex	Recharge
	28.10.14	1	Unspecified	100	100	104.6	114.8	Neither	Anti-clockwise	Top
97.1	25.09.03	1	Unspecified	100	100	129	194.6	Both	Anti-clockwise	Top
	22.03.11	1	Unspecified	100	94.5	154.6	121.8	Sharp gradient	Clockwise	Recession
	26.12.11	2	Unspecified	100	100	106.8	159.7	Sharp gradient	Anti-clockwise	Top
	16.11.13	1	Unspecified	100	100	149.5	140.4	Sharp gradient	Complex	Recession
109.9	08.06.97	2	Debris flow/ avalanche	100	100	129.1	140.7	Sharp gradient	Anti-clockwise	Complex
	11.08.05	1	Unspecified	100	100	115.2	123.7	Sharp gradient	Complex	Complex
	04.06.13	2	Debris avalanche & unspecified	83.1	69.1	117.4	91.3	Prolonged high sat.	Complex	Recession
109.42	16.08.03	1	Debris avalanche	100	93.4	165.7	141.2	Both	Anti-clockwise	Recession
	05.09.06	1	Unspecified	84.7	93.5	84.7	93.5	Sharp gradient	Linear	Top
122.9	28.07.93	1	Unspecified	100	100	112.1	118.6	Sharp gradient	Clockwise	Recession
	24.09.04	6	Unspecified	100	100	144.5	149.2	Both	Complex	Top
	27.09.04	2	Unspecified	83.9	98.5	103.7	112.2	Neither	Complex	Recession
	04.05.06	1	Unspecified	100	100	101.9	122.8	Sharp gradient	Anti-clockwise	Recharge
	11.04.11	1	Debris flow	90.4	100	90.4	134.4	Sharp gradient	Anti-clockwise	Top

Table 22 continues										
122.9	12.04.11	1	Unspecified	100	89.2	134.4	108.2	Sharp gradient	Anti-clockwise	Recession
	09.06.13	4	Debris avalanche	95.1	95.9	96.6	96.6	Sharp gradient	Clockwise	Recession
	14.08.13	1	Unspecified	100	86.9	107	91.3	Sharp gradient	Clockwise	Recession
	22.06.14	2	Debris avalanche & unspecified	100	100	117.6	120.2	Sharp gradient	Clockwise	Recession
	23.06.14	1	Debris avalanche	100	88.3	120.2	100.1	Sharp gradient	Clockwise	Recession
122.11	05.05.00	1	Unspecified	100	100	124.5	119.6	Sharp gradient	Complex	Recharge
	19.06.10	1	Unspecified	100	100	157	135	Sharp gradient	Clockwise	Recession
122.17	17.03.90	1	Unspecified	47.3	93.7	47.3	93.7	Sharp gradient	Complex	Recharge
	08.05.95	1	Unspecified	100	100	150.6	144.4	Both	Complex	Recession
	12.05.97	1	Unspecified	100	100	140.2	150.2	Both	Anti-clockwise	Recharge
	21.04.00	1	Unspecified	100	100	135	139.5	Both	Anti-clockwise	Complex
	23.04.00	1	Unspecified	100	100	146.3	146.2	Both	Complex	Complex

Appendix II – Parameters of the DDD model

*Table 20) Parameters of the DDD model with comment and method of estimation. Model parameters calibrated are marked in bold. In the method of estimation, * indicates parameters obtained through experience in calibrating DDD for gauged catchments in Norway. These parameters are set at a fixed value, that are within the recommended range for the HBV model (Sælthun, 1996). The GIS analyses are carried out using the national 25 m x 25 m DEM* (www.statkart.no).

Parameter	***Comment***	***Method of estimation***	***Value***	***Ref***
Hypsographic curve	11 values describing the quantiles 0 to 100.	GIS		
Ws [%]	Max liquid water content in snow	Calibrated	5	
Hfelt	Mean elevation of catchment	GIS		
Sc	Correction factor for precipitation as snow	Calibrated		
Pc	Correction factor for precipitation	Calibrated		
TX [°C]	Threshold temperature rain/snow	Calibrated		
TS[°C]	Threshold temperature melting/ freezing	Calibrated		
CX [mm°C^{-1}day^{-1}]	Degree-day factor for melting snow	Calibrated		
Cglac [mm°C^{-1}day^{-1}]	Degree-day factor for melting glacier Ice	*	1.5 x θ_{CX}	Sælthun (1996)
CFR [mm°C^{-1}day^{-1}]	Degree-day factor for freezing	*	0.02	Sælthun (1996)
Area [m2]	Catchment area	GIS		
maxLbog [m]	Max distance distribution of bogs	GIS		
midLbog [m]	Mean distance distribution of bogs	GIS		
Bogfrac	Fraction of bogs in catchment	GIS		
Zsoil	Areal fraction of zero distance to the river network for soils	GIS		
Zbog	Areal fraction of zero distance to the river network for bogs	GIS		
NOL	Number of storage levels	Std. value	5	Skaugen and Onof (2014)
Cx	Coefficient of variation for spatial distribution of snow	Calibrated		

$\boldsymbol{\alpha_0}$	Scale parameter of unit precipitation	Estimated from observed spatial variability of precipitation		
D	Decorrelation length of spatial precipitaiton	Estimated from observed spatial variability of precipitation		
Cea [mm°C^{-1}day^{-1}]	Degree day factor for evapotranspiration	Calibrated		
R	Ratio defining field capacity	Std. value	0.3	Skaugen and Onof (2014)
δ	Shape parameter of gamma distributed recession characteristic λ	Estimated from recession		
β	Scale parameter of gamma distributed recession characteristic λ	Estimated from recession		
V_r [ms-1]	Mean celerity in river	Calibrated		
m_{Rd} [m]	Mean distance distribution to the river network	GIS		
s_{Rd} [m]	Standard deviation of distances distribution of the river network	GIS		
R_{dmax}	Max of distance distribution in river network	GIS		
M [mm]	Max subsurface water reservoir/Mean of subsurface water reservoir	Estimated from recession and MAD		
$\bar{\boldsymbol{d}}$ [m]	Mean of distance distribution for hillslope	GIS		
d_{max} [m]	Max of distance distribution for hillslope	GIS		
Glacfrac	Fraction of bogs in catchment	GIS		
m_{Gl} [m]	Mean of distance distribution for glaciers	GIS		
s_{GL} [m]	Standard deviation of distance distribution for glaciers	GIS		
Areal fraction of glaciers in elevation zones	Ten values	GIS		

Appendix III – Temporal dynamics of saturation

Temporal dynamics of saturation (given in % of M) for all landslide events with the number of days on the x-axis and storage on y-axis. The day of the landslide event are indicated (day 21).

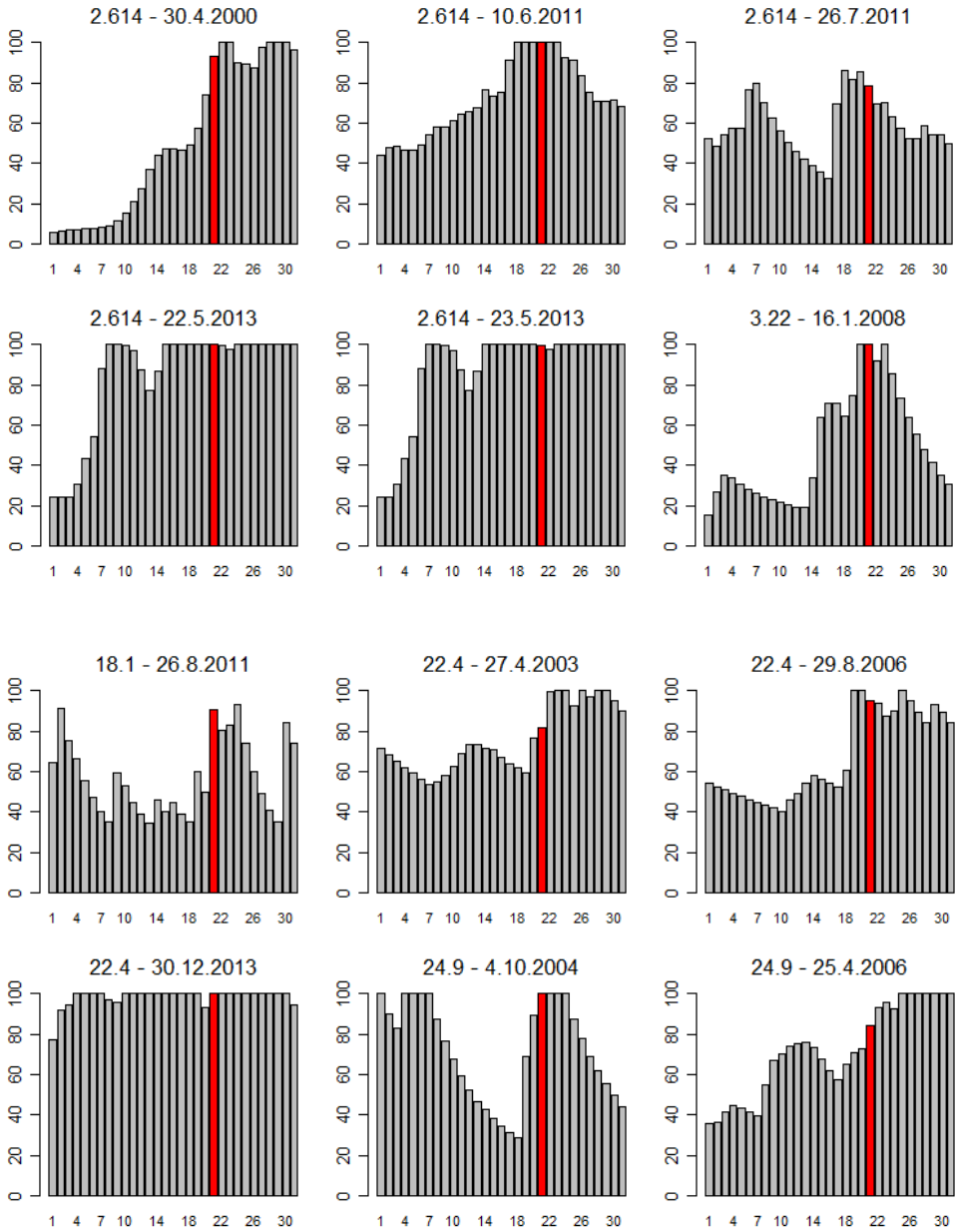

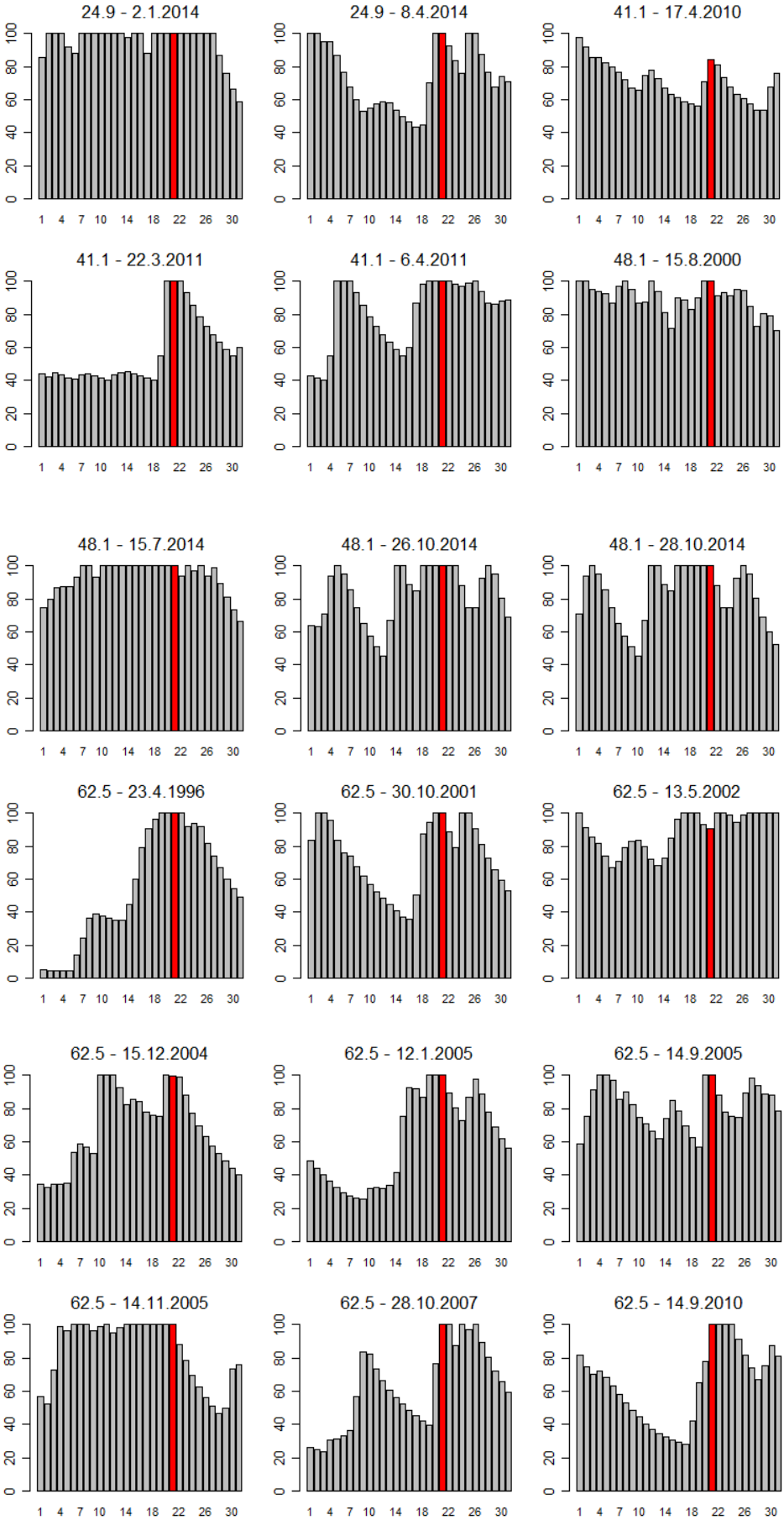
24.9 - 2.1.2014
24.9 - 8.4.2014
41.1 - 17.4.2010
41.1 - 22.3.2011
41.1 - 6.4.2011
48.1 - 15.8.2000
48.1 - 15.7.2014
48.1 - 26.10.2014
48.1 - 28.10.2014
62.5 - 23.4.1996
62.5 - 30.10.2001
62.5 - 13.5.2002
62.5 - 15.12.2004
62.5 - 12.1.2005
62.5 - 14.9.2005
62.5 - 14.11.2005
62.5 - 28.10.2007
62.5 - 14.9.2010
0 20 40 60 80 100
1 4 7 10 14 18 22 26 30

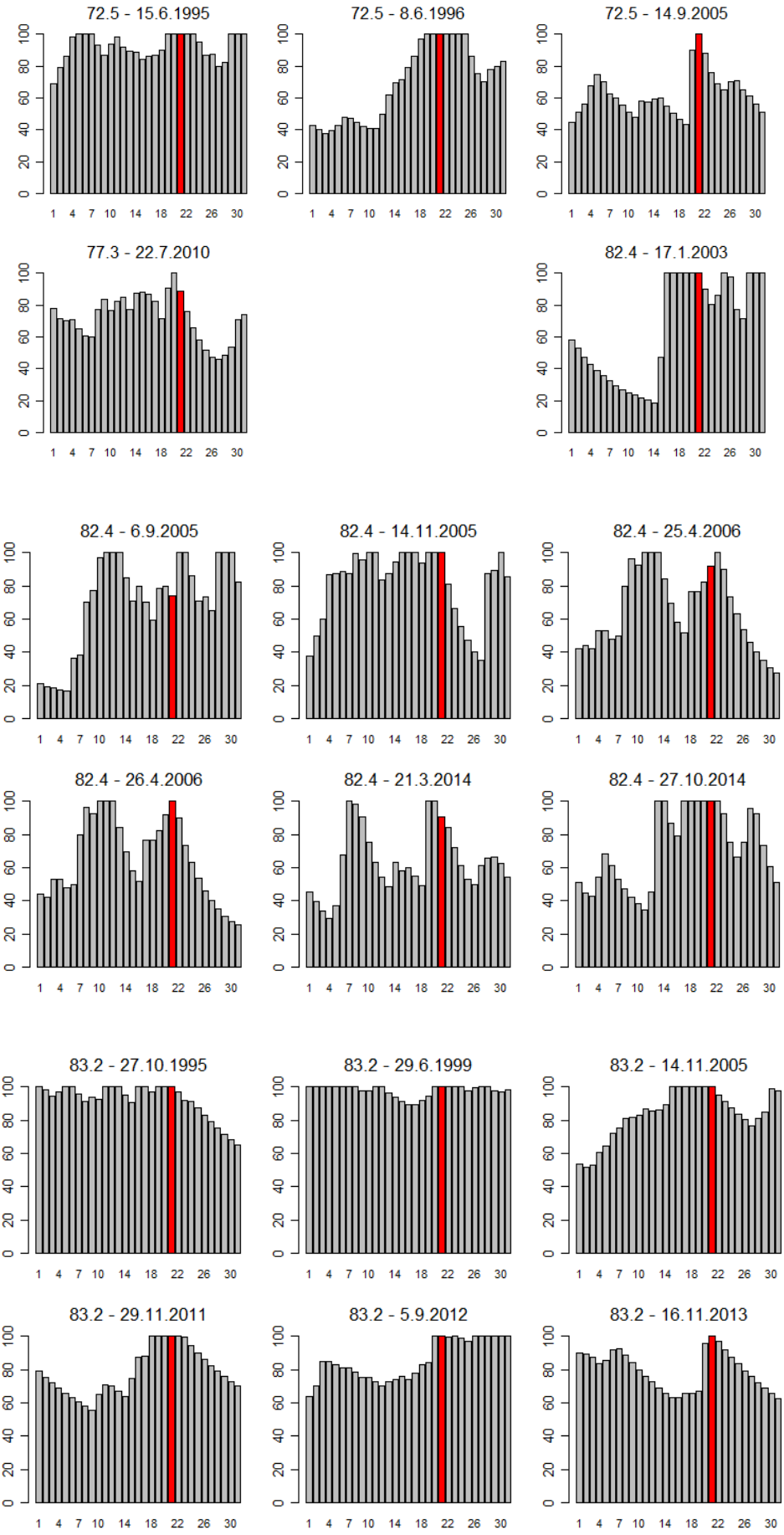
72.5 - 15.6.1995
72.5 - 8.6.1996
72.5 - 14.9.2005
77.3 - 22.7.2010
82.4 - 17.1.2003
82.4 - 6.9.2005
82.4 - 14.11.2005
82.4 - 25.4.2006
82.4 - 26.4.2006
82.4 - 21.3.2014
82.4 - 27.10.2014
83.2 - 27.10.1995
83.2 - 29.6.1999
83.2 - 14.11.2005
83.2 - 29.11.2011
83.2 - 5.9.2012
83.2 - 16.11.2013

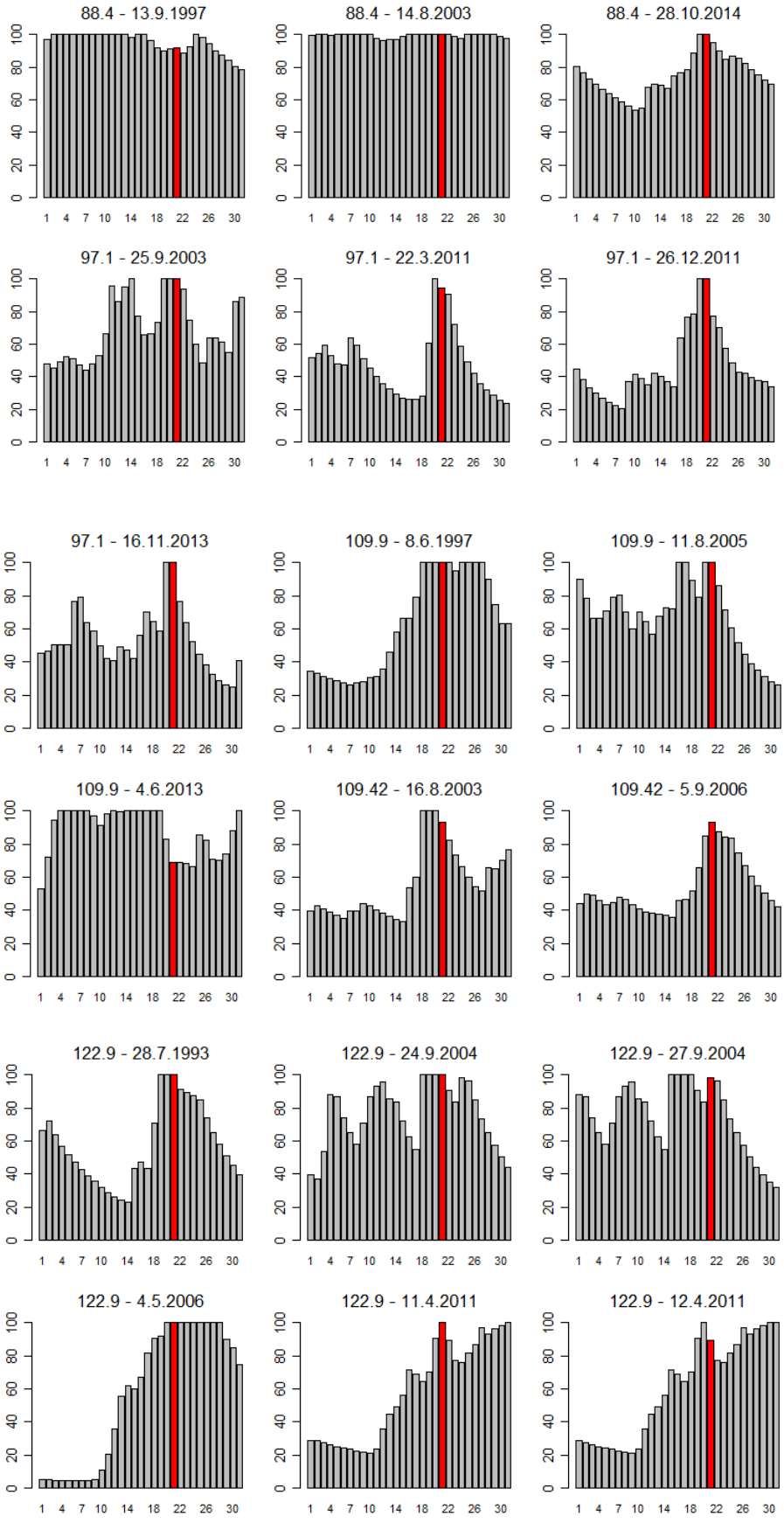
88.4 - 13.9.1997
88.4 - 14.8.2003
88.4 - 28.10.2014
97.1 - 25.9.2003
97.1 - 22.3.2011
97.1 - 26.12.2011
97.1 - 16.11.2013
109.9 - 8.6.1997
109.9 - 11.8.2005
109.9 - 4.6.2013
109.42 - 16.8.2003
109.42 - 5.9.2006
122.9 - 28.7.1993
122.9 - 24.9.2004
122.9 - 27.9.2004
122.9 - 4.5.2006
122.9 - 11.4.2011
122.9 - 12.4.2011
0 20 40 60 80 100
1 4 7 10 14 18 22 26 30

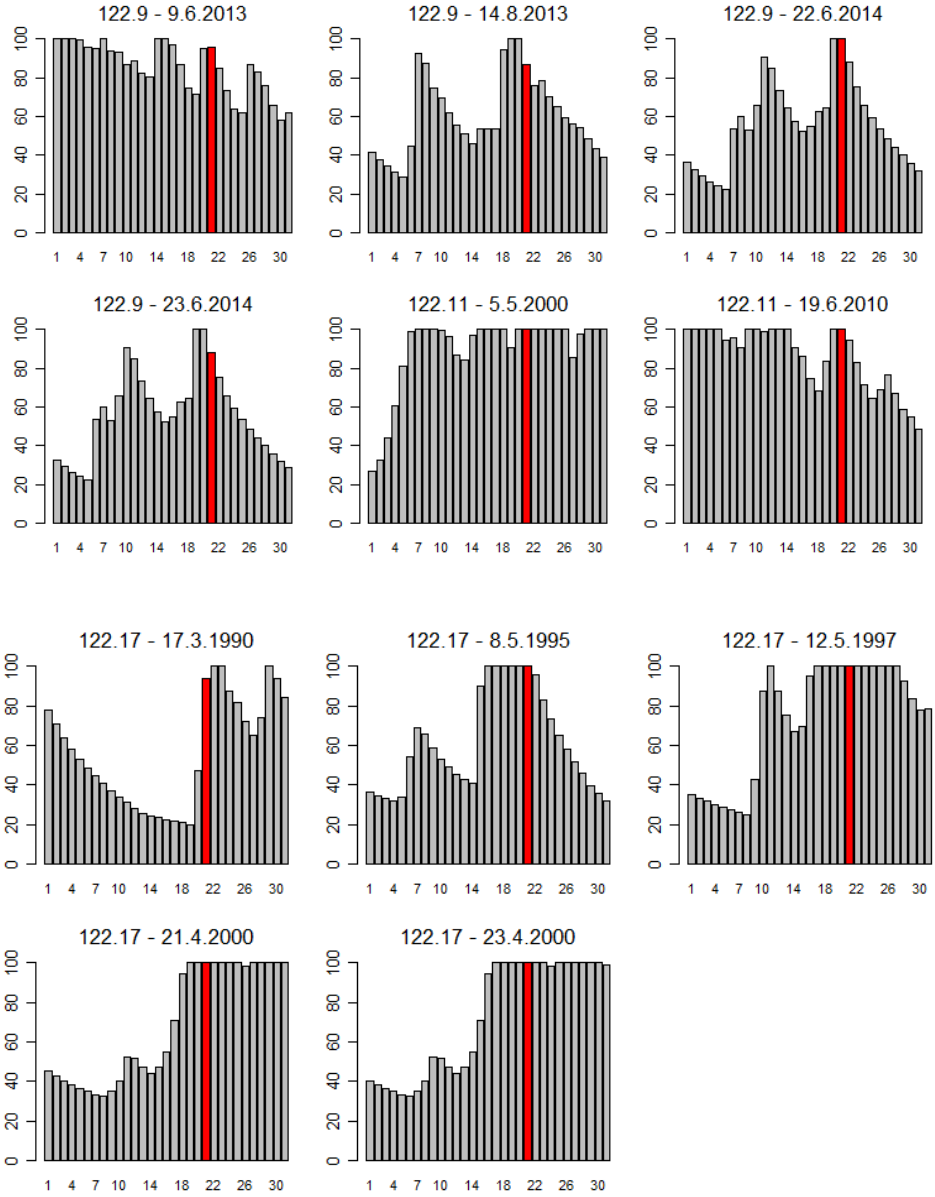
122.9 - 9.6.2013
122.9 - 14.8.2013
122.9 - 22.6.2014
122.9 - 23.6.2014
122.11 - 5.5.2000
122.11 - 19.6.2010
122.17 - 17.3.1990
122.17 - 8.5.1995
122.17 - 12.5.1997
122.17 - 21.4.2000
122.17 - 23.4.2000
0 20 40 60 80 100
1 4 7 10 14 18 22 26 30

Appendix IV – Temporal dynamics of saturation including overland flow

Temporal dynamics of saturation including overland flow (given in % of M) for all landslide events with the number of days on the x-axis and storage on y-axis. The day of the landslide event are indicated (day 21). The black horizontal line indicates maximum storage capacity (S=M).

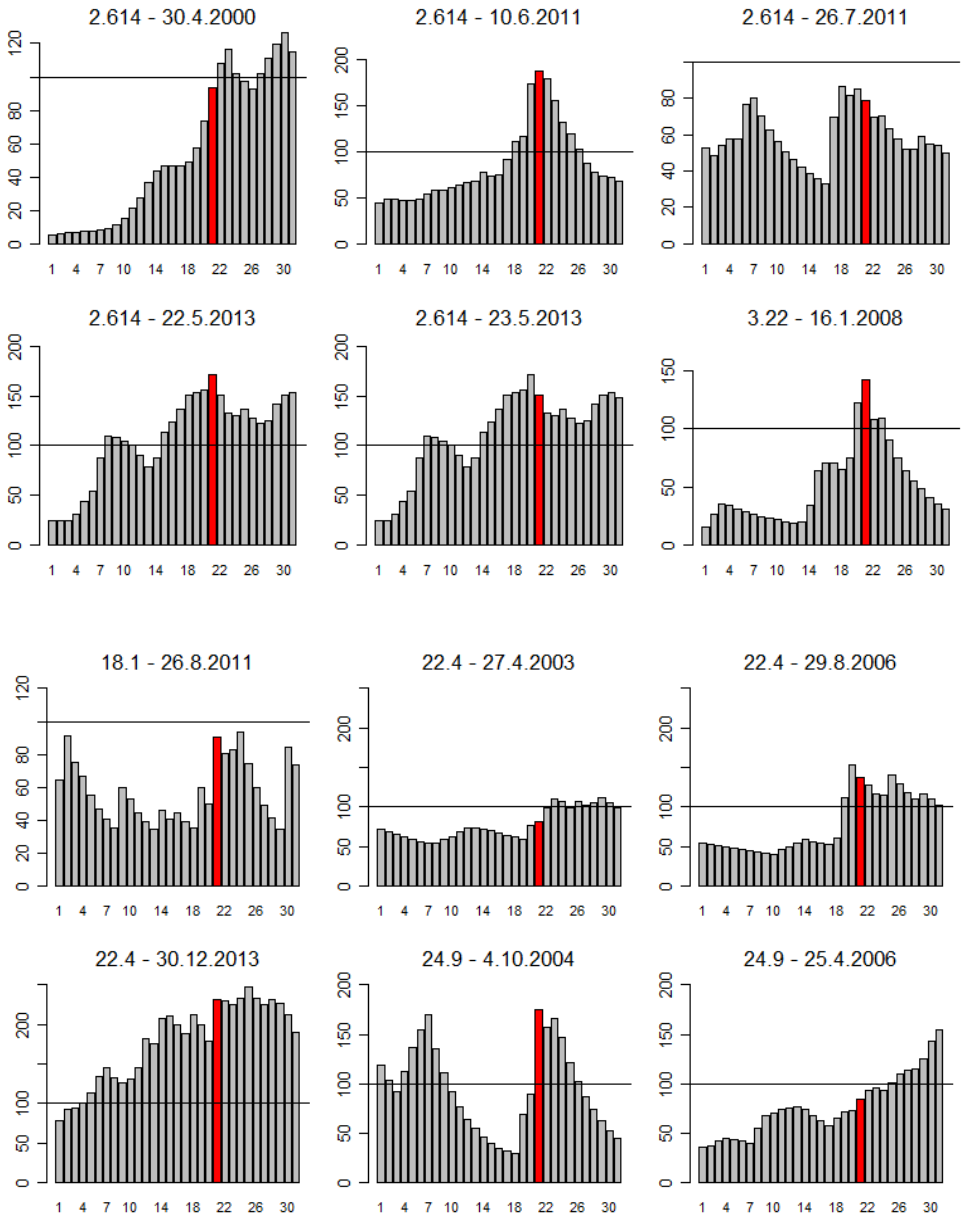

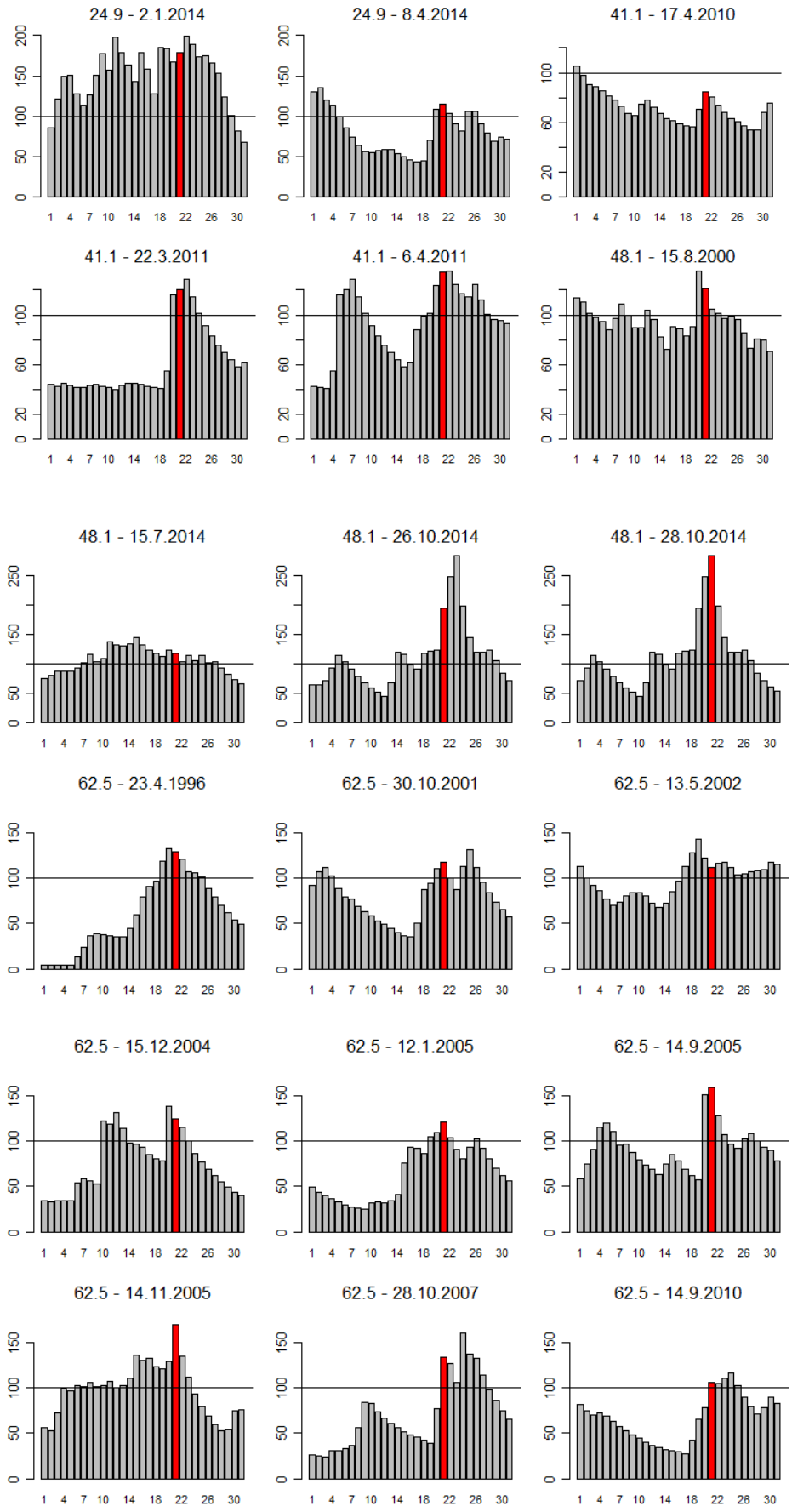
24.9 - 2.1.2014
24.9 - 8.4.2014
41.1 - 17.4.2010
41.1 - 22.3.2011
41.1 - 6.4.2011
48.1 - 15.8.2000
48.1 - 15.7.2014
48.1 - 26.10.2014
48.1 - 28.10.2014
62.5 - 23.4.1996
62.5 - 30.10.2001
62.5 - 13.5.2002
62.5 - 15.12.2004
62.5 - 12.1.2005
62.5 - 14.9.2005
62.5 - 14.11.2005
62.5 - 28.10.2007
62.5 - 14.9.2010

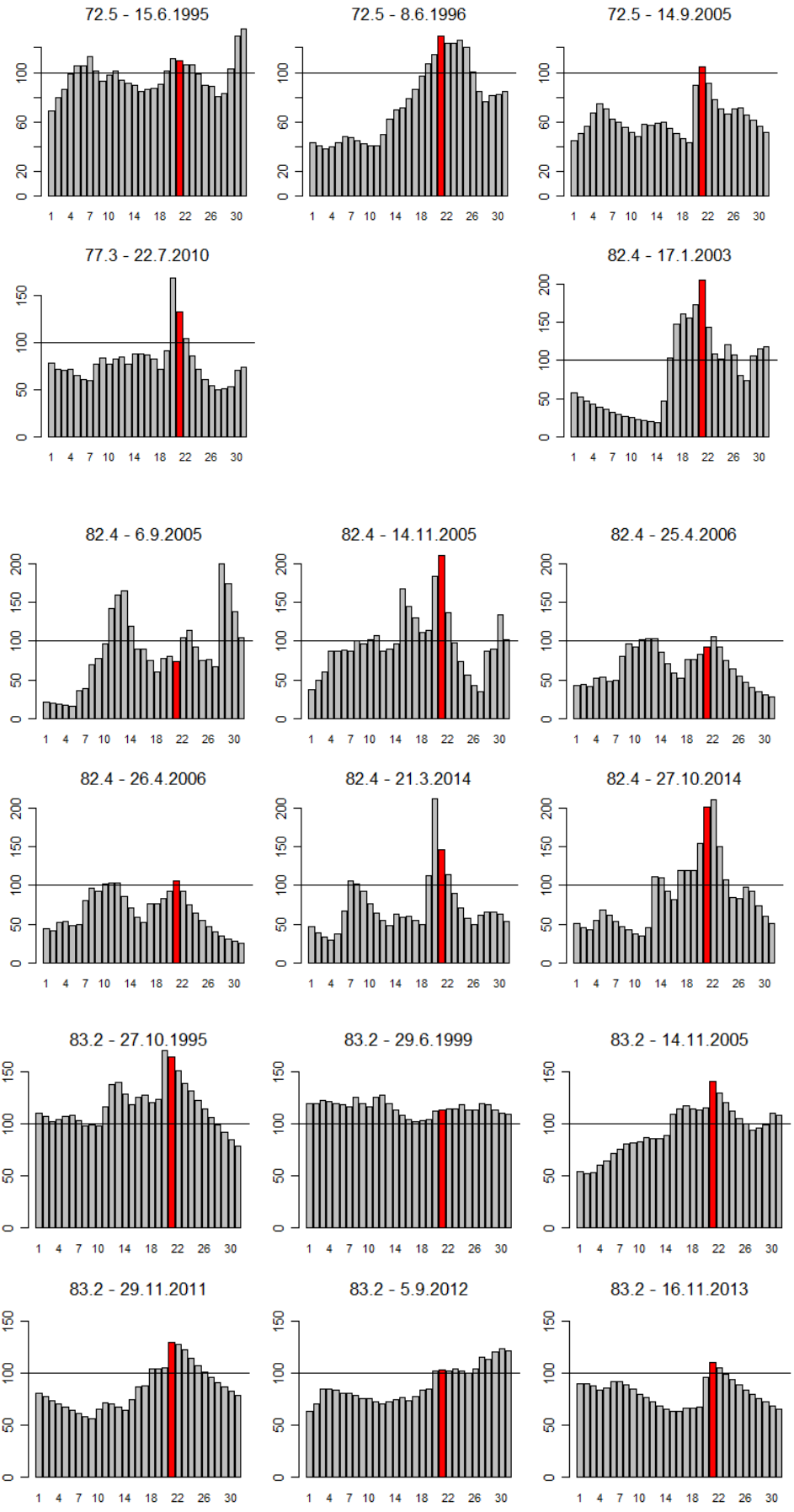
72.5 - 15.6.1995
72.5 - 8.6.1996
72.5 - 14.9.2005
77.3 - 22.7.2010
82.4 - 17.1.2003
82.4 - 6.9.2005
82.4 - 14.11.2005
82.4 - 25.4.2006
82.4 - 26.4.2006
82.4 - 21.3.2014
82.4 - 27.10.2014
83.2 - 27.10.1995
83.2 - 29.6.1999
83.2 - 14.11.2005
83.2 - 29.11.2011
83.2 - 5.9.2012
83.2 - 16.11.2013

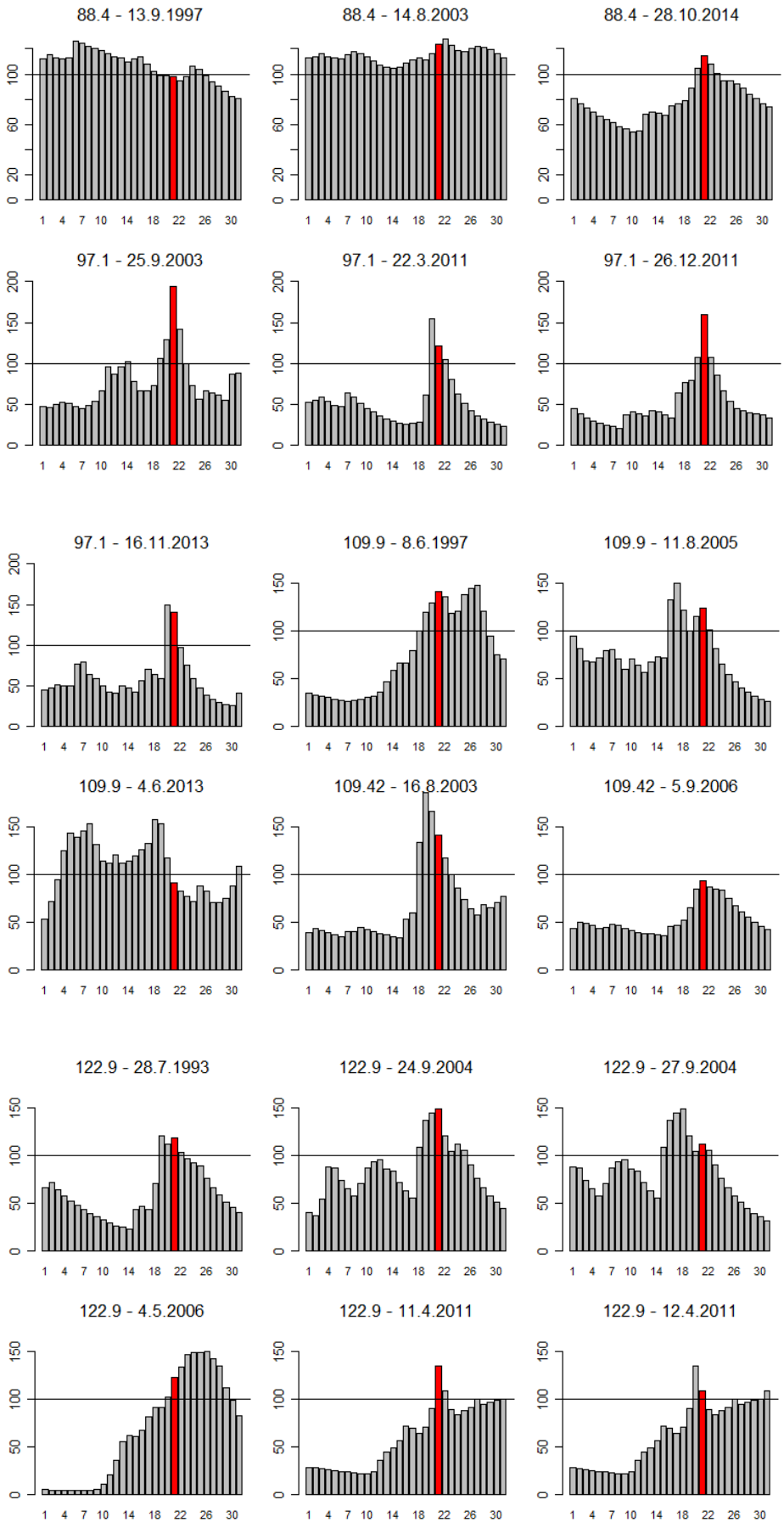
88.4 - 13.9.1997
88.4 - 14.8.2003
88.4 - 28.10.2014
97.1 - 25.9.2003
97.1 - 22.3.2011
97.1 - 26.12.2011
97.1 - 16.11.2013
109.9 - 8.6.1997
109.9 - 11.8.2005
109.9 - 4.6.2013
109.42 - 16.8.2003
109.42 - 5.9.2006
122.9 - 28.7.1993
122.9 - 24.9.2004
122.9 - 27.9.2004
122.9 - 4.5.2006
122.9 - 11.4.2011
122.9 - 12.4.2011

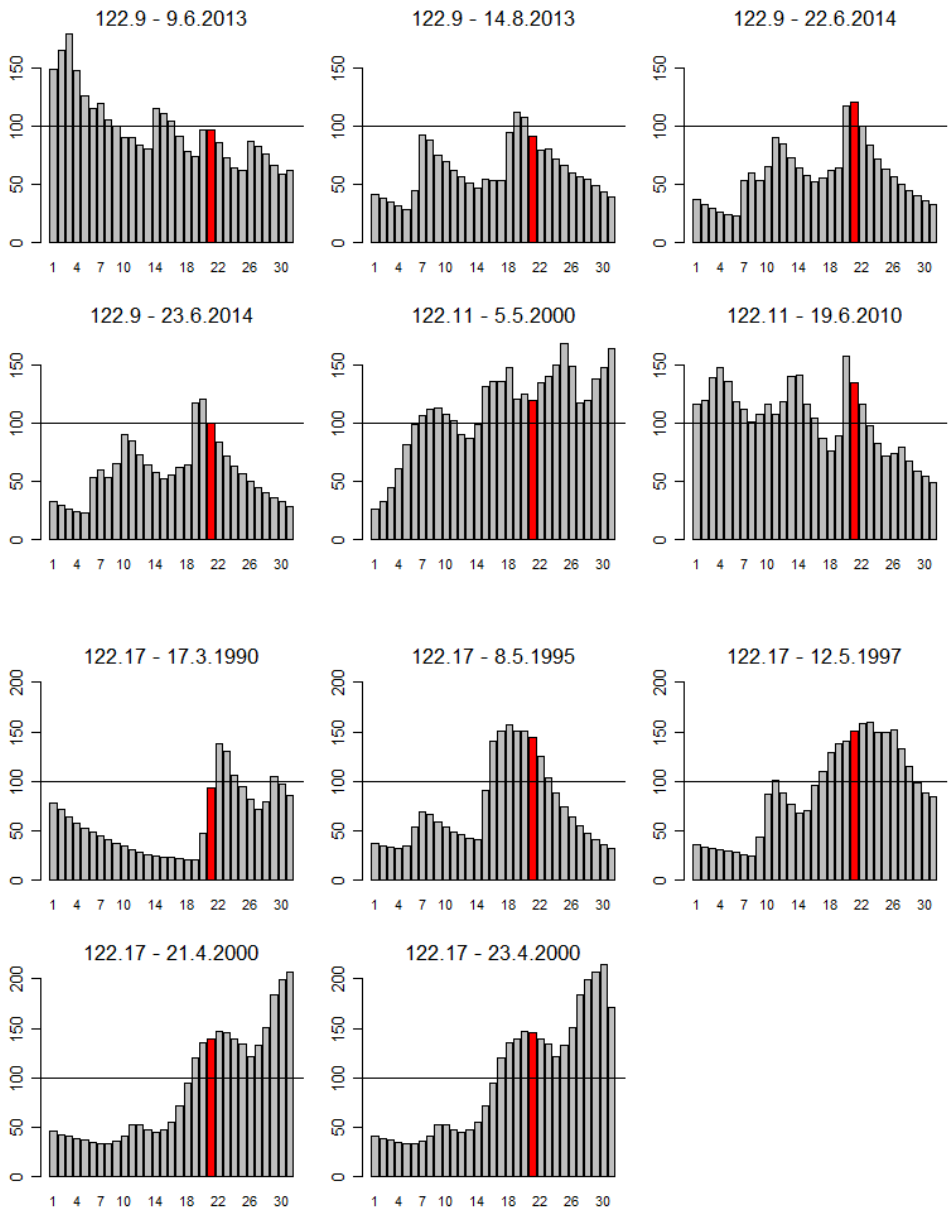
122.9 - 9.6.2013
122.9 - 14.8.2013
122.9 - 22.6.2014
122.9 - 23.6.2014
122.11 - 5.5.2000
122.11 - 19.6.2010
122.17 - 17.3.1990
122.17 - 8.5.1995
122.17 - 12.5.1997
122.17 - 21.4.2000
122.17 - 23.4.2000
0 50 100 150 200
1 4 7 10 14 18 22 26 30

Appendix V – Storage - Discharge Hysteresis

Storage–discharge hysteresis with corresponding rainfall. In the bar plot of rainfall [mm] (days on the x-axis) the blue bar indicates the day of the landslide. In the hysteresis, storage [mm] is on x-axis, discharge [mm/day] on y-axis. The number of days denote the direction of the loop. The red dot indicates the day of the landslide. The blue, stippled line indicate the maximum storage capacity (M).

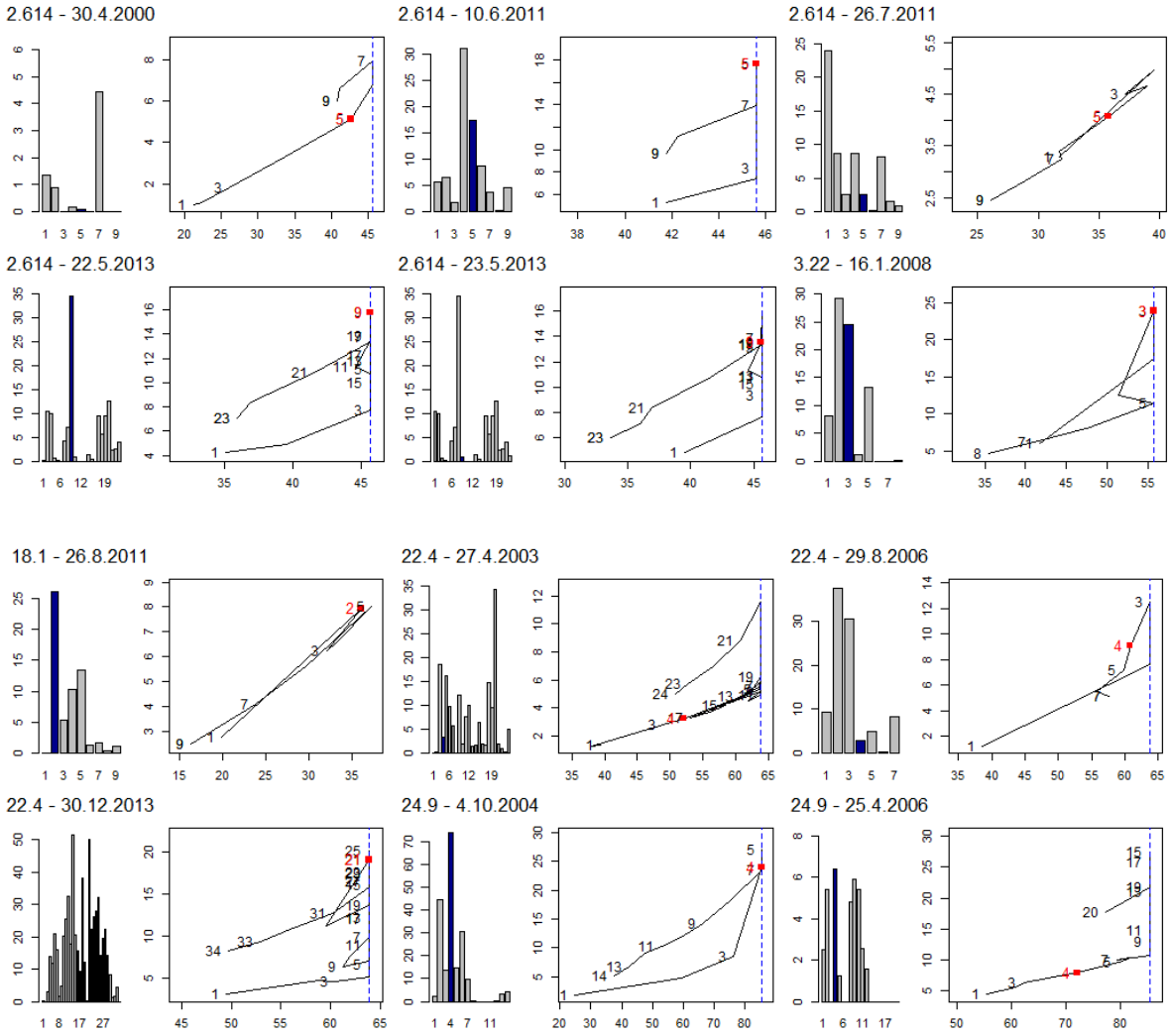

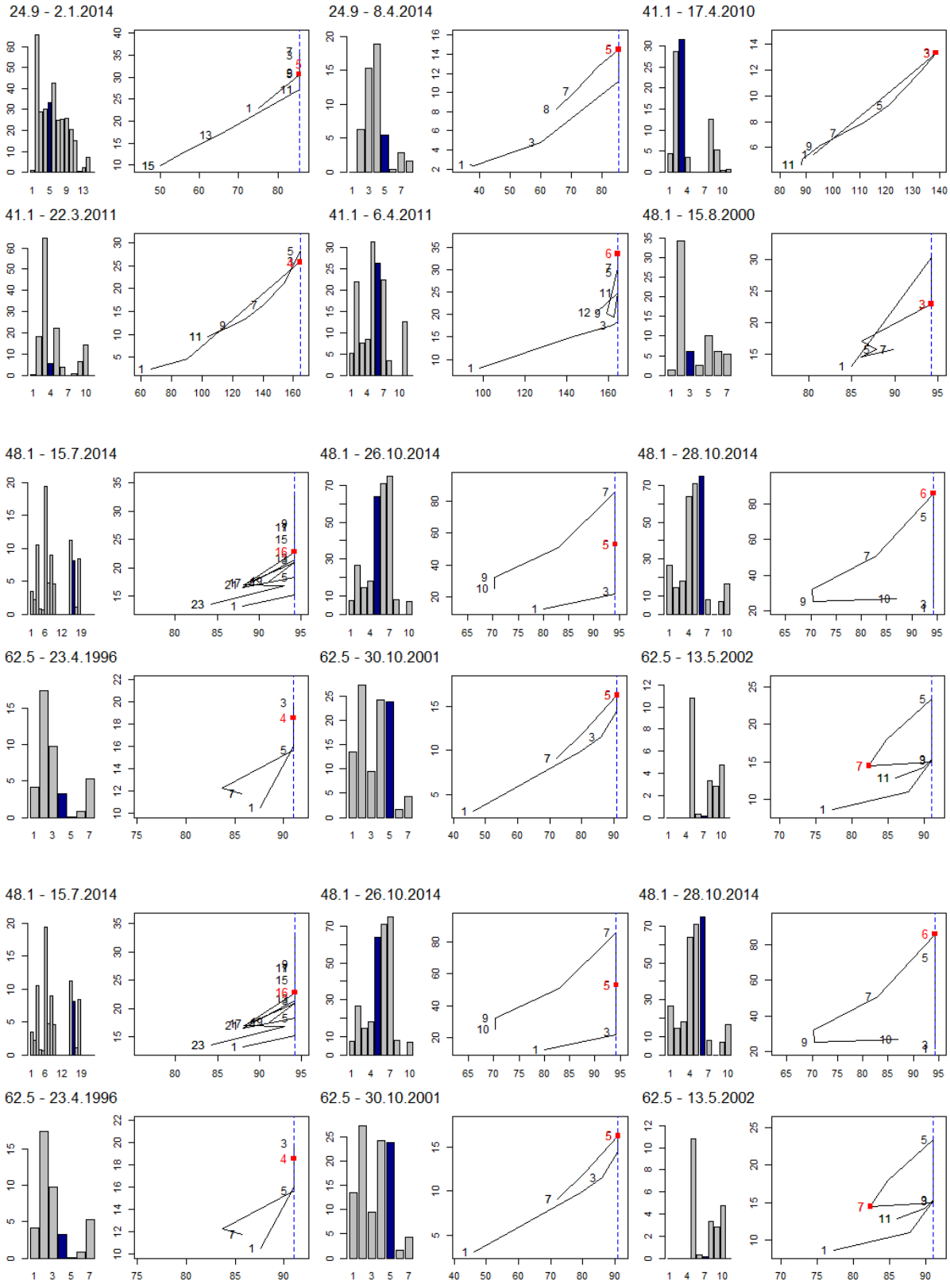
24.9 - 2.1.2014
24.9 - 8.4.2014
41.1 - 17.4.2010
41.1 - 22.3.2011
41.1 - 6.4.2011
48.1 - 15.8.2000
48.1 - 15.7.2014
48.1 - 26.10.2014
48.1 - 28.10.2014
62.5 - 23.4.1996
62.5 - 30.10.2001
62.5 - 13.5.2002
48.1 - 15.7.2014
48.1 - 26.10.2014
48.1 - 28.10.2014
62.5 - 23.4.1996
62.5 - 30.10.2001
62.5 - 13.5.2002

62.5 - 15.12.2004

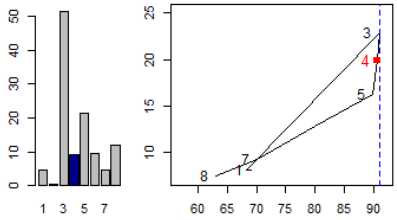

62.5 - 12.1.2005

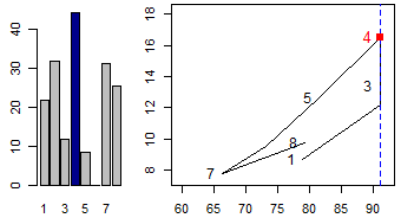

62.5 - 14.9.2005

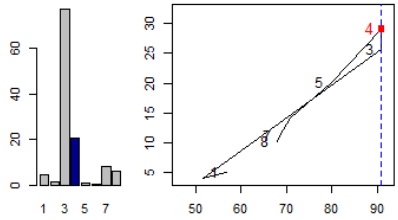

62.5 - 14.11.2005

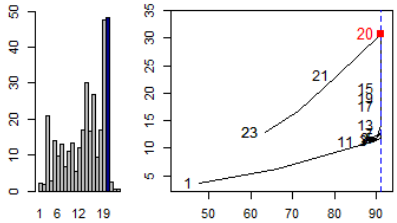

62.5 - 28.10.2007

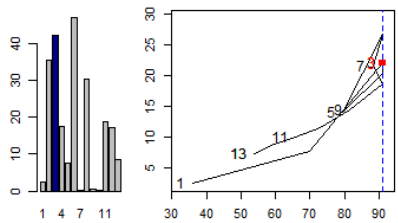

62.5 - 14.9.2010

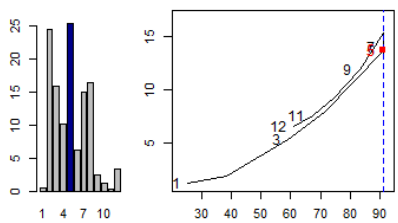

72.5 - 15.6.1995

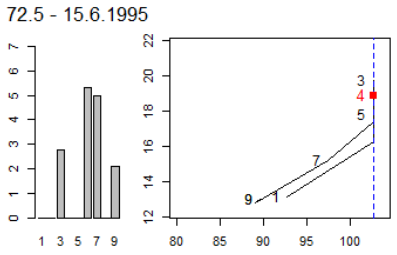

72.5 - 8.6.1996

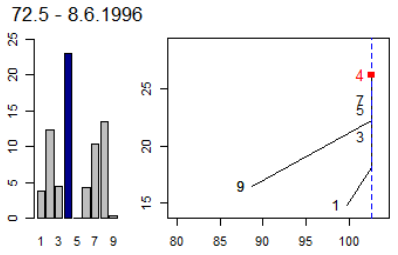

72.5 - 14.9.2005

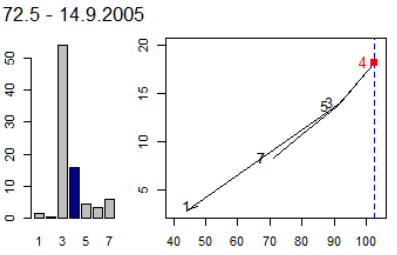

77.3 - 22.7.2010

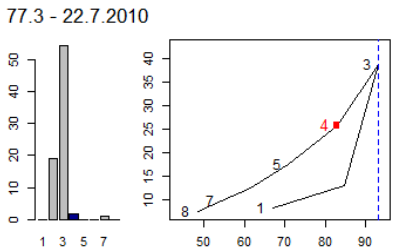

82.4 - 17.1.2003

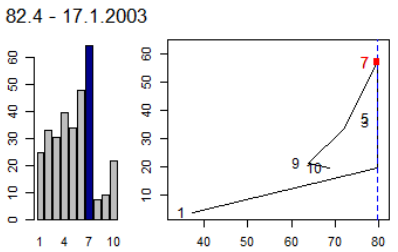

82.4 - 6.9.2005

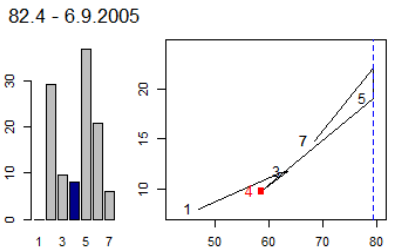

82.4 - 14.11.2005

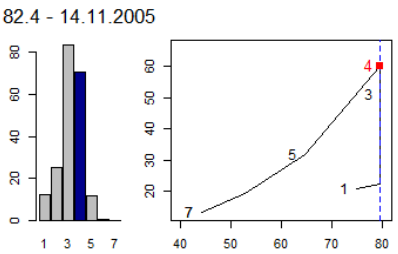

82.4 - 25.4.2006

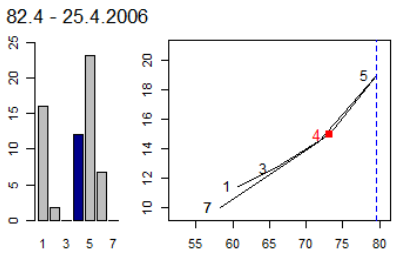

82.4 - 26.4.2006

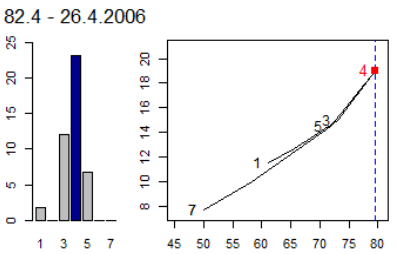

82.4 - 21.3.2014

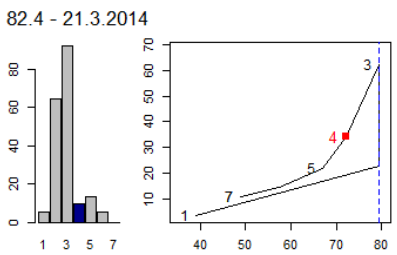

82.4 - 27.10.2014

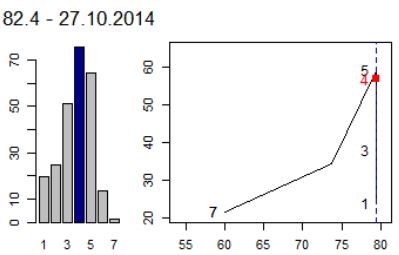

83.2 - 27.10.1995

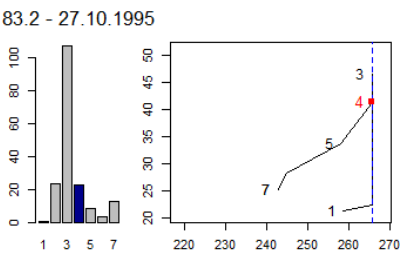

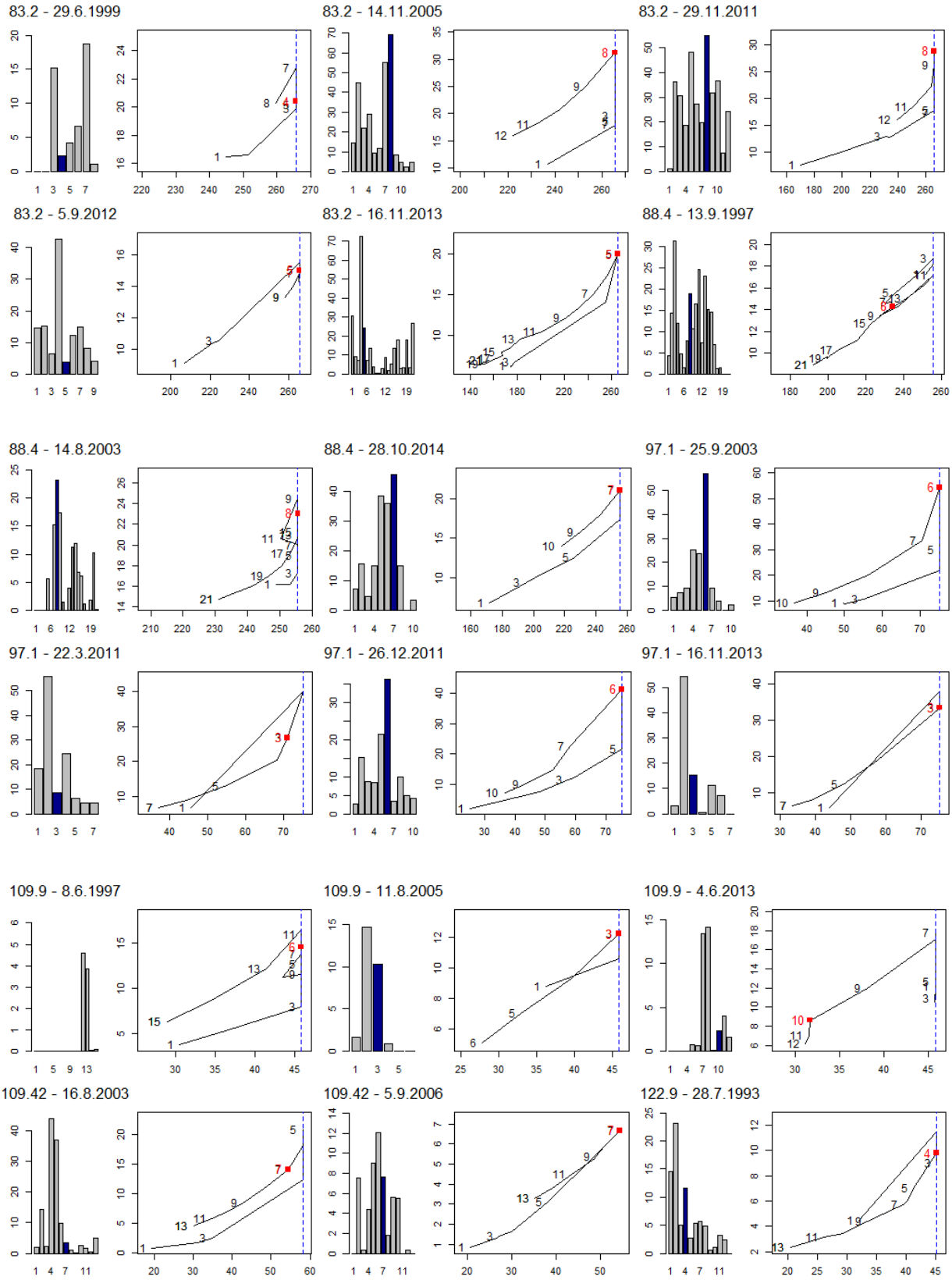
83.2 - 29.6.1999
83.2 - 14.11.2005
83.2 - 29.11.2011
83.2 - 5.9.2012
83.2 - 16.11.2013
88.4 - 13.9.1997
88.4 - 14.8.2003
88.4 - 28.10.2014
97.1 - 25.9.2003
97.1 - 22.3.2011
97.1 - 26.12.2011
97.1 - 16.11.2013
109.9 - 8.6.1997
109.9 - 11.8.2005
109.9 - 4.6.2013
109.42 - 16.8.2003
109.42 - 5.9.2006
122.9 - 28.7.1993

122.9 - 24.9.2004

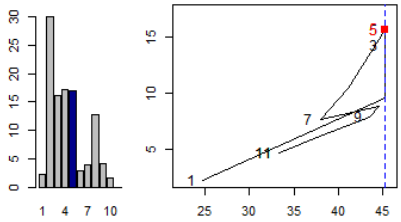

122.9 - 27.9.2004

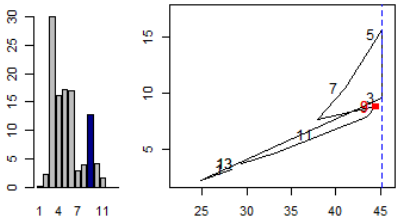

122.9 - 4.5.2006

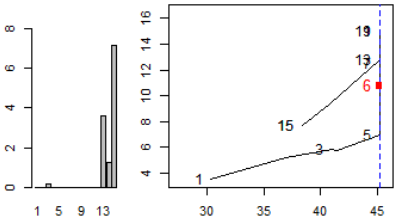

122.9 - 11.4.2011

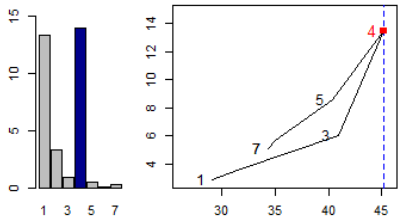

122.9 - 12.4.2011

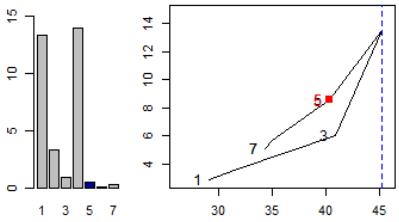

122.9 - 9.6.2013

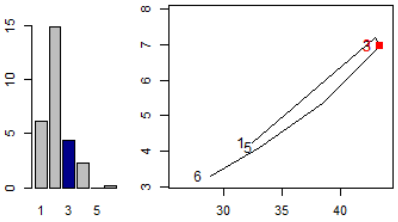

122.9 - 14.8.2013

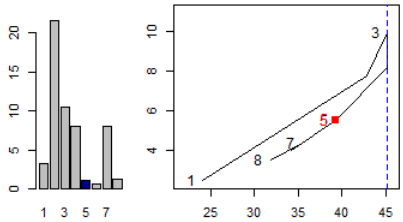

122.9 - 22.6.2014

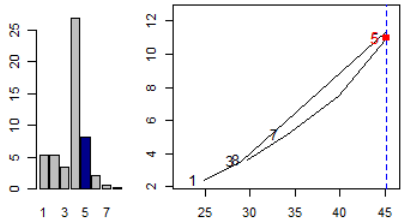

122.9 - 23.6.2014

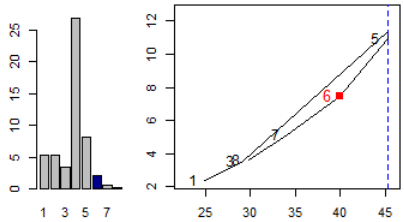

122.11 - 5.5.2000

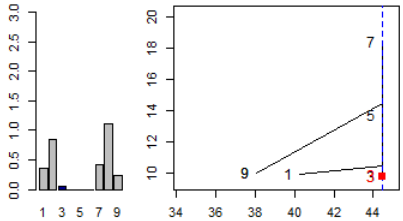

122.11 - 19.6.2010

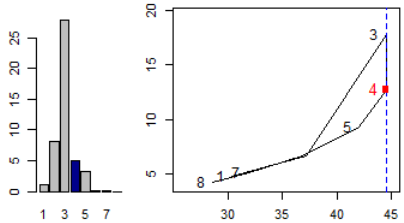

122.17 - 17.3.1990

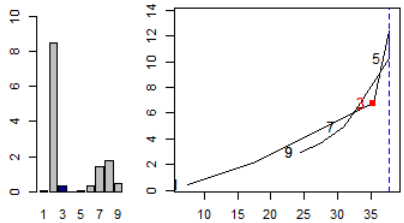

122.17 - 8.5.1995

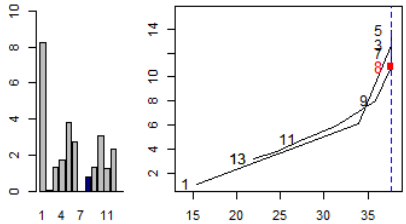

122.17 - 12.5.1997

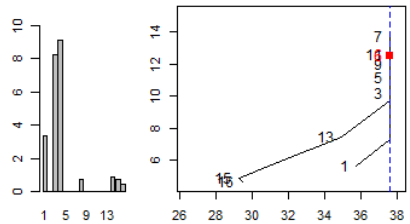

122.17 - 21.4.2000

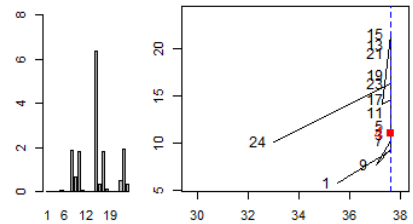

122.17 - 23.4.2000